Design and application of circular RNAs for protein sponging and modulation of alternative splicing

Dissertation

vorgelegt von

Anna Didio

(Master of Science in Biology)

zur Erlangung des akademischen Grades

doctor rerum naturalium

(Dr. rer. nat.)

Institut für Biochemie

der Justus-Liebig-Universität Gießen

Gießen, November 2020

Die vorliegende Arbeit wurde am Institut für Biochemie des Fachbereichs 08 der Justus-Liebig-Universität Gießen in der Zeit von November 2017 bis November 2020 unter der Leitung von Prof. Dr. Albrecht Bindereif angefertigt.

Dekan:
Prof. Dr. Jürgen Janek
Physikalisch-Chemisches Institut
Justus-Liebig-Universität Gießen

1. Gutachter:
Prof. Dr. Albrecht Bindereif
Institut für Biochemie
Fachbereich für Biologie und Chemie
Justus-Liebig-Universität Gießen

2. Gutachter:
Prof. Dr. Elena Evguenieva-Hackenberg
Institut für Mikro- und Molekularbiologie
Fachbereich für Biologie und Chemie
Justus-Liebig-Universität Gießen

Contents

Summary

The presented work focuses on the design, production, and application of circular RNA (circRNA) for sequestration of RNA-binding protein hnRNP L and modulation of alternative splicing of *CD45*. For that, we first focused on circRNA expression systems and applied either tRNA-based, Tornado ribozyme-driven or *in vitro* intron type I-based circRNA expression systems, as well as *in vitro*-generated circRNAs. In addition, we developed several circRNA expression constructs based on the platelet-specific circRNA *Plt-circR4*.

HnRNP L is a global regulator of alternative splicing, binding preferentially to CA-rich RNA sequences. Therefore, we designed and applied in HeLa cells circRNAs containing CA-rich sequences. Direct *in vivo* hnRNP L/circRNA interactions were captured by RNA immunoprecipitation (RIP) and alternative splicing of hnRNP L target genes was analyzed by RT-PCR. Interestingly, we observed hnRNP L delocalization from the predominant nuclear localization, which resulted in equal hnRNP L distribution between nucleus and cytoplasm in HeLa cells.

As a part of the hnRNP L-regulated alternative splicing network, we targeted the gene coding for *CD45*, an essential regulator of T- and B-cell antigen receptor signaling. Therefore, we generated *in vitro* designer antisense circRNAs targeting splice sites, intron, or each of the three variable exons 4, 5, and 6 of the *CD45* pre-mRNA as a proof of principle for developing designer antisense circRNAs that function in alternative splicing modulation. Consequently, we co-transfected a *CD45* minigene construct together with the antisense circRNAs into HeLa cells and analyzed splicing patterns of *CD45* minigene affected by antisense circRNAs. Specific splicing patterns were detected for each antisense circRNA variant applied, and these changes were determined to be at least partially of post-transcriptional nature.

Overall, we conclude that designer circRNAs have high potential for modulating activities of RNA-binding proteins or for alterations of particular alternative splicing events. They represent a promising alternative to pharmacological inhibition of proteins and can be applied in a way similar to antisense splice-switching oligonucleotides targeting individual splicing events.

Zusammenfassung

Die hier vorgelegte Arbeit konzentriert sich auf das Design, die Produktion und die Anwendung von zirkulärer RNA (circRNA) zur Sequestrierung des RNA-Bindeproteins hnRNP L und zur Modulation des alternativen Spleißens von *CD45*. Zu diesem Zweck konzentrierten wir uns zunächst auf circRNA-Expressionssysteme und verwendeten entweder tRNA-basierte, Tornado Ribozym-gesteuerte oder *in vitro* Intron-Typ-I-basierte circRNA-Expressionssysteme sowie enzymatisch *in vitro* generierte circRNAs. Zusätzlich entwickelten wir mehrere circRNA-Expressionskonstrukte basierend auf der circRNA *Plt-circR4*.

HnRNP L ist ein globaler Regulator des alternativen Spleißens, der bevorzugt an CA-reiche RNA-Sequenzen bindet. Daher designten und verwendeten wir circRNAs, die CA-reiche Sequenzen enthielten in HeLa Zellen. Direkte *in vivo* hnRNP L/circRNA-Wechselwirkungen wurden durch RNA-Immunpräzipitation (RIP) erfasst und alternatives Spleißen von hnRNP L-Zielgenen wurde durch RT-PCR analysiert. Interessanterweise konnte nach circRNA Transfektion in HeLa Zellen eine Delokalisierung von hnRNP L beobachtet werden, von einer vorwiegend nukleären Lokalisation hin zu einer gleichmäßigen Verteilung zwischen Kern und Zytoplasma.

Zur Untersuchung des hnRNP L-regulierten alternativen Spleißnetzwerks fokussierten wir uns auf *CD45*, ein essentieller Regulator der T- und B-Zell Antigen-Rezeptor-Signalübertragung. Dafür wurden *in vitro* designer-antisense-circRNAs generiert, die gegen Spleißstellen, ein Intron oder eins der drei variablen Exons 4, 5 und 6 des *CD45*-Gens gerichtet sind. Dies dient als grundsätzliches Prinzip für den Einsatz von designer-antisense-circRNAs als Regulatoren des alternativen Spleißens. Zur Analyse der verschiedenen *CD45*-Spleißmuster wurde ein *CD45*-Minigen-Konstrukt zusammen mit den antisense-circRNAs in HeLa-Zellen co-transfiziert. Hierbei wurden spezifische Spleißmuster detektiert, die teilweise auf posttranskriptionelle Effekte zurückgeführt werden können.

Zusammenfassend lässt sich sagen, dass designer-circRNAs das Potential zur Modulation der Aktivität von RNA-Bindungsproteinen sowie bestimmter alternativer Spleißereignisse haben. Sie stellen eine vielversprechende Alternative zur pharmakologischen Inhibition von Proteinen dar und können auf ähnliche Weise wie antisense-splice-switching-Oligonukleotide angewendet werden, die auf individuelle Spleißprozesse abzielen.

1. Introduction

1.1 Splicing of mRNA

In eukaryotes, the majority of protein-coding genes contain introns that have to be processed in order to allow correct translation. Therefore, eukaryotic pre-mRNA transcripts undergo a maturation process. First, pre-mRNA is capped with 7-methylguanosine at the 5′-end. Second, non-coding sequences (introns) are removed and the protein-coding sequences, termed “exons” are spliced together. Finally, the mature mRNA is cleaved and polyadenylated, namely ~200 adenylate residues, forming a poly-adenosine [poly(A)] tail, are attached to the 3′-end of the mRNA. Since the splicing phenomenon and the presence of introns in protein-coding genes were first discovered (Berget *et al*., 1977; Chow *et al*., 1977), it turned out to be essential for eukaryotic gene expression. Different eukaryotes have their own characteristic average intron content and length. In human, protein-coding genes contain on average eight introns with the median length approximately 3.3 kb (Lander *et al*., 2001). Exons are normally much shorter and, in comparison to introns, their sequence is highly conserved as they usually code for protein sequence.

There are four known mechanisms of splicing described for eukaryotes. Namely, two mechanisms of intron group I and II splicing, tRNA splicing, and pre-mRNA splicing governed by the spliceosome. Among eukaryotes, group I and II introns are present mainly in organelle genomes. The introns of both groups are spliced by ribozymes, without protein catalysis (mechanism of a two-step transesterification reaction). Specific to group I introns is the conserved intron structure and the necessity of an external guanosine cofactor (Cech, 1990). Group II introns resemble nuclear pre-mRNA splicing, as they require conserved splice sites and the presence of the branch point adenosine (Michel & Ferat, 1995; Bonen & Vogel, 2001). Interestingly, some data imply shared functional and structural similarity of spliceosomal components, namely the small nuclear RNA (snRNAs) with the protein-free catalytic core of group II introns (reviewed by Sharp, 1991). In contrast to protein-free splicing, pre-mRNA splicing is carried out by the spliceosome with >100 cofactor proteins. The main constituents of the spliceosome are uridine-rich U1, U2, U4, U5, and U6 small nuclear ribonucleoproteins snRNPs, as well as a large set of proteins. Each snRNP is in turn composed of the respective snRNA, seven Sm proteins (LSm proteins for U6), and several snRNP-specific proteins.

Over the last 40 years, numerous biochemical, genetic, and cryo-electron microscopy studies provided structural insights into the splicing mechanism (reviewed in Wilkinson *et al*., 2020). In particular, it was shown that splicing implies numerous interactions of the spliceosomal components with the pre-mRNA. Recognition of sequences at the exon-intron boundaries by the spliceosome is the determining factor for splicing, namely the intron dinucleotide GU at its 5′ end and AG at its 3′ end. Therefore, these RNA interactions with the spliceosome are

defined by three important sites: the 5′ splice site (5′SS), branch point adenosine (BP-A) in the downstream portion of the intron, and the 3′ splice site (3′SS), where all of them are determined by short conserved sequences. The biochemical mechanism of the spliceosomal intron removal implicates two sequential transesterification reactions (Fig. 1.1A). In the first reaction, the 2′OH of the branch point adenosine performs a nucleophilic attack at the 5′SS phosphodiester group, forming a lariat intermediate. In the second reaction, the 3′OH of the 5′SS attacks the phosphodiester group at the 3′SS, bringing two exons together and releasing the intron lariat as an unusual 2′-5′-branched structure.

The spliceosome continuously assembles and re-assembles its components, consequently leaving and joining the complex, directly on the pre-mRNA substrate molecule (Fig. 1.1B). Recently, it was shown that the formation of the spliceosome is possible across the intron (intron definition model), as well as across the exon (exon definition model). These two models coexist and can result in the same spliceosome structure even on the same pre-mRNA (Li *et al*., 2019). In the early stage of spliceosome assembly, the U1 snRNP recognizes the 5′SS, where the U1 snRNA base-pairs with the pre-mRNA 5′SS consensus sequence (E complex). The next step is the binding of U2 snRNP to the BP sequence, also mediated by base-pairing of the U2 snRNA with the respective pre-mRNA sequence, which forms the A complex. The DEAD-box helicase Prp28 releases the 5′SS from U1 snRNP and transfers it to the U6 snRNA within the U4/U6/U5 tri-snRNP complex, which joins the spliceosome last (Staley & Guthrie, 1999). Subsequently, the B complex is formed: U6 snRNA becomes separated from U4 snRNA by the RNA helicase Brr2 (Raghunathan & Guthrie, 1998) and the U6 snRNA contains the active site coordinating the two catalytic metal ions (Steitz & Steitz, 1993; Hang *et al*., 2015). The attachment of the Prp19-associated complex (NTC) and the Prp19-related complex (NTR) to the spliceosome marks the formation of the B^{act} complex. These two proteins stabilize the active site of the splicesome (Chan *et al*., 2003). Further spliceosome complex remodeling is mediated by the DEAH-box helicases Prp2, Prp16, and Prp22 (Cordin *et al*., 2012). Particularly, Prp2 remodels the spliceosome active site (Semlow *et al*., 2016), which designates the beginning of the first catalytic step (B* complex). U6 snRNA catalyzes both splicing reactions: (i) branching reaction produces the cleaved 5′SS and the lariat-intron intermediate, (ii) Prp16 promotes BP sequence release from the active site, where the 5′SS is subsequently ligated to the 3′SS (Fica *et al*., 2013). Finally, the post-splicing P complex is formed. Prp22 releases the spliced exons from the spliceosomal components, which are recycled for the next rounds of splicing, while most of the intron lariats are debranched and degraded (Clement *et al*., 1999).

In sum, the spliceosome-directed intron excision is driven by the activity of the RNA-dependent ATPases/helicases, which leads to the recruitment/dissociation of specific splicing

factors that enable the reaction. By the mechanism of action, the spliceosome can be called a protein-directed metalloribozyme (reviewed in Wilkinson *et al*., 2020).

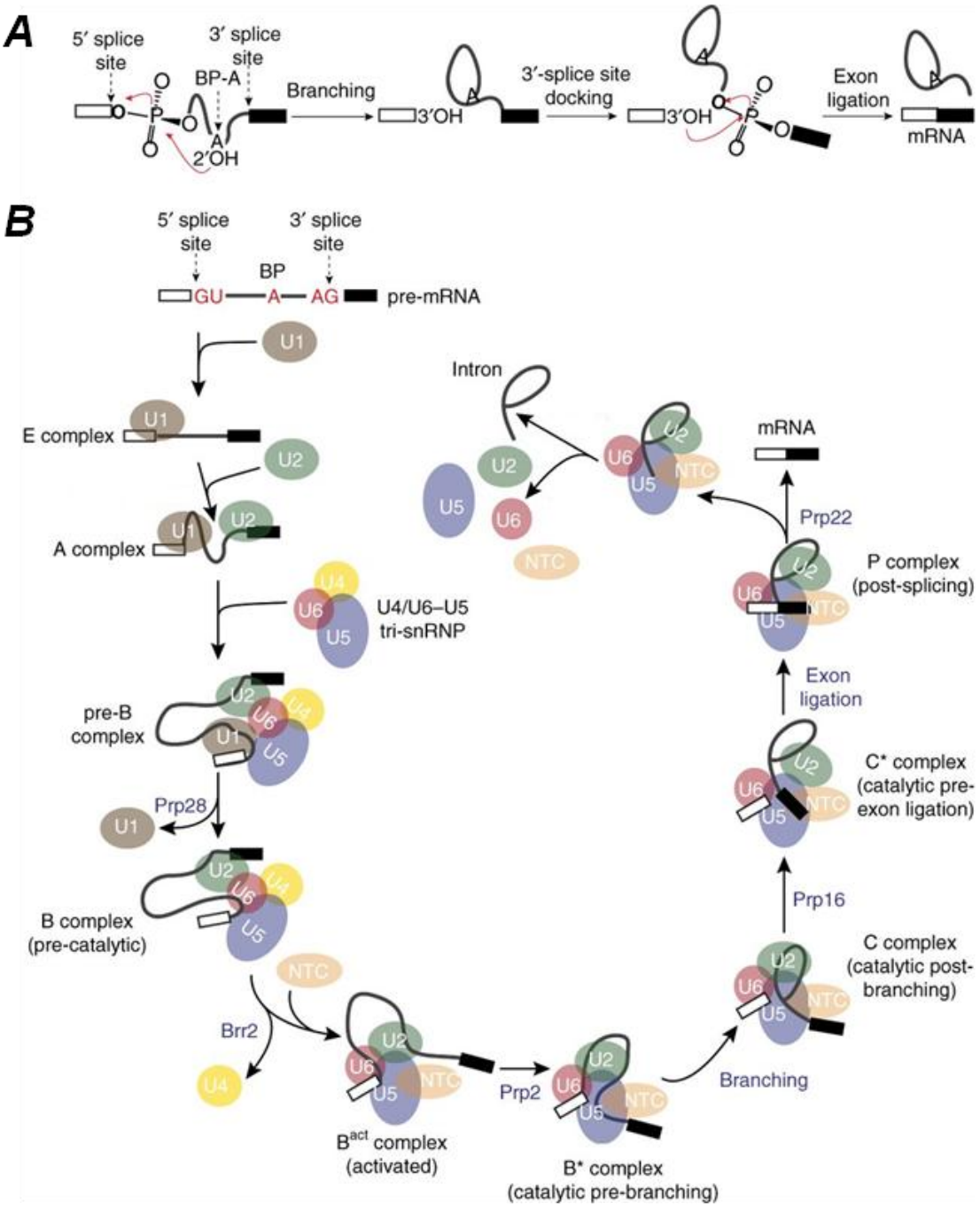

Figure 1.1 Schematic of the spliceosome cycle (from Fica & Nagai, 2017).
(A) Chemical mechanism of the two-step transesterification reaction in pre-mRNA splicing. Red arrows indicate nucleophilic attacks. 2′OH of the BP-A (branch point adenosine) attacks the 5′SS phosphate. In the second reaction, the free 3′OH of the 5′SS attacks the phosphate of the 3′SS.
(B) Spliceosome complex remodeling along the spliceosome cycle (explanation in the text).

Finally, a rare class of introns (less than 0.5%) which are flanked by AT/AC and other dinucleotides (instead of the canonical GT/AG) are spliced by the U11 and U12 snRNA-dependent minor spliceosome (reviewed by Turunen *et al*., 2013).

1.2 Alternative splicing

Many individual protein-coding genes are known to produce multiple mRNA species from a single pre-mRNA due to alternative splicing. Such mRNAs are a source of an additional protein complexity, as they often produce functionally different protein products. Alternative splicing increases proteome diversity, thereby allowing regulation of tissue differentiation and development. Human transcriptome studies showed that transcripts from ~95% of multiexon human genes undergo alternative splicing (Pan *et al*., 2008; Wang *et al*., 2008). High-resolution mass spectrometry analysis of diverse human tissues and cells showed that 37% of all detected proteins could be annotated to protein-coding genes which generate >2 protein isoform; among them 34% were identified with isoform-specific peptides (Kim *et al*., 2014). However, not all alternatively spliced mRNAs produce functionally different proteins; namely, the changes can involve translation efficiency, protein stability or localization. Additionally, alternative splicing may lead to the introduction of a premature termination codon, which causes nonsense-mediated decay (NMD) and mRNA transcript elimination.

Fig. 1.2A illustrates the five basic patterns of alternative splicing. Some regulated exons can either be included in the mature mRNA or skipped (exon skipping). Exons can be shortened or enlarged by using alternative 5′SS or 3′SS for splicing. Exons can as well be included in a mutually exclusive manner (mutually exclusive exons). Finally, in some cases, the introns are retained in the mRNA (intron retention). Alternative poly(A) site selection and suppression of multiple exons gives another interesting pattern for mRNA diversity (not shown). In addition to this, several splicing patterns can also occur in one mRNA (Fig. 1.2B). Therefore, alternative splicing adds up an extra level of mRNA isoform complexity.

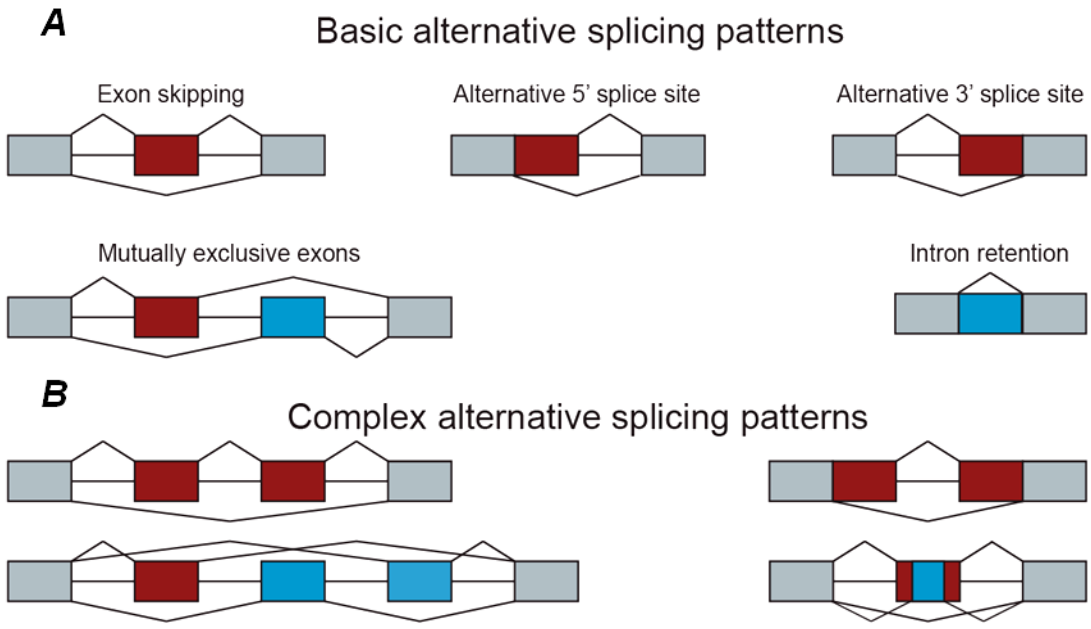

Figure 1.2 Schematic of alternative splicing patterns (modified from Park *et al*., 2018).
Colored boxes represent exons. Constitutive and alternative splicing patterns are shown with grey lines. Blue and red boxes represent alternatively spliced elements.

In the past, obtaining comprehensive data on the alternative splicing variants was restrained due to technological limitations. In particular, reverse transcription polymerase chain reaction (RT-PCR) and expressed sequence tags (ESTs) techniques for the detection of alternatively spliced mRNAs are rather laborious and have low throughput. RT-PCR and splicing microarray strategies are limited to known splicing events. Since 2008, alternative splicing has been comprehensively analyzed by RNA sequencing (RNA-seq), which allowed the discovery of novel mRNA isoforms, their quantification, and estimation of their expression levels (Wang *et al*., 2008). Thereby, recent advances in high-throughput sequencing (e.g. using Illumina and Nanopore sequencing) allowed detailed transcriptomic analysis.

Many splicing isoforms have been assigned to specific biological functions *in vivo*. One striking example of alternative splicing importance in development is *Drosophila* somatic sex determination pathway, which combines a cascade of three alternative splicing processes (reviewed in Förch & Valcárcel, 2003). In males, the inclusion of the third exon in the *sxl* mRNA with the stop codon leads to the formation of the truncated mRNA. In females, the full-length mRNA lacks exon 3, therefore leading to the production of the long protein isoform. The presence or absence of the full-length Sxl protein affects alternative splicing of *tra* and, subsequently, *dsx* mRNA. Sxl protein binds to intronic regulatory elements of the *tra* pre-mRNA with high uridine content. In males, the absence of the Sxl protein leads to the production of the non-coding *tra* mRNA. In females, Tra protein is produced, which affects the alternative splicing in *dsx* mRNA, causing male- and female-specific Dsx protein isoforms to be produced.

Alternative splicing is regulated by a coordinated network of RNA-protein interactions, both spatially (cell type-specific) and temporally (during development). This regulation is implemented through so-called *cis*-elements and *trans*-factors. *Cis*-acting elements reside within the pre-mRNA and include the splice sites (5′SS and 3′SS), BP sequence, and polypyrimidine tract, which are recognized by the spliceosomal machinery just like in case of canonical splicing (see above). Besides these canonical splicing signals, there are auxiliary *cis*-elements that include splicing enhancers and silencers. These *cis*-elements reside either in exons or introns of the pre-mRNA, and can accordingly be classified as exonic splicing enhancers (ESEs), exonic splicing silencers (ESSs), intronic splicing enhancers (ISEs), and intronic splicing silencers (ISSs). In general, these splicing regulatory elements recruit *trans*-acting splicing factors (RNA-binding proteins, RBPs) that activate or suppress splice site recognition or spliceosome assembly by various mechanisms, thereby promoting or repressing intron splicing (reviewed in Wang & Burge, 2008).

ESEs and ESSs are located in exons and respectively promote or inhibit the inclusion of the exon they reside in. ESEs are often very short purine-rich elements, which recruit serine-arginine-rich (SR) protein family, thus facilitating spliceosomal assembly (Graveley &

Maniatis, 1998). ESSs repress splicing by recruiting members of the heterogeneous nuclear ribonucleoprotein (hnRNP) class. ISEs and ISSs correspondingly enhance or inhibit the usage of adjacent splice sites or exons from an intronic location. One example of these elements is CA-rich sequences, which were shown to act either as intronic splicing activators or silencers (Hui *et al.*, 2005; Hung *et al.*, 2008). These *cis*-regulatory-elements and the recruited *trans*-factors are illustrated in Fig. 1.3.

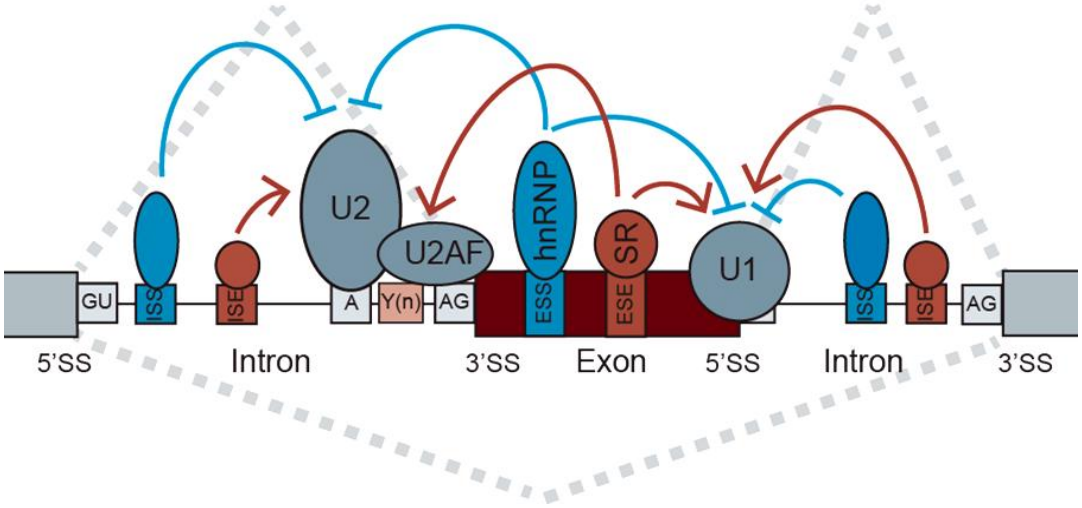

Figure 1.3 Schematic of the protein-RNA interaction network in alternative splicing (modified from Park *et al*., 2018).
Cis-elements within the pre-mRNA include the canonical splicing elements 5′splice site (5′SS), branch point adenosine (A), polypyrimidine tract [Y(n)], and 3′ splice site (3′SS), as well as the auxiliary *cis*-elements exonic splicing enhancers (ESEs), exonic splicing silencers (ESSs), intronic splicing enhancers (ISEs), and intronic splicing silencers (ISSs). 5′SS is recognized by the U1 snRNP, branch site – by the U2 snRNP complex, 3′SS and Y(n) are bound by the U2AF proteins. ISS and ESS elements recruit hnRNP proteins, which hinder binding of the spliceosomal components to the pre-mRNA. ISE and ESE elements are bound by SR proteins, which promote splicing. GU and AG dinucleotides are conserved the first and last two nucleotides of the intron, respectively.

In sum, different splicing decisions exhibit a broad spectrum of molecular and physiological outcomes, influencing such processes as development and cell differentiation.

1.3 Alternative splicing as a therapeutic target in human diseases

Studying alternative splicing regulation is crucial when its disruption leads to pathological conditions or disease. It was estimated, that between 15% and 60% of disease-causing mutations lead to aberrancies in splicing (reviewed in Wang & Cooper, 2007).

Such diseases can be treated by correcting the aberrant gene expression by splice-switching oligonucleotides (SSOs), a type of antisense oligonucleotides (ASO) of 16 – 25 nucleotides long, which specifically target splicing (reviewed by Havens & Hastings, 2016). When targeted by ASOs, undesired mRNA isoforms can be degraded by RNAse H or RNA interference (RNAi). Alternatively, SSOs can modulate splicing by preventing splicing factors from binding to the target pre-mRNA (steric blocking). For that, SSOs are designed to target specific splice sites or other *cis*-elements (Fig. 1.4), thereby redirecting protein production

towards isoforms with restored function. SSOs can inhibit splicing by blocking a cryptic splice site, generated by a mutation, or downregulating a particular protein by exon skipping. For therapeutic splicing activation, SSOs are designed to target splicing silencer elements, thereby switching on the splice site weakened by a mutation or *cis*-activating regulatory element. SSO-induced skipping of individual exons results either in disruption of the reading frame and mRNA nonsense-mediated decay or maintaining the reading frame and production of shorter semi-functional protein isoforms. When an aberrant alternative splicing event leads to the introduction of the premature termination codon and NMD, SSO therapy targeting this mRNA can restore the full-length mRNA and, as a consequence, protein production (Lim *et al*., 2020).

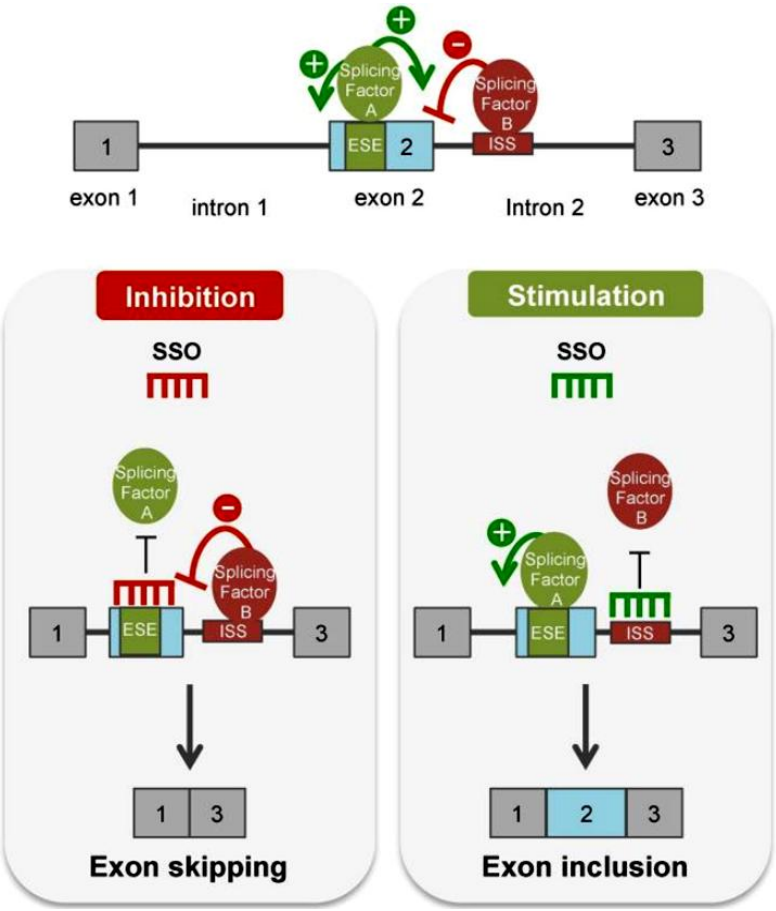

Figure 1.4 Modulation of alternative splicing with splice-switching oligonucleotides (SSOs) by steric blocking (from Havens & Hastings, 2016).
Exonic splicing enhancer (ESE) and intronic splicing silencer (ISS) elements recruit *trans*-factors, which facilitate or abrogate splicing (splicing factor A and B, respectively). Antisense nucleotides that bind these elements create a steric block, which prevents binding of a *trans*-factor. This, in turn, disrupts splicing resulting in exon skipping (left) or leads to exon inclusion when a negatively acting splicing factor is blocked (right).

To improve pharmacological properties, ASOs are often synthesized with chemical modifications. Phosphorothioate (PS) backbone increases stability and protects against digestion by nucleases. 2′-O-methyl (2′OMe) and 2′-O-methoxyethyl (2′-MOE) ribose

modifications are also implicated in order to increase the half-life of ASOs. In addition to that, 2′OMe- and 2′-MOE-modified ASOs exhibit higher stability of complementary base hybridization. Phosphorodiamidate morpholino (PMO) ASOs have overall neutral charge, which improves their tolerability *in vivo*.

For clinical applications, ASOs can be injected into the blood as unformulated drugs, where they can be bound by circulating plasma proteins and enter cells by endocytosis (reviewed by Dowdy, 2017). Recently, attempts have been made for the optimization of ASO delivery by packaging into biodegradable lipid nanoparticles in cultured human cells and animal model (Yang *et al*., 2020).

Deletions and other mutations that result in skipping of exons 45 – 55 in the *DMD* gene prevent the expression of dystrophin protein and cause Duchenne muscular dystrophy (Muntoni *et al*., 2003). Males with such mutations experience severe neuromuscular impairment starting in early childhood. In approximately 13% of cases, patients can be treated with 30-nucleotide antisense PMO oligonucleotide eteplirsen, approved by FDA in 2016 (Mendell *et al*., 2013, 2016). Eteplirsen is designed to bind the ESE in exon 51, causing exon 51 skipping and restoration of the *DMD* reading frame, which leads to the production of a truncated but partially functional dystrophin protein isoform.

Another example is spinal muscular atrophy (SMA) caused by insufficient production of the SMN protein from the *SMN1* gene, which is the most common genetic cause of infant mortality. A therapeutic strategy for SMA treatment relies on the restoration of the protein expression from the *SMN1*-paralogous gene, *SMN2*. *SMN2* differs from *SMN1* by a C>T mutation in the exon 7, which abrogates ESE site normally recognized by the splicing factor SRSF1 (Cartegni *et al*., 2006). *SMN2* exon 7 splicing can be restored by a 2′-MOE antisense oligonucleotide, called nusinersen, which blocks an ISS in intron 7 of *SMN2* (Singh *et al*., 2006). Nusinersen targeting this ISS is predicted to block the hnRNP A1 binding, to cause mRNA secondary structure rearrangements, and to prevent an inhibitory interaction with downstream sequences within intron 7 (reviewed by Ottesen, 2017).

Recently, attempts were made in the treatment of multiple sclerosis by ASOs. The severity of multiple sclerosis positively correlates with the expression of the α subunit of integrin receptors (integrin alpha-4). Antisense oligonucleotides targeting the *ITGA4* transcript were designed to induce skipping of its individual exons, and thereby reduce protein expression (Aung-Htut *et al*., 2019). After screening ASOs with 2′OMe base modifications on a PS backbone in fibroblasts, several ASO were also synthesized as peptide-linked PMOs and tested in a mouse model of multiple sclerosis, which resulted in the production of a truncated *ITGA4* mRNA and downregulation of integrin alpha-4 protein.

2′-MOE ASOs with PS backbone are not resistant to RNase H, so they can eliminate the malfunctioning mRNA isoforms directing them to RNase H degradation upon ASO binding

(Ackermann *et al*., 2016). Such a mechanism is used for treating hypercholesterolemia. ASO mipomersen is a PS-based *APOB*-antisense drug, hybridizing to pre-mRNA of *APOB* (Raal *et al*., 2010). DNA-RNA heteroduplex recruits RNase H, which cleaves the mRNA, therefore reducing the amount of apolipoprotein B and, as a consequence, hindering release of LDL-cholesterol in blood.

Alternative splicing can also be controlled through siRNA-mediated gene silencing. As functioning siRNAs (Robb *et al*., 2005) and then later also their cofactor proteins (Gagnon *et al*., 2014) were discovered in the nuclei of various human cells, siRNA-based alternative splicing modulation of therapeutic protein isoforms was introduced. First, in a study on fibronectin extra domain I alternative exon (Alló *et al*., 2009). SiRNAs targeting sequences which surround the alternative exon prevented efficient Pol II elongation and led to exon inclusion. Liu *et al.* (2015) demonstrated argonaute 2-dependent dystrophin exon 51 skipping triggered by siRNAs targeting this exon for the treatment of Duchenne muscular dystrophy. Therefore, exon 51 skipping restores a reading frame and eliminates a premature stop codon.

To sum up, the application of ASOs represents a powerful tool for the therapy of alternative splicing defects. The chemistry of therapeutic ASOs depends on a particular splicing defect and should be individually selected for each specific case.

1.4 HnRNP L, a global regulator of alternative splicing

HnRNP L is a predominantly nuclear 68 kDa protein with four canonical RRM motifs, two glycine- and two proline-rich regions; characterized as a global regulator of RNA processing and alternative splicing.

A study on the human endothelial nitric oxide synthase (*eNOS*) gene provided the first evidence on the role of hnRNP L in regulation of alternative splicing. Intron 13 of the *eNOS* pre-mRNA contains a polymorphic CA-rich ISE element, predominantly bound by hnRNP L, which acts there as a splicing activator (Hui *et al*., 2003). The number of CA repeats within eNOS intron 13 ISE was shown to correlate with the risk of coronary disease (Stangl *et al*., 2000). Since eNOS protein is mainly involved in the regulation of the vascular tone, its splicing regulation by hnRNP L makes this mechanism a potential target for atherosclerosis therapy.

HnRNP L is known to specifically bind CA-rich RNA sequences. CA repeats represent the most common dinucleotide simple-sequence repeat motif in human and mouse transcriptomes (Lander *et al*., 2001; Waterston *et al*., 2002), which makes hnRNP L a ubiquitous RNA-binding protein regulating splicing. CA-rich sequences functioning as widespread regulatory elements were found in many human genes and confirmed by mutational analysis of these CA-rich elements (Hui *et al*., 2005). RNA-binding specificity of hnRNP L was additionally analyzed *in vitro* by applying SELEX (systematic evolution

of ligands by exponential enrichment) approach. Tetranucleotides ranked according to their hnRNP L affinity and four high-score SELEX-derived sequences are shown in Fig. 1.5.

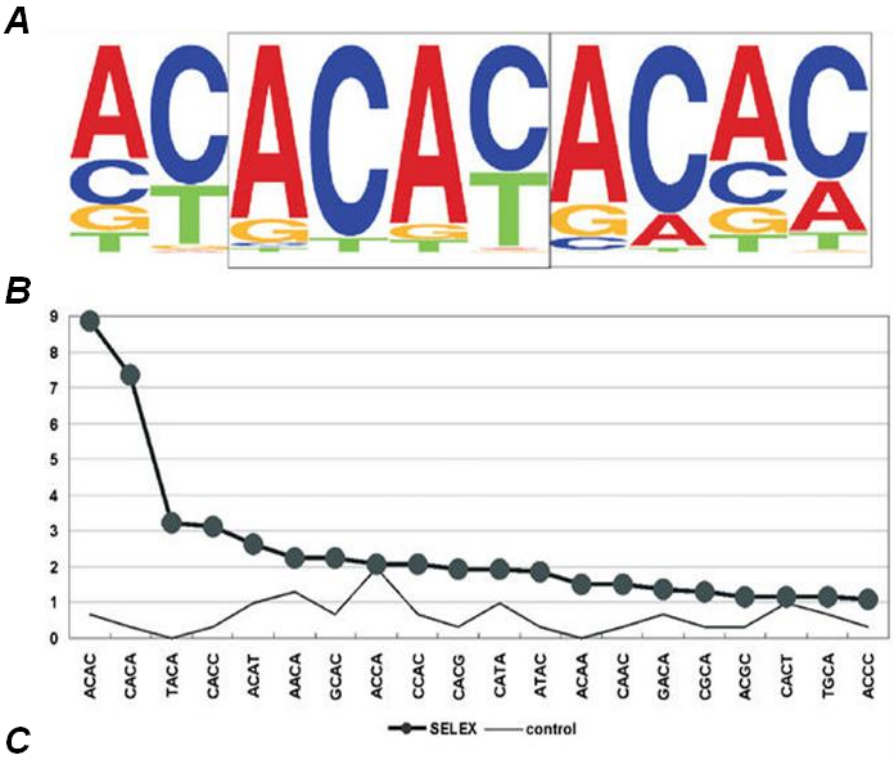

C

#	Sequence	K_D (nM)
51	ATACATGACACACACACGCA	7.2±5.1
55	CACACACACTACACCACAC	8.1±2.4
1	CACACCACAACGGCACCACA	11.7±2.6
63	TGCATCTACGTACACACACA	17.6±3.1

Figure 1.5 RNA-binding specificity of hnRNP L determined by SELEX (from Hui *et al*., 2005).
(A) The 10-nucleotide consensus sequence. The letter height reflects the frequency of each nucleotide. Two boxes mark two conserved tetranucleotide motifs.
(B) Frequency of the 20 most common tetranucleotide motifs among selected hnRNP L-binding sequences. Vertical axes represent the percentage of the total.
(C) Four SELEX-derived sequences with the high-score motifs shown in red, low score motifs are underlined. K_D values are represented with standard deviations, $p < 0.05$.

Alternative splicing targets of hnRNP L were identified by microarray approach comparing hnRNP L knockdown and control samples, where hnRNP L was shown to act as an activator (*MYL6*, *FAM48A*, *PAPOLA*) or repressor (*TJP1*, *FALZ*, *PARK7*) of alternative splicing (Hung *et al*., 2008). Additionally, hnRNP L was found to be involved in poly(A) site selection and suppression of multiple exons. Mechanisms of hnRNP L alternative splicing regulation are summarized in Fig. 1.6.

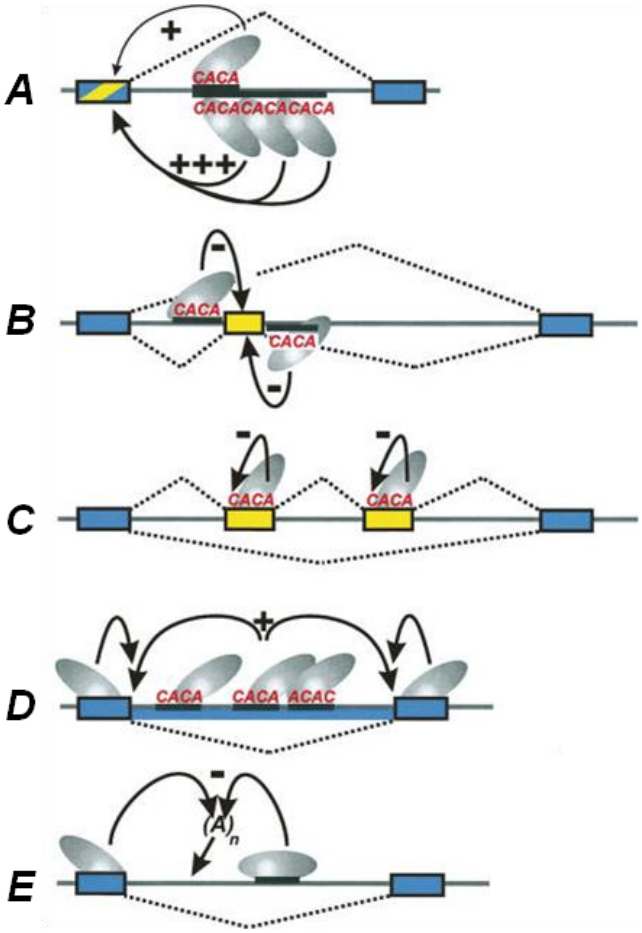

Figure 1.6 Schematics of hnRNP L alternative splicing regulation (from Hung *et al*., 2008).
Activator (+) and repressor (-) hnRNP L functions, CA-rich motifs (CACA), constitutive (blue) and regulated (yellow) exons are marked.
(A) HnRNP L binds to CA-rich ISEs leading to an alternative exon inclusion.
(B) Binding of hnRNP L to CA-rich ISS elements results in the repression of cassette-type exons.
(C) HnRNP L suppresses multiple exons by acting on ESE elements.
(D) Binding of hnRNP L to CA-rich ISE or ESE leads to intron splicing.
(E) HnRNP L represses alternative internal poly(A) site acting on exonic or intronic regulatory sequences.

The *HNRNPL* gene itself has a long CA-rich cluster in intron 6, which was identified as a conserved ISE element, followed by a so-called poison cassette exon 6A. Binding of hnRNP L protein to its regulatory CA-rich region in intron 6 leads to the inclusion of the poison exon 6A, which introduces a premature termination codon, inducing NMD (Rossbach *et al*., 2009). This autoregulation loop supports homeostasis of this ubiquitously acting splicing factor. Similar homeostatic regulation mechanisms were also shown for many other RBPs, which manifests the importance of their proteostasis in numerous transcription events (Müller-McNicoll *et al*., 2019).

The study on the hnRNP L autoregulation loop revealed the involvement of its closely related paralog hnRNP L-like (hnRNP LL), which also contains the corresponding poison exon regulated by hnRNP L, therefore its homeostasis is controlled in a manner similar to hnRNP L autoregulation (Rossbach *et al*., 2009). HnRNP LL was shown to preferably bind

CA-rich sequences (Rossbach *et al*., 2009) and affect alternative splicing (Oberdoerffer *et al*., 2008).

One interesting example of hnRNP L and LL regulation of alternative splicing is the case of *CD45* splicing (described in Chapter 1.5). A detailed study on *CD45* regulatory elements revealed an interplay between hnRNP L and LL regulation and the combinatorial alternative splicing model (Preussner *et al*., 2012). HnRNP L and LL were shown to be differentially expressed in various B-cell lines, correlating with the splicing patterns of *CD45* transcripts, where exon 4 is repressed by hnRNP L and LL, exon 5 is passively co-repressed, and exon 6 is repressed by hnRNP LL alone.

The detailed mechanism of hnRNP L alternative splicing modulation is not completely understood. A study on hnRNP L individual-nucleotide resolution crosslinking-immunoprecipitation in combination with deep-sequencing (iCLIP-Seq) demonstrated an overlapping between hnRNP L and microRNA (miRNA) 3′UTR binding sites, which suggests a hnRNP L versus miRNA competition model for mRNA turnover regulation (Rossbach *et al*., 2014).

A study on murine hematopoietic stem cells (HSC) demonstrated the role of hnRNP L in haematopoiesis (Gaudreau *et al*., 2016). HnRNP L-depleted HSC displayed impaired blood cell differentiation, increased apoptosis rates, and mitochondrial stress. Further analysis demonstrated a new role of hnRNP L as a transcription regulator. Cells lacking hnRNP L accumulated the death receptor TrailR2. TrailR2 signaling activates Caspase-8 protein cleavage and a downstream cell death signaling pathways. The promoter region of *TrailR2* pre-mRNA was shown to be occupied by hnRNP L, which suggests hnRNP L as a regulator of TrailR2 expression (Gaudreau *et al*., 2016). HnRNP L is also involved in an interplay between enhancer RNA seRNA-1, Pol II, and H3K36me3 on Mb locus which contributes to myogenic differentiation (Zhao *et al*., 2019). In this study, hnRNP L was shown to bind CAAA motive on seRNA-1. Notably, disruption of this interaction led to the downregulation of transcription from the *Mb* locus.

In sum, hnRNP L is involved in numerous regulatory networks, mainly based on alternative splicing, which makes this protein an interesting target for molecular interventions and a potential therapeutic target for disease therapy, altering splicing of malfunctioning hnRNP L-dependent transcripts.

1.5 Alternative splicing of *CD45*

The *CD45* gene, also called *protein tyrosine phosphatase receptor type C* (*PTPRC*), encodes a trans-membrane protein-tyrosine phosphatase expressed in all differentiated hematopoietic cells, except for erythrocytes and plasma cells. It contains a highly glycosylated extracellular domain, a transmembrane domain, and two cytoplasmic protein tyrosine phosphatase domains. In T cells, CD45 modulates immune response by

dephosphorylating the inhibitory tyrosines of Src family protein tyrosine kinases, which are responsible for phosphorylation of T-cell receptor (Xu & Weiss, 2002).

CD45 represents one of the first mammalian genes where alternative splicing has been described. In particular, it was studied in T-cell activation, where several mRNA isoforms with different combinations of exon 4, 5, and 6 were discovered (Streuli *et al*., 1987). Specifically, resting T-cells predominantly express “full-inclusion” form, containing all three exons (R456), and partial inclusion forms (R45, R56, and R5). Upon activation, naive T-cells switch to exons 4 – 6 skipped form (R0), which hinders signaling via the T-cell receptor (Birkeland *et al*., 1989). The alternatively spliced *CD45* exons encode a highly glycosylated extracellular domain. It was shown, that the R0 CD45 protein isoform is more prone to homodimer formation than the inclusion forms. Larger CD45 isoforms exist predominantly as monomers, where homodymer formation is impeded by sialylation and O-glycosylation of the alternatively spliced exons. In other words, alternative splicing determines the equilibrium between CD45 protein monomers and dimers, which in turn regulates the threshold of signal transduction (Hermiston *et al*., 2003).

Later, studies on T-cells demonstrated that hnRNP L and LL proteins play a decisive role in alternative splicing of these exons (Lynch & Weiss, 2000; Oberdoerffer *et al*., 2008). As shown by House & Lynch (2006), hnRNP L inhibits splicing after the spliceosomal A complex formation by targeting an ESS, thereby regulating exon 4 inclusion in *CD45* transcript. CA-rich silencer elements in exons 4 and 6 were additionally confirmed by mutational analysis (Preussner *et al*., 2012).

The function of CD45 in B-cells is not very clear. Interestingly, one non-catalytic function of CD45 was discovered: Coughlin *et al*. (2015) demonstrated CD45-driven modulation of the inhibitory B-cell antigen co-receptor CD22. Thereby, CD45 regulates tonic B-cell receptor signaling. Similar to T-cells, B-lymphocytes were also shown to “lose” *CD45* alternative exons upon differentiation (Hathcock *et al*., 1992). Likewise, *CD45* alternative splicing in B-cells is also controlled by the interplay between hnRNP L and LL proteins. HnRNP LL expression correlates with the development stage of B-cells, while hnRNP L is expressed at similar levels in most of the B-cell lines, which suggests that hnRNP LL might mediate B-cell differentiation (Preussner *et al*., 2012; Chang *et al*., 2015). According to the suggested *CD45* alternative splicing regulation model (Fig. 1.7), ESS in exon 4 can be suppressed by hnRNP L and LL, exon 5 does not contain regulatory sequences and can only be co-repressed, while exon 6 could be regulated only by hnRNP LL. Therefore, the predominant *CD45* isoforms in each particular cell line are determined by hnRNP L versus LL expression (Preussner *et al*., 2012). Other protein factors were also shown to affect CD45 splicing. For instance, the CCCTC-binding factor (CTCF) can be co-transcriptionally recruited to exon 5 genomic DNA, which pauses RNA polymerase II and enhances exon 5 inclusion (Shukla *et al*., 2011).

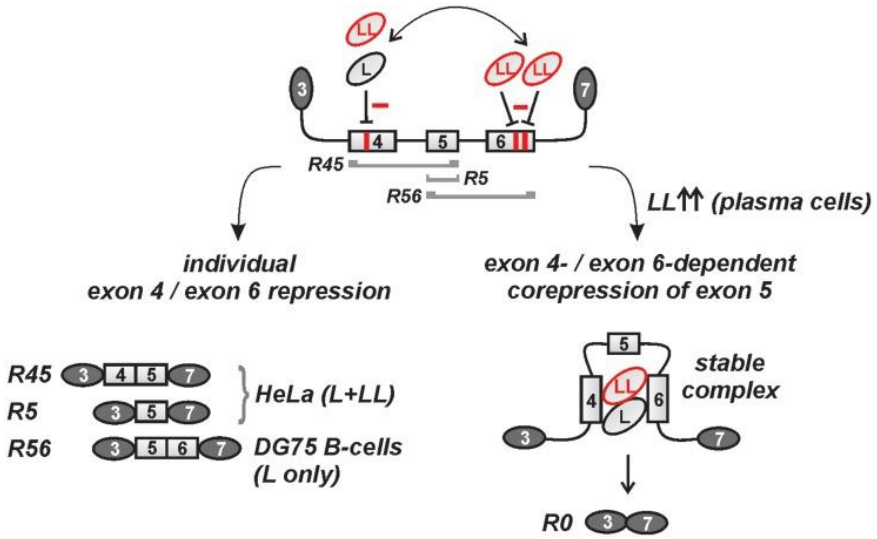

Figure 1.7 Model of *CD45* alternative splicing (from Preussner *et al*., 2012).
The final outcome of a splice reaction depends on the levels of hnRNP L and LL proteins. In the presence of both hnRNP L and LL, inclusion/skipping of alternatively spliced exons 4, 5, and 6 results in predominant R45 and R5 mRNA CD45 isoforms. In DG75 cells, where no hnRNP LL is present, R56 form is produced. Cross-exon 4 – 6 interaction together with high hnRNP L and LL levels may lead to the formation of a stable RNP complex, in which exon 5 is looped out. Then all three exons can also be skipped, generating the R0 form.

1.6 Circular RNA

Circular RNAs (circRNAs) represent a new class of covalently closed transcripts, which are now known to be a common output of many eukaryotic protein-coding genes. The first identified circRNA was characterized as a viroid plant pathogen (Sanger *et al*., 1976). Several approaches demonstrated circular conformation of these viroids: Single-stranded circRNA structures were visualized by electron microscopy, while the attempts to label 5′ or 3′ RNA ends were unsuccessful. Unlike for viroids, a circRNA discovered in the hepatitis delta virus, a satellite virus of the hepatitis B virus, was shown to code for protein components of its self-replication system, expanding knowledge about the circRNA and its functions (Kos *et al*., 1986; Weiner *et al*., 1988).

Yet another type of circRNA was found with the discovery of circRNA produced from rRNA type I introns in *Tetrahymena (*Grabowski *et al.*, 1981). In addition to that, circRNAs were also found in archaea, where they are formed as an intermediate in rRNA processing (Kjems & Garrett, 1988). CircRNA was first discovered in metazoa in a study on scrambled exons in human and rodent cells, where it was shown, that four *DCC* (netrin 1 receptor) transcripts contain exons positioned in a “wrong” order, however preserving the canonical splice site connections (Nigro *et al*., 1991). In this study, circRNA was described as a product of pre-mRNA splicing where the upstream donor 5′SS connects to the downstream acceptor 3′SS, a process later termed backsplicing.

Shortly after the study on scrambled exons, the first direct evidence on circRNA production from a nuclear pre-mRNA was obtained, where the circRNAs from *ETS-1* transcripts were

characterized by a predominant cytoplasmic localization and stability for at least 48 h upon actinomycin D treatment (Cocquerelle *et al*., 1993).

Since then, many genes, such as the rat cytochrome *P450 2C24* (Zaphiropoulos, 1996), human cytochrome *P450 2C18*, gene coding for the rat androgen-binding protein (Zaphiropoulos, 1997), human dystrophin gene (Surono *et al*., 1999), and Na/Ca exchanger gene 1 (Li & Lytton, 1999) were found to produce circRNA transcript isoforms. However, circRNAs were very long considered to be a product of aberrant splicing. They did not attract much attention until the availability of high-throughput RNA sequencing in combination with specific bioinformatic approaches, leading to circRNA re-discovery between 2012 and 2014, when several hallmark publications announced its occurrence, ubiquity, and novel functions. The studies on chromosomal rearrangements in normal and cancer cells by RNA-seq analysis revealed multiple abundant RNA transcripts of circular configuration and concluded that the circRNAs represent a general phenomenon in eukaryotic gene expression (Salzman *et al*., 2012; Jeck *et al*., 2013). Interestingly, many of newly detected circRNAs were more abundant than their corresponding linear isoforms. However, not all identified RNA-seq circRNA reads should be interpreted as such. To minimize the detection of potential artifacts of reverse transcription and other false-positive reads, it is important to use at least two algorithms to identify circRNAs, and additionally validate *de novo* circRNAs by Northern blot or RT-PCR (Jeck & Sharpless, 2014; Hansen, 2018). As most circRNAs are expressed at relatively low levels, several additional steps, such as rRNA depletion, poly(A) depletion, and RNase R treatment are often introduced in RNA-seq library preparation for a more efficient circRNA detection.

Further comprehensive analysis of the circRNA content demonstrated tissue- and developmental stage-dependent circRNA expression (Memczak *et al*., 2013). The high abundance of the circRNA and its differential expression were noted especially for the central nervous system, which was confirmed for human, mouse, and *Drosophila* (Rybak-Wolf *et al*., 2015). Moreover, circRNAs were found to be conserved across species. Namely, in the same study comparing mammalian and mouse brain circRNAs, around one-third of all detected circRNAs were shown to share both splice sites, while the other third shared one splice site, which demonstrates a high conservation rate and supports the hypothesis of circRNA functionality. Additionally, the analysis of human circRNAs from the protein-coding genes and their circular orthologues in mice revealed significantly higher conservation in the third codon position in comparison to the exons without the circular output (Memczak *et al*., 2013). Later, circRNA-coding exons were also shown to be more conserved in comparison to their flanking exons (Rybak-Wolf *et al*., 2015).

Most of the exonic circRNAs accumulate in the cytoplasm. However, little is known about their export from the nucleus. Huang *et al*. (2018) suggested a length-dependent mechanism

of circRNA export to the cytoplasm: In humans, spliceosome RNA helicase DDX39B (UAP56) drives the export of long (>1300 nt) circRNAs, whereas the short circRNAs (<400 nt) require DDX39A (URH49).

A common degradation pathway of circRNA has not been discovered yet. Liu *et al*. (2019) demonstrated circRNA digestion by cytoplasmic endonuclease RNase L, which cleaves many viral and cellular transcripts after UN dinucleotides, where N is any nucleotide. In some particular cases, circRNAs can be eliminated from cytoplasm via packaging into extracellular vesicles (Preußer *et al*., 2018).

1.7 Splicing of circRNA: Sequence determinants and protein factors

CircRNAs can originate from introns, intron lariats, exon skipping, or direct backsplicing. Exonic circRNA also can contain retained introns. However, most of the identified circRNAs are intron-free exonic circRNA formed by backsplicing. Backsplicing results in a circRNA formation from a linear precursor, when the splicing reaction involves a downstream splice donor and an upstream splice acceptor of the same pre-mRNA molecule.

Several factors contribute to the backsplicing reaction. One of them is the mRNA sequence determinants (*cis*-factors). One of the first studies on the circRNA biogenesis determinants was the study on *Sry* transcripts discovered in mouse testis (Capel *et al*., 1993). It was shown that the circular RNA isoform represents more than 90% of all *Sry* transcripts, indicating that its formation is favored over that of a linear molecule. The single exon forming the circRNA is flanked by near-perfectly complementary sequences. Therefore, it was hypothesized, that potentially any hybridization between intronic repeat regions within a pre-mRNA molecule could lead to the generation of a circular spliced RNA product. Further research on *Sry* circRNA expression demonstrated that 400 nt inverted repeats flanking the circularizing exon is sufficient for circularization of ectopically expressed *Sry* circRNA (Dubin *et al*., 1995).

Previously, the number of repetitive elements flanking circRNA and their degree of complementarity, as well as the distance between them, were shown to affect the splicing outcome and, therefore, circular to linear product ratios (Zhang *et al*., 2014). Jeck *et al*. (2013) demonstrated enrichment of complementary Alu elements (approximately 300 nt) in circRNA flanking introns. Liang & Wilusz (2014) assayed *ZKSCAN1* (zinc finger protein with KRAB and SCAN domains 1) circRNA formation and its flanking sequence prerequisites. *ZKSCAN1* produces a circRNA from joined exon 2 and 3, which is facilitated by upstream and downstream introns containing one and two Alu elements, respectively. In case of *ZKSCAN1* exons 2 – 3 circularization, 87 nt of an upstream and 59 nt of a downstream intronic flanking sequence are sufficient for circularization.

However, bioinformatic analyses determined that circularizing exons are not always flanked with complementary repeats (Zhang *et al*., 2016). Thus, it can be assumed that there are no

common sequence determinants for all circRNA, except for splice sites (Starke *et al*., 2015). It was found that human circRNAs are spliced through the canonical splicing motif AG–GT in 99% of all validated circRNAs (Vo *et al*., 2019).

In addition to the spliceosomal machinery, several *trans*-factors, namely RNA-binding proteins (RBPs), were found to be involved in circRNA biogenesis (Fig. 1.8). One of them is RNA helicase DHX9, which unwinds dsRNA and recruits ADAR protein, and thus prevents backsplicing (Aktaş *et al*., 2017). ADAR (adenosine deaminase acting on RNA) converts adenosine to inosine in RNA duplexes. Changing an A–U to I–U in a Watson-Crick pair destabilizes the duplex and results in partial unwinding of dsRNA. ADAR knockdown results in overall higher circRNA abundance, confirming its role in circRNA biogenesis (Fig. 1.8B; Rybak-Wolf *et al*., 2015). On the opposite, alternative splicing factor Quaking (QKI) contributes to backsplicing reaction as it binds flanking introns, subsequently forms dimers, thus bringing the splice sites into close proximity (Fig. 1.8C). Conn *et al*. (2015) found hundreds of circRNAs to be regulated by QKI during human epithelial-mesenchymal transition. Removal and addition of QKI binding sites in circRNA flanking introns correspondingly hindered or enhanced circRNA production, suggesting a global role of QKI in circRNA biogenesis. In addition to that, circRNA formation can be regulated by FUS, hnRNP L, and SR proteins (Errichelli *et al*., 2017; Fei *et al*., 2017; Kramer *et al*., 2015).

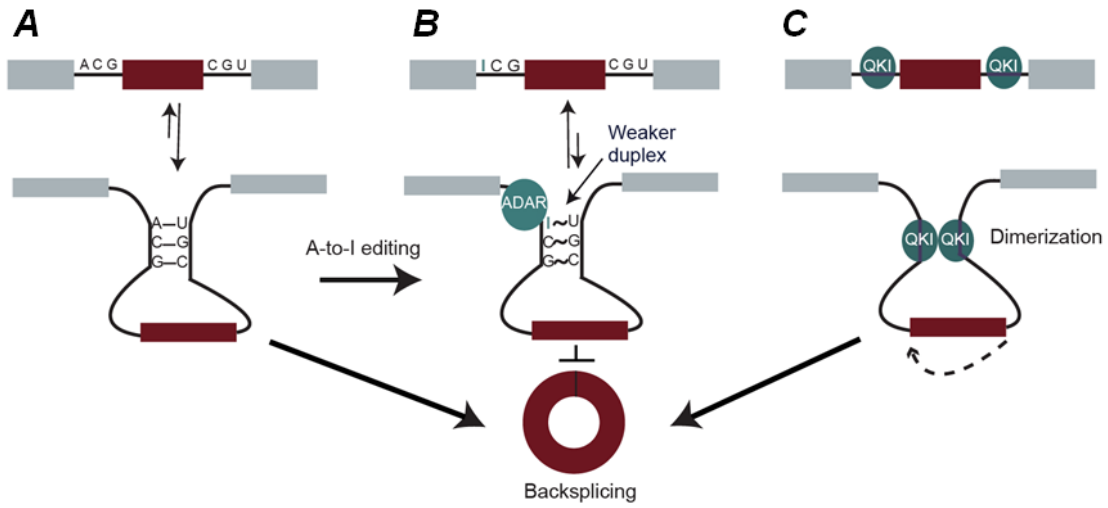

Figure 1.8 Protein factors contribute to backsplicing (adapted from Barrett & Salzman, 2016).
(A) Schematics of circRNA formation. Complementary intronic regions surrounding the circularizing exon base-pair with each other, which supports the circRNA formation.
(B, C) Protein factors impacting the biogenesis of circRNA. When ADAR protein is present, it edits and weakens dsRNA within intronic complementary sequences, which represses RNA circularization ***(B)***. QKI protein binds intronic sequences, forms homodimers and, as a consequence, looping exon which facilitates circRNA formation ***(C)***.

Finally, components of canonical spliceosomal machinery also influence circRNA formation. Both pharmacological inhibition and knockdown of individual spliceosomal components, resulted in higher circRNA levels (Liang *et al*., 2017; Wang *et al*., 2019). One possible

explanation for this is when spliceosomal components are limiting, spliceosome assembles across-exon, according to the exon definition model, often resulting in backsplicing and generation of circRNA (Li *et al*., 2019).

1.8 CircRNA expression systems in human cells

To study the functionality of endogenous circRNAs, as well as to implement artificial circRNAs in cell systems, it is important to establish a reliable circRNA expression system. CircRNA can be prepared *in vitro*, implementing *in vitro* T7 transcription from synthetic DNA oligonucleotides and subsequent chemical or enzymatic RNA ligation (Müller & Appel, 2017; Breuer & Rossbach, 2020). However, different sequences are known to exhibit different circularization efficiency. To stabilize the RNA secondary structure of flanking sequences, a stem region surrounding the circularizing sequence of interest can be introduced, therefore stabilizing the base-pair interactions across an exon. Further, this circRNA can be directly transfected in a desired cell system. Generally, *in vitro* circRNA production is more suitable for shorter RNAs.

Wesselhoeft *et al*. (2018) introduced an *in vitro* circRNA production system based on a vector with group I self-splicing introns [permuted intron-exon (PIE)] from *Anabaena* pre-tRNA. The vector additionally contains homology arms and spacers flanking the circularizing exonic region. After *in vitro* transcription from the PIE vector, circRNA is formed by autocatalytic, enzyme-free ligation. As a result of intermolecular instead of intramolecular reaction, circRNA concatemers can also be formed. Other products of the reaction are flanking introns. The presence of these products generated additionally to the circRNA requires the downstream RNase R treatment and HPLC purification.

An alternative to *in vitro*-produced circRNA is a vector-based system (Tatomer *et al*., 2017). The first vector for transient circRNA expression was based on the ciRS-7 pre-mRNA backbone with the splice sites from the circularizing exon and the endogenous flanking intronic sequences (Hansen *et al*., 2013). Interestingly, circRNA from this vector was expressed only after incorporation of the upstream flanking sequence in an inverted orientation in the downstream intron. This is consistent with the observation that the circRNAs are generated from the exons surrounded by intronic complementary regions. However, low RNA production and inefficient circularization have led to further attempts in the field and the development of a vector based on the human *ZKSCAN1* gene (Liang & Wilusz, 2014). This vector included human *ZKSCAN1* circRNA splice sites surrounded by the intronic regions containing upstream AluSq2 and downstream AluJr and AluSz sequences. Again, the major outcome of splicing appeared to be a linear mRNA.

An interesting alternative to the exonic circRNA vector-based expression systems was presented by Lu *et al*. (2015) and Noto *et al*. (2017). The introduced vector is based on the intron from the *Drosophila* tRNA:Tyr_{GUA} gene. The strategy relies on the excision of the tRNA

intron, which follows by its circularization driven by the endogenous RtcB ligase (RNA 2′,3′-cyclic phosphate and 5′-OH ligase). The transcription in this vector is driven by U6 promoter and additionally boosted by the first 27 nucleotides of U6 snRNA, which promote γ-monomethyl phosphate 5′ capping (Good *et al*., 1997) and enhances the stability of the expressed RNA.

For direct visualization of the expressed circRNA in living cells or in a total RNA sample on a gel, fluorescent RNA aptamers such as Broccoli can be introduced (Lu *et al*., 2015). These aptamers were generated by applying the SELEX strategy, selected based on their ability to bind fluorophores and activate fluorescence. They fold in a highly stable RNA structure and can retain fluorophore molecules. Fluorescent Broccoli aptamer is an improved 49-nt long RNA which activates the fluorescence of DFHBI fluorophore (Filonov *et al*., 2014). Broccoli can be used in mammalian or bacterial live-cell imaging for direct localization of RNA molecules. Moreover, in-gel Broccoli imaging represents an alternative to the Northern blot detection (Filonov *et al*., 2015).

A new level of circRNA expression with almost no detectable linear RNA by-products was achieved with the introduction of ribozymes. The Tornado [Twister-optimized RNA for durable overexpression (Litke & Jaffrey, 2019)] circRNA expression cassette includes the U6 promoter and the Broccoli aptamer flanked by ribozyme combinations of upstream Twister P3 U2A and downstream Twister P1. The naturally occurring Twister ribozyme class discovered by bioinformatic prediction represents one of the fastest classes of ribozymes (Roth *et al*., 2014). Twister ribozymes undergo self-cleavage and produce 5′ hydroxyl and 2′,3′-cyclic phosphate ends, identical to the TSEN-driven pre-tRNA intron excision in tRNA splicing (described below). Similar to the strategy introduced by Lu *et al*. (2015), the circRNA expression cassette contains corresponding tRNA intronic sequences for RNA ligation by the tRNA-specific endogenous RtcB ligase.

1.9 Functions of endogenous circRNAs and their potential application

Although a single unified function of circRNA is still not clear, there are several individual examples of circRNA functionality. Mouse Sry and human CDR1as (ciRS-7) circRNAs have conserved miRNA target sites and act as miRNA sponges. The CDR1as circRNA contains >70 near-perfectly complementary binding sites for sequestration of the miRNA miR-7 (Hansen *et al*., 2013; Memczak *et al*., 2013). In addition to that, CDR1as contains a binding site for miR-671. Opposite to miR-7 binding, miR-671 bound to CDR1as recruits Argonaute 2 (AGO2) and drives CDR1as cleavage (Hansen *et al*., 2013). CDR1as knockout experiments in mice demonstrated significant downregulation of miR-7 and accumulation of miR-671 in several brain parts normally expressing CDR1as, which suggests that CDR1as can act as miRNA sponge for miR-7 storage or delivery, and this mechanism could be controlled by the miR-671 (Piwecka *et al*., 2017). Downregulation of miR-7 can be explained by its binding to

other targets, thereby directing miR-7 degradation in absence of CDR1as (Kleaveland *et al*., 2018). Another example is the mouse Sry circular RNA, which contains 16 binding sites for miR-138 (Hansen *et al*., 2013). Most other circRNAs either present in cells in very low amounts or contain few miRNA-binding sites, which suggests the miRNA sponging as a very unique circRNA function.

Another proposed role of circRNA is a template for protein translation. Yang *et al*. (2017) demonstrated pervasive N6-methyladenosine (m6A)-initiated protein translation from circRNAs in human cells. Two further studies on particular cap-independent protein translation from endogenous circRNAs confirmed the presence of protein but lacked an evidence on protein functionality (Legnini *et al*., 2017; Pamudurti *et al*., 2017). However, this still remains a controversial issue in the circRNA field (reviewed by Schneider & Bindereif, 2017).

Holdt *et al*. (2016) investigated the atheroprotective role of the circRNA *ANRIL* (*circANRIL*) produced from the long non-coding RNA *ANRIL*, which was shown to generate circles along with the linear RNA. Circular *ANRIL* isoform is expressed 10-fold higher than the linear one. The circularizing exons 5-6-7 are surrounded by Alu repeats, which are conserved in primates. *circANRIL* binds PES1 which is a component of the key regulator of 60S ribosome subunit biogenesis, thereby preventing rRNA maturation. Therefore, impaired ribosome biogenesis leads to increased apoptosis and restrains proliferation, which exhibits an atheroprotective effect of *ANRIL* circRNA in human vascular tissues.

Although many circRNAs have been discovered so far, the functions of a majority of them remain unclear. The function of circRNAs may also directly reside in their biogenesis: When backsplicing occurs, the biogenesis of the full-length mRNA is blocked (Ashwal-Fluss *et al*., 2014).

As circRNAs are metabolically stable, they can serve as potential biomarker candidates for a wide range of clinical applications. To estimate the biomarker potential of circRNAs, Memczak *et al*. (2015) studied circRNA detection in human peripheral whole blood, where more than four thousand circRNA candidates were identified by RNA-seq. In addition to that, circRNAs were found to correlate with various human pathologies, such as cardiovascular diseases (Holdt *et al*., 2016) and disorders of the nervous system (Errichelli *et al*., 2017). However, a recent expanding interest to circRNA biomarkers revealed a need for circRNA characterization and standardization of circRNA validation (Pfafenrot & Preußer, 2019).

Only few circRNAs have assigned functions so far. Although, there are examples when knockdown or ectopic expression of certain circRNAs results in specific molecular phenotypes (Garikipati *et al*., 2019; Piwecka *et al*., 2017). To sum up, further research is needed on circRNA functionality.

1.10 Splicing of tRNA

Transfer RNA (tRNA) is an essential component of protein translation. Metazoan pre-tRNA is transcribed by RNA polymerase III, then 5′ leader and 3′ trailer sequences are removed by RNase P and RNase Z, respectively. Some tRNAs also contain an intron which is spliced out by the tRNA splicing endonuclease (TSEN; Paushkin *et al*., 2004). TSEN2 and TSEN34 catalytic components of TSEN complex cleave the 5′ exon-intron and the 3′ intron exon, respectively (Trotta *et al*., 1997), after which tRNA exons are ligated. Among 388 human tRNA genes, 28 were confirmed to contain an intron (7%). The percentage of intron containing tRNA genes is species-specific and reaches over 50% in some cases (Chan & Lowe, 2019; Schmidt & Matera, 2020). If present, tRNA introns are almost always located one nucleotide 3′ to the anticodon.

Pathways of tRNA splicing can be divided into “healing and sealing” and “direct ligation”. In yeast and plants (“healing and sealing”), Rlg1/Trl1 complex phosphorylates the 5′ end of the 3′ exon, opens the 2′,3′-cyclic phosphate on the 5′ exon, ligates the tRNA molecule, and phosphorylates the 5′ end of the intron, leading to its degradation by exonuclease Xrn1. In archaea and metazoans (“direct ligation”), RtcB directly ligates the exons and intron ends, generating tRNA and tRNA intronic circRNA (tricRNA) (Popow *et al*., 2011; reviewed in Popow *et al*., 2012).

The functions of the tRNA introns are still not clear. One rather exeptional example of the tRNA intron functionality is its requirement for a leucine tRNA methylation by the methyltransferase Trm4 in *Schizosaccharomyces pombe* (Müller *et al*., 2019).

1.11 CircRNAs in human platelets

Platelets are produced in bone marrow and are involved in clot formation. Although they lack nuclei, platelets exhibit active RNA metabolism (Denis *et al*., 2005). Platelets and their RNA content are especially interesting for diagnostic purposes as platelets are a major source of extracellular vesicles in blood. Platelets were shown to exhibit high RNA stability and to have high circRNA content (Preußer *et al*., 2018). Among all hematopoietic cells, platelets (together with erythrocytes) contain an unusually high concentration of circRNAs (Nicolet *et al*., 2018), although it remains unclear whether this high circRNA abundance results from the general high RNA stability in platelets, or if they can be produced outside of the nucleus. CircRNA was also shown to be more abundant in differentiated platelets in comparison with their progenitor cells, megakaryocytes (Nicolet *et al*., 2018). However, the role of circRNAs in platelet differentiation has not been determined yet. For some genes, only the circular isoforms were detected to be present in platelets (Alhasan *et al*., 2016). One of them is a circRNA *Plt-circR4*, derived from the third exon of the *Plt-circR4* gene, located on the minus strand (Fig. 1.9; Preußer *et al*., 2018). This circRNA is exclusively expressed in platelets; however, its function still remains unknown. The whole third exon (878 nt) and the

surrounding *Plt-circR4* sequences were identified as the DNA mariner transposon of the *HsMar1* sub-family. These elements mobilize within the host genome by a cut-and-paste mechanism. *HsMar1* encodes a mariner transposase that is flanked by inverted terminal repeats. These repeats are located 140 bp upstream and 195 bp downstream from 5′SS and 3′SS ends of *Plt-circR4* exon 3, respectively. Originally, inverted terminal repeats of the *HsMar1* transposons are involved in its mobility throughout the genome. In the context of circRNA formation, these inverted repeats are unusually short, comprising only 28 nt both up- and downstream, including one mismatch. However, they were shown to play a decisive role in the formation of circRNA *Plt-circR4* (Dr. Christian Preusser, data not published).

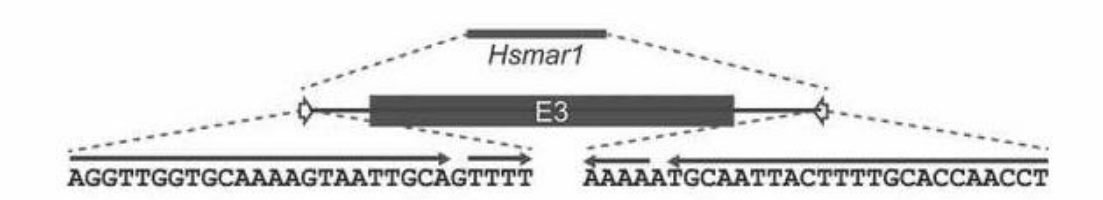

Figure 1.9 Schematic of *Hsmar1* transposon including exon 3 of *Plt-circR4 (*adapted from Preußer *et al*., 2018*).*
The exon-intron structure of *Plt-circR4* genomic locus with the surrounding inverted repeats (arrows) shows exon 3 (E3) and enlarged inverted repeat sequences.

Taken together, these results make the platelet-specific circRNA *Plt-circR4* a suitable model for studying RNA circularization determinants, where unusually short flanking regions may be adapted for developing of alternative circRNA expression vectors.

1.12 Specific aims of this work

In this study, we focus on the design, expression, and functional characterization of artificial circRNAs. First, we tested several circRNA expression constructs based on a platelet-specific *Plt-circR4* circRNA. Next, we focused on tRNA-based, PIE, and Tornado circRNA expression systems. Our main aim was to develop and functionally characterize designer circRNAs. As a model system, we used circRNA targeting hnRNP L, a global alternative splicing regulator. Therefore we cloned sequences with high affinity to hnRNP L into PIE and Tornado vectors and directly transfected or expressed these circRNAs in HeLa cells. Direct *in vivo* hnRNP L/circRNA interactions were captured by RNA immunoprecipitation (RIP), and alternative splicing of hnRNP L target genes was analyzed by RT-PCR.

Many attempts have been made in the field of therapeutic nucleic acids for splicing modulation. To study if circRNAs can be developed into splicing modulators, we designed and produced *in vitro* circRNAs with antisense sequences to various *cis*-elements in the *CD45* pre-mRNA. First, the alternative splicing patterns of *CD45* were analyzed in an ectopic *CD45* minigene expression system in HeLa cells, with the co-transfected *CD45* antisense circRNAs. Second, we tested these circRNAs on endogenous *CD45* in the DG75 B-cell line.

In sum, we tested and characterized several designer artificial circRNAs. Our observations strongly argue for their high potential as a novel class of therapeutic RNAs, to be applied when deregulated RNA-binding proteins cause human disease, or for modulation of aberrant splicing patterns in pathological conditions.

2. Materials

2.1 Chemicals and reagents

Actinomycin D	Sigma-Aldrich
Agarose	Roth
Ammonium persulfate (APS)	BioRad
Blocking reagent	Roche
Boric acid	Roth
Bovine serum albumin (BSA)	Roche
Bromphenol blue	Merck
CDP-Star chemiluminescent substrate	Sigma-Aldrich
Chloroform	Roth
Deoxynucleotide triphosphates (dNTPs)	Peqlab
DFHBI	Sigma-Aldrich
Digoxigenin (DIG) RNA labeling mix	Roche
Dimethyl pyrocarbonate (DMPC)	Sigma-Aldrich
Dulbecco's Modified Eagle's medium (DMEM)	Gibco
Ethanol (EtOH)	Roth
Ethidium bromide	Roth
Ethylenediaminetetraacetic acid (EDTA)	Roth
Fetal bovine serum (FBS)	Gibco
Formaldehyde	Roth
Glycerol	Roth
Glycogen	Peqlab
Hoechst 33342	Sigma-Aldrich
Isopropanol	Roth
Lipofectamine 2000 transfection reagent	Thermo Scientific
Lipofectamine MessengerMax mRNA transfection reagent	Thermo Scientific
Lumi-Light Western blotting substrate	Roche
Magnesium chloride ($MgCl_2$)	Merck
Maleic acid	Roth
Methanol	Roth
Milk powder (fat-free)	Roth
NorthernMax hybridization buffer	Ambion
OptiMEM	Gibco
Phenol/chloroform/isoamylalcohol (25:42:1)	Roth
Phosphate-buffered saline (PBS), X10	Gibco
Potassium chloride (KCl)	Roth

Protein-A/G dynabeads	Thermo Scientific
Rotiphorese gel 30% (37.5:1)	Roth
RPMI medium	Invitrogen
Sodium acetate	Merck
Sodium chloride (NaCl)	Roth
Sodium citrate	Roth
Sodium hydroxide (NaOH)	Roth
Sodium dodecyl sulfate (SDS)	Roth
Super Optimal Broth (SOC) medium	Invitrogen
SYBR Gold solution	Roche
Tetramethylethylenediamine (TEMED)	Biorad
Tris(hydroxymethyl)aminomethane (Tris)	Roth
Trizol reagent	Thermo Scientific
TRIzol-LC	Ambion
Trypsin EDTA solution	Gibco
Tryptone	Roth
TurboFect *in vitro* transfection reagent	Thermo Scientific
Tween 20	Sigma-Aldrich
Urea	Roth
Yeast extract	Roth
Yeast tRNA	Roche
β-mercaptoethanol	Sigma-Aldrich

2.2 Kits

Bioanalyzer Nano RNA chip kit	Agilent
Bioanalyzer Small RNA chip kit	Agilent
DIG-detection system	Roche
Gel extraction kit	QIAGEN
HiScribe T7 High Yield RNA synthesis kit	New England Biolabs
Luna qPCR reaction mix	New England Biolabs
Monarch RNA cleanup kit	New England Biolabs
NE-PER nuclear and cytoplasmic extraction reagents	Thermo Scientific
Norgen total RNA purification kit	Norgen Biotek
Nucleofector™ kit V	Lonza
Plasmid Maxi kit	QIAGEN
QIAprep Spin Miniprep kit	QIAGEN
QIAquick gel extraction kit	QIAGEN
qScript cDNA synthesis kit	Quantabio

qScript Flex cDNA kit	Quantabio
Qubit quantification assay kit, RNA BR	Thermo Scientific
Quick Spin RNA columns	Roche
RNeasy Mini kit	QIAGEN

2.3 Enzymes

*Afl*II	New England Biolabs
*Apa*I	New England Biolabs
*Bam*HI-HF	New England Biolabs
*Bgl*II	New England Biolabs
*Hin*dIII-HF	New England Biolabs
*Nhe*I-HF	New England Biolabs
*Not*I-HF	New England Biolabs
RNase R	Epicenter
RNaseOUT	Thermo Scientific
RQ1 DNase	Promega
*Sac*II	New England Biolabs
T4 DNA Ligase	New England Biolabs
T4 RNA Ligase	New England Biolabs
Taq polymerase	Purified by Silke Schreiner
TURBO DNase	Invitrogen
*Xba*I-HF	New England Biolabs
*Xho*I	New England Biolabs

2.4 Antibodies

Anti-Digoxigenin-AP Fab coupled to alkaline phosphatase	Roche
Anti-FLAG monoclonal antibody	Sigma-Aldrich
Anti-GAPDH monoclonal antibody 71.1	Sigma-Aldrich
Anti-hnRNP L monoclonal antibody 4D11	Sigma-Aldrich
Anti-IGF2 (IMP3) polyclonal antibody 3199196	Millipore
Anti-Mouse IgG peroxidase antibody	Sigma-Aldrich
Anti-Rabbit IgG peroxidase antibody	Sigma-Aldrich

2.5 Plasmids

Plt-circR4

Plt-circR4-exp

Plt-circR4-control

Plt-circR4-X3-control

Plt-circR4-X5-control

Plt-circR4-X10-control

tricRNA

Broccoli tricRNA

CA-SELEX tricRNA

PIE

pcDNA3-PIE-circ

PIE-CA-SELEX X4

PIE-CA-SELEX X8

PIE-CA-SELEX X16

PIE-CA-SELEX X32

PIE-$(CA)_{100}$

PIE-control

Tornado

pAV-U6+27-Tornado-Broccoli (control Broccoli)

Tornado $(CA)_{20}$

Tornado CA-SELEX X2

Tornado CA-SELEX X4

pAV-U6+27-Tornado-F30-Broccoli

Tornado CA-SELEX X4 Broccoli

Tornado $(CA)_{100}$ Broccoli

Tornado control Broccoli (control)

CD45

CD45 2/3-4-5-6-7 minigene

2.6 Molecular weight markers

DNA DIG-labeled Molecular Weight Marker VIII	Roche
GeneRuler DNA Ladder Mix	Thermo Scientific
GeneRuler Low Range (LR) DNA Ladder	Thermo Scientific
Riboruler High/Low Range (HR/LR) RNA Ladder	Thermo Scientific
PeqGOLD Protein-Marker IV	Peqlab

2.7 Laboratory equipment

Agfa Curix 60 processing machine (developing machine)	AGFA
ÄKTApurifier	GE Healthcare
Axio Observer Z1 fluorescence microscope	Zeiss
Bioanalyzer 2100	Agilent
BLX 254 UV-crosslinker	Biolink
Centrifuge 5424	Eppendorf

Excella Eco-170 CO_2 incubator	New Brunswick Scientific
G:Box gel documentation	Syngene
HB-1000 hybridization oven	UVP
Heraeus Multifuge X1R centrifuge	Thermo Scientific
InLab Expert Pro-ISM pH meter	Mettler Toledo
INTAS Imager Transilluminator ChemiDoc MP	Bio-Rad
Micropipettors (0.5 µl to 1000 µl)	Eppendorf, Gilson
Mini PROTEAN electrophoresis system	Biorad
Moxi Z Mini automated cell counter	ORFLO Technologies
NanoDrop 1000 spectrophotometer	Thermo Scientific
Nucleofector™ 2b device	Lonza
Pipetus pipet filler	Hirschmann
Qubit 2.0 fluorometer	Invitrogen
Realplex Mastercycler (thermocycler)	Eppendorf
Subcell GT agarose gel system	BioRad
SureBeads magnetic rack	BioRad
Systec DB-23 autoclave	Systec
Thermo Scientific Safe 2020 (laminar flow)	Thermo Scientific
Thermomixer L057	Kisker
TMS inverted phase contrast microscope	Nikon
Trans-Blot semi-dry transfer cell	BioRad
Trans-Blot Turbo transfer system	BioRad
Veriti thermal cycler	Applied Biosystems
Vortex-Genie2	Scientific Industries

2.8 Consumables

Culture bottles with filter (75 cm^2)	Greiner Bio-One
Cell culture dishes 100 X 20 mm	Sarstedt
Cell culture plates (6, 12, 24 wells)	Sarstedt
Chemiluminescent detection films	GE Healthcare
Eppendorf tubes (1.5 ml, 2 ml; Safe Lock)	Sarstedt
Falcon tubes (15 ml, 50 ml)	Sarstedt
Multiply PCR strips and lids	Sarstedt
Phase lock gel tubes	5Prime
Pipette tips (10, 20, 2000, 1250 ml)	Sarstedt
qPCR Seal optical clear films	VWR
qPCR semi-skirted plates	VWR
Sterile serological pipettes (5, 10, 25, 50 ml)	Greiner

2.9 Oligonucleotides

Table 2.1 RNA-oligonucleotides. The siRNAs were obtained from Sigma-Aldrich.

siRNA oligonucleotides	
human hnRNPL 3′ UTR 1581	GACAUUUCUCUUUCCUUUATT
luciferase GL2	CGUACGCGGAAUACUUCGATT

Table 2.2 DNA-oligonucleotides. Desalted dry oligonucleotides were chemically synthesized (Sigma-Aldrich). All the oligonucleotides given represent the sequence from 5′ to 3′ end.

Real-time PCR primers	
Housekeeping genes	
ACTB fwd	GTGGAACGGTGAAGGTGACA
ACTB rev	GGGACTTCCTGTAACAACGCA
GAPDH fwd	TGCACCACCAACTGCTTAGC
GAPDH rev	GGCATGGACTGTGGTCATGAG
snoRD U78 fwd	GTGTAATGATGTTGATCAAATGT
snoRD U78 rev	TTCTTCAGTGTTACCTTTGTCTA
U6 fwd	CTCGCTTCGGCAGCACATA
U6 rev	GCTTCACGAATTTGCGTGTCA
Plt-circR4	
circ control fwd	GGAGGTGACAACATGGAGGG
circ control rev	CCGGCTGCCAACATAATCTGC
precursor control fwd	GGAGGTGACAACATGGAGGG
precursor BGH rev	AGGAAAGGACAGTGGGAGTG
Tornado	
$(CA)_{20}$ circ fwd	TCGGCGTGGACTGTAGAAC
$(CA)_{20}$ circ rev	TGTGTGTGTGTGTGGCGG
$(CA)_{100}$ Broccoli circ fwd	GGTCGGCGTGGACTGTAG
$(CA)_{100}$ Broccoli circ rev	GATACGAATATCTGGACCCGACCGTC
CA-SELEX X2 circ fwd	TCGGCGTGGACTGTAGAAC
CA-SELEX X2 circ rev	CATGTATGCGGCCGCACT
CA-SELEX X4 circ fwd	CAAGATGTGGCCGCGGTC
CA-SELEX X4 circ rev	ATGTATGGATCCGCGGCCG
CA-SELEX X4 Broccoli circ fwd	GGTCGGCGTGGACTGTAG
CA-SELEX X4 Broccoli circ rev	GATACGAATATCTGGACCCGACCGTC
control Broccoli circ fwd	GGTCGGCGTGGACTGTAG
control Broccoli circ rev	GATACGAATATCTGGACCCGACCGTC
CD45	
CD45 total (ex7) fwd	TGCCTACCTTAATGCCTCTGA
CD45 total (ex7) rev	TGGTTGAAATGACAGCGCTT

RT-PCR primers

Housekeeping and other endogenous genes

ACTB fwd	TGGACTTCGAGCAAGAGATG
ACTB rev	GTGATCTCCTTCTGCATCCTG
CAMSAP1 circ fwd	CCCTGATGATGGCCTACACT
CAMSAP1 circ rev	TGTGCTCCTGCTCATACTGG
CAMSAP1 lin rev	GGACCTTTTGATGAGCTGGA
CAMSAP1 circ fwd	CCCTGATGATGGCCTACACT
IFN-1β fwd	TGGGAGGATTCTGCATTACC
IFN-1β rev	CAGCATCTGCTGGTTGAAGA
GAPDH fwd	GAGTCAACGGATTTGTGCGT
GAPDH rev	GATCTCGCTCCTGGAAGATG
PKR fwd	AGCGAACAAGGAGTAAGGGA
PKR rev	AGCAAGAATTAGCCCCAAAGC
snoRD U78 fwd	GTGTAATGATGTTGATCAAATGT
snoRD U78 rev	TTCTTCAGTGTTACCTTTGTCTA
U1 fwd	GCGAGGCTTATCCATTGCAC
U1 rev	GCAGTCCCCCACTACCACAA
U6 fwd	CTCGCTTCGGCAGCACATA
U6 rev	GCTTCACGAATTTGCGTGTCA

Plt-circR4

circ control fwd	GGAGGTGACAACATGGAGGG
circ control rev	CCGGCTGCCAACATAATCTGC
precursor control fwd	GGAGGTGACAACATGGAGGG
precursor BGH rev	AGGAAAGGACAGTGGGAGTG

tricRNA

tricRNA Broccoli divergent fwd	GTCGAGTAGAGTGTGGGCTCGT
tricRNA Broccoli divergent rev	GATACGAATATCTGGACCCGACCGTC
tricRNA Broccoli prec fwd	CCTTCGATAGCTCAGTTGGT
tricRNA Broccoli prec divergent rev	GATACGAATATCTGGACCCGACCGTC

PIE

$(CA)_{100}$ circ fwd	CACACACACAAGATCCACTA
$(CA)_{100}$ circ rev	TGTGTGTGTGTGGATCCTCT
CA-SELEX circ fwd	CACACGCAAGATCTCGAGAA
CA-SELEX circ rev	TGAACCCACACGACCGTTTA
control circ fwd	AGGATTGAGGATCGTTTCGCA
control circ rev	CGGACTGGCTTTCTACGTGT

Tornado

$(CA)_{20}$ circ fwd	TCGGCGTGGACTGTAGAAC
$(CA)_{20}$ circ rev	TGTGTGTGTGTGTGGCGG
$(CA)_{100}$ Broccoli circ fwd	GGTCGGCGTGGACTGTAG

$(CA)_{100}$ Broccoli circ rev	GATACGAATATCTGGACCCGACCGTC
CA-SELEX X2 circ fwd	TCGGCGTGGACTGTAGAAC
CA-SELEX X2 circ rev	CATGTATGCGGCCGCACT
CA-SELEX X4 circ fwd	CAAGATGTGGCCGCGGTC
CA-SELEX X4 circ rev	ATGTATGGATCCGCGGCCG
CA-SELEX X4 Broccoli circ fwd	GGTCGGCGTGGACTGTAG
CA-SELEX X4 Broccoli circ rev	GATACGAATATCTGGACCCGACCGTC
control Broccoli circ fwd	GGTCGGCGTGGACTGTAG
control Broccoli circ rev	GATACGAATATCTGGACCCGACCGTC
control circ fwd	AGGATGAGGATCGTTTCGCA
control circ rev	CGGACTGGCTTTCTACGTGT

hnRNP L alternative splicing targets

ARGBP2 fwd	CTTGGAGATCTTACAATGATGGC
ARGBP rev	GTTTCCATTCACTGTTATCTGGC
BPTF (FALZ) fwd	TCATCAAACCTTTGCTACATGG
BPTF (FALZ) rev	CTGACTGGTACCTGTACTTGATG
CC2D2A fwd	CCAGGGAAAGAGGTAGAAAGGAC
CC2D2A rev	GTCCTCGGCATCATCACCAT
C5orf42 fwd	CAGTTCCATCGTCTGCAGAGT
C5orf42 rev	CTTGCAGCCGTTTCCACAAT
CARS2 fwd	CTGCTGTGTTTGGTGCCATC
CARS2 rev	TCCACCACACCATGCAAGG
DAF fwd	TCCCACCAACAGTTCAGAAAC
DAF rev	GTCCTGGAAACAGGTGTACTCC
HMMR fwd	AGATACTACCTTGCCTGCTTCA
HMMR rev	GCCTTGCTTCCATCTTTTCCA
DLG1 fwd	GCATTGCTGGAGGTGTTGGA
DLG1 rev	TGGTGATATCAGGTGGTGCA
GPBP1 fwd	TCCTGAGTATGAGAGAGAACCAA
GPBP1 rev	TCTTAACTGGCTGTGACGGA
PAPOLA fwd	GAGTCAAGAGGACATCCTCACC
PAPOLA rev	AGAGGCCAACAGAGAAGCC
PPP3CB fwd	AGTGGAGTGTTAGCTGGAGGA
PPP3CB rev	CCGAGGTGGCATTCTCTCAT
RIF1 fwd	TCCATACCATGCCCAACAGA
RIF1 rev	GAGTTGTCCCAGGCCTCTTG
TJP1 fwd	ATATCCTCCTTACTCACCACAAG
TJP2 rev	TTCAAAACATGGTTCTGCCTC
WHSC1 fwd	TTCCACGGCAGCATCTTCAG
WHSC1 rev	AGTCACTCCTCGCTCAGACT

CD45

CD45 ex2/3 fwd	GGCAAAGCCCAACACCTTCCCCCACTG
CD45 ex7 rev	GGGCTCAGAGTGGTTGTTTC
CD45 ex2/3 fwd (for circRNA Ex7)	AGAAGTATTTGTGACAGGGCA
CD45 ex7 rev (for circRNA Ex7)	TGAAATGACAGCGCTTCCAG
CD45 ex5 rev	GAAGGTGAGGCGTCTGTACT

CD45 ex5 fwd	AGTACAGACGCCTCACCTTC
CD45 ex9 rev	CTGAAACTTTTCAACCCCTGGTGGCAC
circRNA Ex4 ESS fw	GCAGTGGTGTGAGTAGGCTT
circRNA Ex4 ESS rev	CCCGCAAGCACCTTTGAG
circRNA Ex5 fw	GTGGGAAGGTGAGGCTTACA
circRNA Ex5 rev	CCTCTGCGCTTACTCCCTAC

Short-living mRNAs (actinomycin D-experiment)

FOXO3 fwd	GACAAACGGCTCACTCTGTC
FOXO3 rev	AGTTCCCTCATTCTGGACCC
MYC fwd	GCTGCTTAGACGCTGGATTT
MYC rev	CTCCTCCTCGTCGCAGTAG
ZNF260 fwd	GCCATGGTCGTCTTTGTCTG
ZNF260 rev	GGAACAAAGCAGCATCCCAA

Cloning primers

Plt-circR4

5 repeats downstream fwd	ATAGCGGCCGCAGGATGTGTTTGAGCCTAGTC
5 repeats downstream rev	AGGAAAGGACAGTGGGAGTG
5 repeats upstream fwd	AGTCTTAAGAGACCCAAGCTGGCTAGC
5 repeats upstream rev	CCGGCTGCCAACATAATCTGC

Oligonucleotides for cloning

Plt-circR4

2X upstream repeat fwd	CTGGCTAGCAGGTTGGTGCAAAAGTAATTGCAGTTTTTAG GTTGGTGCAAAAGTAATTGCAGTTTTTGCTAGCCTG
2X upstream repeat rev	CAGGCTAGCAAAAACTGCAATTACTTTTGCACCAACCTAA AAACTGCAATTACTTTTGCACCAACCTGCTAGCCAG
2X downstream repeat fwd	TAAGGGCCCAAAAATGCAATTACTTTTGCACCAACCTAAA AATGCAATTACTTTTGCACCAACCTGGGCCCGTT
2X downstream repeat rev	AACGGGCCCAGGTTGGTGCAAAAGTAATTGCATTTTTAGG TTGGTGCAAAAGTAATTGCATTTTTGGGCCCTTA
4X upstream repeat fwd	CTGGCTAGCCGCGGAGGTTGGTGCAAAAGTAATTGCAGT TTTTAGGTTGGTGCAAAAGTAATTGCAGTTTTTAGGTTGGT GCAAAAGTAATTGCAGTTTTTAGGTTGGTGCAAAAGTA
4X upstream repeats rev	CAGGCTAGCGGTACCAAAAACTGCAATTACTTTTGCACCA ACCTAAAAACTGCAATTACTTTTGCACCAACCTAAAAACTG CAATTACTTTTGCACCAACCTAAAAACTGCAATTAC
4X downstream repeats fwd	TAAGGGCCCCCTGCAGGAAAAATGCAATTACTTTTGCACC AACCTAAAAATGCAATTACTTTTGCACCAACCTAAAAATGC AATTACTTTTGCACCAACCTAAAAATGCAATTAC
4X downstream repeats rev	AACGGGCCCGCGGCCGCAGGTTGGTGCAAAAGTAATTGC ATTTTTAGGTTGGTGCAAAAGTAATTGCATTTTTAGGTTGG TGCAAAAGTAATTGCATTTTTAGGTTGGTGCAAAAG

tricRNA

CA-SELEX51 SacII fwd	GGATACATGACACACACACGCAGTGGCCGC
CA-SELEX51 SacII rev	GGCCACTGCGTGTGTGTGTCATGTATCCGC

PIE

CA-SELEX X4 in PIE fwd	TGAGGATCCATACATGACACACACACGCAATATATACATG ACACACACACGCAATATATACATGACACACACACGCAATA TATACATGACACACACACGCAAGATCTCGAGCTAA
CA-SELEX X4 in PIE rev	TTAGCTCGAGATCTTGCGTGTGTGTGTCATGTATATATTG CGTGTGTGTGTCATGTATATATTGCGTGTGTGTGTCATGT ATATATTGCGTGTGTGTGTCATGTATGGATCCTCA

Tornado

CA-SELEX X4 fwd	GGCCGCGGATCCATACATGACACACACACGCAATATATA CATGACACACACACGCAATATATACATGACACACACACGC AATATATACATGACACACACACGCAAGATGTGGCCGC
CA-SELEX X4 rev	GGCCACATCTTGCGTGTGTGTGTCATGTATATATTGCGT GTGTGTGTCATGTATATATTGCGTGTGTGTGTCATGTATA TATTGCGTGTGTGTGTCATGTATGGATCCGC
CA-SELEX X4 Broccoli fwd	ATGATGGGTCCCAGAGGATCCATACATGACACACACAC GCAATATATACATGACACACACACGCAATATATACATGAC ACACACACGCAATATATACATGACACACACACGCAAGAT CTCGAGAAGGGTCCCATCATT
CA-SELEX X4 Broccoli rev	AATGATGGGACCCTTCTCGAGATCTTGCGTGTGTGTGTC ATGTATATATTGCGTGTGTGTGTCATGTATATATTGCGTG TGTGTGTCATGTATATATTGCGTGTGTGTGTCATGTATG GATCCTCTGGGACCCATCAT
CA-SELEX X2 fwd	GGCCGCATACATGACACACACACGCAATACATGACACAC ACACACACGCAGTCGCCGC
CA-SELEX X2 rev	GGCCACTGCGTGTGTGTGTCATGTATTGCGTGTGTGTGT CATGTATGC
$(CA)_{20}$ fwd	GGCCGCCACACACACACACACACACACACACACACACA CACACACAGT
$(CA)_{20}$ rev	GGCCACTGTGTGTGTGTGTGTGTGTGTGTGTGTGTGT GTGTGTGGC

Oligonucleotide templates for preparation of antisense circRNA

CD45

Ex4 3'SS 30 OR fwd	TAATACGACTCACTATAGGGAGTAAGCTTGCTGTAGTCA ATCCTGTTAATTAATGGAAAAGCTTACAGTA
Ex4 3'SS 30 OR rev	TACTGTAAGCTTTTCCATTAATTAACAGGATTGACTACAG CAAGCTTACTCCCTATAGTGAGTCGTATTA
Ex4 ESS 30 OR fwd	TAATACGACTCACTATAGGGAGTAAGCGGTGCTTGCGGG TGAGAATGCAGTGGTGTGGCTTACAGTA
Ex4 ESS 30 OR rev	TACTGTAAGCCACACCACTGCATTCTCACCCGCAAGCACC GCTTACTCCCTATAGTGAGTCGTATTA
Intr4 30 OR fwd	TAATACGACTCACTATAGGGAGTAAGCCATCAGTCTTCCC CCACTGGAGATGAATAAGCTTACAGTA
Intr4 30 OR rev	TACTGTAAGCTTATTCATCTCCAGTGGGGGAAGACTGATG GCTTACTCCCTATAGTGAGTCGTATTA
Scrambled 30 OR fwd	TAATACGACTCACTATAGGGAGTAAGCGTGCGGCATGAA GTGGCGGTTGAGGTGTGTGCTTACAGTA
Scrambled 30 OR rev	TACTGTAAGCACACACCTCAACCGCCACTTCATGCCGCAC GCTTACTCCCTATAGTGAGTCGTATTA
Ex4 3'SS 40 OR fwd	TAATACGACTCACTATAGGGAGTAAGCCATCTTTGCTGTA GTCAATCCTGTTAATTAATGGAAAATGGCTTACAGTA

Ex4 3'SS 40 OR rev	TACTGTAAGCCATTTTCCATTAATTAACAGGATTGACTACA GCAAAGATGGCTTACTCCCTATAGTGAGTCGTATTA
Ex4 ESS 40 OR fwd	TAATACGACTCACTATAGGGAGTAAGCTCAAAGGTGCTTG CGGGTGAGAATGCAGTGGTGTGAGTAGGCTTACAGTA
Ex4 ESS 40 OR rev	TACTGTAAGCCTACTCACACCACTGCATTCTCACCCGCAA GCACCTTTGAGCTTACTCCCTATAGTGAGTCGTATTA
Ex4 5'SS 40 OR fwd	TAATACGACTCACTATAGGGAGTAAGCAACAACTTTTGTG TGCCAACCTGTGGTATTAAAAGCACTAGCTTACAGTA
Ex4 5'SS 40 OR rev	TACTGTAAGCTAGTGCTTTTAATACCACAGGTTGGCACAC AAAAGTTGTTGCTTACTCCCTATAGTGAGTCGTATTA
Intr4 40 OR fwd	TAATACGACTCACTATAGGGAGTAAGCGAGATCATTACAT CAGTCTTCCCCCACTGGAGATGAATAAGCTTACAGTA
Intr4 40 OR rev	TACTGTAAGCTTATTCATCTCCAGTGGGGGAAGACTGATG TAATGATCTCGCTTACTCCCTATAGTGAGTCGTATTA
Ex6 ESS 40 OR fwd	TAATACGACTCACTATAGGGAGTAAGCAACTGGGTCTGTA GGAAAGGTGCTGGCTGTACTCCTCTCTGCTTACAGTA
Ex6 ESS 40 OR rev	TACTGTAAGCAGAGAGGAGTACAGCCAGCACCTTTCCTAC AGACCCAGTTGCTTACTCCCTATAGTGAGTCGTATTA
Scrambled 40 OR fwd	TAATACGACTCACTATAGGGAGTAAGCCGGTGAGGTGGA TATTAACGGTGGCAAGGTCATGTGAGGTGCTTACAGTA
Scrambled 40 OR rev	TACTGTAAGCACCTCACATGACCTTGCCACCGTTAATATC CACCTCACCGGCTTACTCCCTATAGTGAGTCGTATTA
Ex5 40 OR fwd	TAATACGACTCACTATAGGGAGTAAGCGCAGAGGGCGTC TGCGAGTCTGCGTGCGTGGGAAGGTGAGGCTTACAGTA
Ex5 40 OR rev	TACTGTAAGCCTCACCTTCCCACGCACGCAGACTCGCAG ACGCCCTCTGCGCTTACTCCCTATAGTGAGTCGTATTA
Ex7 40 OR fwd	TAATACGACTCACTATAGGGAGTAAGCGGGCTCAGAGTG GTTGTTTCAGAGGCATTAAGGTAGGCATGCTTACAGTA
Ex7 40 OR rev	TACTGTAAGCATGCCTACCTTAATGCCTCTGAAACAACCA CTCTGAGCCCGCTTACTCCCTATAGTGAGTCGTATTA

Oligonucleotides for circRNA qPCR standards (absolute quantification)

Tornado

T7 OR CA-SELEX X4 Broccoli fwd	TAATACGACTCACTATAGGGAGTAAGCAACCATGCCGAGT GCGGCCGCTTGCCCGGAGACGGTCGGGTCCAGATATTC GTATCTGTGGCCGCGGTCGGCGTGGACTGTAGGCTTACA GTA
T7 OR CA-SELEX X4 Broccoli rev	TACTGTAAGCCTACAGTCCACGCCGACCGCGGCCACAGA TACGAATATCTGGACCCGACCGTCTCCGGGCAAGCGGCC GCACTCGGCATGGTTGCTTACTCCCTATAGTGAGTCGTAT TA
T7 OR CA-SELEX X4 fwd	TAATACGACTCACTATAGGGAGTAAGCAACCATGCCGAG TGCGGCCGCGGATCCATACATGCAAGATGTGGCCGCGG TCGGCGTGGACTGTAGGCTTACAGTA
T7 OR CA-SELEX X4 rev	TACTGTAAGCCTACAGTCCACGCCGACCGCGGCCACATC TTGCATGTATGGATCCGCGGCCGCACTCGGCATGGTTGC TTACTCCCTATAGTGAGTCGTATTA

Oligonucleotides for Northern blot riboprobe

tricRNA

Riboprobe CA-SELEX fwd	GGCTCGTGGCCGCGGATACATGACACACACACGCAGTG GCCGCGGTGTTGAAAGTGCGGCCGCGAGACGGTCGGGT CCAGATATTCGTATCTGTCGAGTACCCTATAGTGAGTCGT ATTA
Riboprobe CA-SELEX rev	TAATACGACTCACTATAGGGTACTCGACAGATACGAATAT CTGGACCCGACCGTCTCGCGGCCGCACTTTCAACACCGC GGCCACTGCGTGTGTGTGTCATGTATCCGCGGCCACGAG CC

**OR* – stem sequence from Jost *et al.* (2018)

3. Methods

3.1 DNA cloning in *E. coli*

For cloning of DNA fragments in plasmids, both were digested with the corresponding restriction enzymes purchased from New England Biolabs, according to the manufacturer's instructions. After digestion, linearized plasmid and the insert were checked on 1% and 2% agarose gels, respectively. Digested DNA was either gel-purified with the QIAquick gel extraction kit (QIAGEN), or purified directly from the digestion reaction with the PB buffer from the QIAprep spin miniprep kit (QIAGEN) and the columns, PE and EB buffers from the QIAquick gel extraction kit. Purified plasmid and the insert were ligated in molar ratios of 1:5 and 1:10 in the total volume of 20 µl. The reaction was performed overnight at 16°C using T4 DNA ligase (New England Biolabs), according to the manufacturer's instructions. Afterwards, the chemically competent KRX *E. coli* cells were transformed with the ligated plasmid DNA, namely 5 µl of the ligation reaction was added to 50 µl of cells and subjected to heat shock at 42°C for 20 sec. Then the cells were grown in 200 µl of SOC medium (Invitrogen) at 37°C on shaker for 1 h. Afterwards, the cells were plated on LB-agar plates supplemented with 100 µg/ml ampicillin. The plates were incubated overnight at 37°C. Single colonies were picked and grown in 3 ml of LB medium (1% tryptone, 0.5% yeast extract, and 1% NaCl) with 100 µg/ml ampicillin. Plasmid clones were isolated with the QIAprep spin miniprep kit and analyzed by the test digestion with the restriction enzymes. After visualizing the test digestions on an agarose gel, the plasmid DNA sequences from positive clones were verified by Sanger sequencing (Microsynth Seqlab). Both DNA strands were checked with corresponding forward and reverse primers, respectively. In order to obtain the plasmids in preparative quantities, KRX *E. coli* cells were transformed with positive clone plasmids and grown overnight at 37°C in 50 ml LB medium. Then, the plasmids were isolated with the Plasmid Maxi kit (QIAGEN). For working with plasmid sequences, SnapGene Viewer 5.0.7 software was used.

3.2 Design of circRNA and cloning of circRNA expression constructs

3.2.1 Use of platelet-derived sequence elements for circRNA expression

To generate a vector for robust circRNA expression, a *Plt-circR4*-derived backbone was used. The primary vector Plt-circR4-exp with one pair of short inverted repeats (2X29 nts) and splice sites was cloned by Marie Mosbach via introduction of *Plt-circR4* introns in pCDNA3.1(+) vector (Fig. 4.1A). The inserts containing two additional inverted upstream and downstream repeats, as well as the overhangs of corresponding restriction sites, were chemically synthesized (Table 2.2), annealed, and cloned into the *Nhe*I and *Apa*I sites, respectively. Both restriction sites are located in close proximity to the original inverted repeats, upstream and downstream from the splice sites. The vector with three pairs of inverted repeats Plt-circR4-X3 was subsequently used for incorporation of the intronic

hnRNP L CA-rich control sequence (339 nts) using *Hin*dIII and *Bam*HI sites of this vector, located between the splice sites, forming Plt-circR4-X3-control. This sequence was cut from the Plt-circR4-control vector provided by Silke Schreiner and was used here as a test sequence. Plt-circR4-X5-control containing five pairs of inverted repeats was generated by incorporation of synthetic annealed oligonucleotides containing additional four inverted repeats in upstream and downstream (*Nhe*I and *Apa*I restriction sites, respectively) of the original vector Plt-circR4-control. Plt-circR4-X10-control comprising 10 pairs of the original inverted repeats was generated by PCR-amplification of 5 inverted repeat sequences from Plt-circR4-X5-control with primers, incorporating additional restriction enzyme recognition sites. Upstream and downstream inverted repeats were cloned into Plt-circR4-X5-control using *Afl*II *and Not*I restriction sites, respectively.

3.2.2 Expression of CA-SELEX sequence in tRNA intronic circular (tric)RNA

pAV-U6+27-pTRIC-Y-Broccoli vector comprised of the tRNA:Tyr_{GUA} (*Drosophila melanogaster*) exons, splice sites, and Broccoli aptamer placed in tRNA intron was generously provided by the laboratory of Prof. Gregory Matera (Lu *et al*., 2015). The CA-rich SELEX#51 sequence (5′-AUACAUGACACACACACGCA-3′) with high affinity to hnRNP L (K_D 7.2 nM) was previously validated as a high-affinity target sequence of hnRNP L (Hui *et al*., 2005). The CA-SELEX insert was incorporated in the vector as the annealed chemically synthesized oligonucleotides flanked with *Sac*II restriction sites. For oligonucleotide sequences, see Table 2.2. CA-SELEX sequence was inserted into *Sac*II-linearized pAV-U6+27-pTRIC-Y-Broccoli (Broccoli tricRNA) plasmid forming a *CA-SELEX* tricRNA (tRNA intronic circRNA) construct, which produces the circRNA of 107 nt in length.

3.2.3 *In vitro* circRNA production by permuted intron-exon splicing strategy

The permuted intron-exon (PIE) backbone (Wesselhoeft *et al*., 2018) was ordered from GeneArt (Thermo Scientific) and cloned into pcDNA3 vector. The resulting pcDNA3-PIE-circ vector contains T7 promoter for *in vitro* transcription, group I self-splicing introns from *Anabaena*, spacers facilitating splicing efficiency, and two short exon fragments. Upon transcription, autocatalytic introns lead to the formation of a direct exon-exon junction, generating circRNA. To clone the construct with four 20 bp CA-rich SELEX sequences, the chemically synthesized oligonucleotides (Table 2.2) were designed containing ATAT linkers (separating the CA-SELEX sequences) and corresponding restriction sites: *Bam*HI at the 5′-end, *Bgl*II and *Xho*I at the 3′-end. The insert was cloned into the pcDNA3-PEI-circ plasmid using *Bam*HI and *Xho*I restriction sites generating a PIE-CA-SELEX X4 vector.

*Bam*HI-HF and *Bgl*II restriction sites forming compatible cohesive ends were used for the next rounds of cloning for the incorporation of additional CA-SELEX sequences. PIE-CA-SELEX X8 was generated by cloning CA-SELEX X4 insert cut with *Bam*HI-HF and *Bgl*II into

the PIE-CA-SELEX X4 vector linearized with *Bam*HI-HF. The PIE-CA-SELEX X16 and pcDNA3-PIE-CA-SELEX X32 vectors were generated using the same cloning strategy, incorporating CA-SELEX X8 and CA-SELEX X16 inserts, respectively. The PIE-CA-SELEX X4, X8, X16, and X32 constructs produce circRNAs of 256, 354, 550, and 942 nts, respectively. The negative control construct includes the 339-bp-long sequence (Rossbach *et al*., 2009), derived from vector sequences, and produces a circRNA of 484 nts. Positive control construct PIE-$(CA)_{100}$, which contains ~100 CA-dinucleotide repeats, was produced by ligation of short CA-repeat sequences joined by *Bam*HI-*Bgl*II linkers. The resulting circRNA $(CA)_{100}$ is 365 nts in length. Both control constructs were cloned by Silke Schreiner.
PIE plasmids were linearized with *Xba*I-HF restriction enzyme and purified with the QIAquick gel extraction kit. PIE circRNA was prepared as described in Wesselhoeft *et al*. (2018). CircRNA precursors were synthesized by run-off *in vitro* transcription using the HiScribe T7 High Yield RNA synthesis kit (New England Biolabs). Plasmid DNA was digested with RQ1 DNase (Promega). Transcribed RNA was column-purified with the Monarch RNA cleanup kit (New England Biolabs). For circularization reactions, samples were supplemented with T4 RNA ligase buffer (New England Biolabs) and GTP to a final concentration of 2 mM. The reaction was heated at 55°C for 8 min and column-purified. Circularization efficiency was assessed on precast 2% agarose E-Gel (Invitrogen). CircRNAs were enriched by RNase R digestion, where 1 U of RNase R (Epicentre) was used for the digestion of 1 µg of RNA; the reaction was incubated at 37°C for 30 min, and 0.5 U of RNase R per 1 µg of RNA was added halfway through the reaction. RNase R-digested RNA was column-purified, and aliquots of 300 ng were visualized on 2% E-Gel. The corresponding linear RNAs were obtained by *in vitro* run-off transcription without the subsequent circularization step. RNA was purified by high-performance liquid chromatography (HPLC) as follows. RNA was loaded onto 4.6x300 mm size exclusion column SRT SEC-2000 with particle size of 5 µm and pore size 2000 Å (Sepax Technologies) and run on ÄKTApurifier high-pressure liquid chromatography system (GE Healthcare). Individual circRNA-containing fractions were collected, combined and precipitated with ethanol. RNA concentration was determined on the Qubit fluorometer (Thermo Scientific).

3.2.4 Expression of circRNA from Tornado constructs

The primary Tornado vectors pAV-U6+27-Tornado-Broccoli and pAV-U6+27-Tornado-F30-Broccoli described by Litke and Jaffrey (2019) were ordered from Addgene. Both vectors are based on pAV vector with the U6+27 promoter [includes the first 27 nucleotides of U6 RNA as described previously (Lu *et al*., 2015)]. The Tornado circRNA expression cassette includes 49 bp sequence of Broccoli aptamer for fluorescent imaging with DFHBI (Filonov *et al*., 2014) flanked by ribozyme combinations of upstream Twister P1 and downstream Twister P3 U2A, and tRNA:Tyr intronic sequences for RNA ligation by tRNA-specific

endonuclease. pAV-U6+27-Tornado-F30-Broccoli vector was designed identically, but also contains a F30 three-way junction with Broccoli on one arm as described by Litke & Jaffrey (2019).

Plasmids based on pAV-U6+27-Tornado-Broccoli vector were made by cloning directly into the Tornado expression cassette at *Not*I and *Sac*II restriction sites, replacing the Broccoli aptamer sequence. Inserts comprising $(CA)_{20}$, CA-SELEX X2, and CA-SELEX X4 with the overhangs corresponding to restriction sites were chemically synthesized as individual oligonucleotides (Table 2.2) and annealed prior to ligation with linearized by *Not*I and *Sac*II vector. Obtained plasmids were named Tornado $(CA)_{20}$, Tornado CA-SELEX X2, and Tornado CA-SELEX X4.

pAV-U6+27-Tornado-F30-Broccoli vector was used for the generation of Tornado CA-SELEX X4 Broccoli construct. Chemically synthesized CA-SELEX X4 oligonucleotides flanked with *Kfl*I overhangs were annealed and cloned into *Kfl*I-linearized plasmid. Tornado $(CA)_{100}$ Broccoli and Tornado control Broccoli were PCR-amplified from the corresponding PIE constructs and cloned in pAV-U6+27-Tornado-F30-Broccoli by Silke Schreiner.

3.2.5 *In vitro* transcription and circularization of antisense circRNA

For targeting *CD45* alternative splicing, designer antisense RNAs were synthesized by *in vitro* transcription, using double-stranded DNA-oligonucleotide templates (Table 2.2) and HiScribe T7 High Yield RNA synthesis kit, followed by RQ1 DNase treatment (10 U per reaction). For circularization, T4 RNA ligase (1.5 U/µg RNA, Thermo Scientific) was used. To eliminate the linear precursor, RNA was treated with RNase R (10 U/µg RNA). After each step, RNA was purified with Monarch RNA cleanup kit and visualized by denaturing polyacrylamide electrophoresis.

3.2.6 RNA secondary structure prediction

RNA secondary structures were predicted using RNAfold ViennaRNA Package server (univie.ac.at) implementing minimum free energy fold algorithm. For circRNA secondary structure prediction, the circular configuration was taken into account.

3.3 Cell culture methods

3.3.1 HeLa cells

HeLa cells were grown in Dulbecco's Modified Eagle's Medium (DMEM, Gibco) supplemented with 10% (v/v) heat-inactivated fetal bovine serum (FBS, Thermo Scientific). HeLa cells were cultured in 10 cm dishes (Sarstedt) and split every 2 – 3 days.

3.3.2 Transfection of circular and linear PIE RNA in HeLa cells

For the time course experiments, HeLa cells were transfected in 24-well plate format using Lipofectamine MessengerMax mRNA transfection reagent (Thermo Scientific) according to

the manufacturer's instructions. 5 x 10^4 cells per well were seeded one day before transfection. For all RNA variants, linear and circular RNA transcripts were transfected in 500 ng quantities. A mock transfection was done in the absence of RNA. For RNA immunoprecipitation experiments, HeLa cells were seeded 1:2 on 10 cm dishes one day before transfection. For each variant, 5 µg of RNA were transfected. The medium was changed 4 h upon transfection. 24 h after transfection, cells were harvested with TRIzol for total RNA isolation with RNeasy columns or, in case of RNA immunoprecipitation, cell pellets were collected.

3.3.3 Transfection of circRNA-expression constructs in HeLa cells

For forward plasmid transfection, cells from 80 – 90% confluent dishes were seeded on 10 cm dishes 1:2 on the day before transfection. Cells were transfected with 10 µg of plasmid using TurboFect transfection reagent (Thermo Scientific) according to the manufacturer's instructions. Mock transfection was performed without adding the plasmid DNA. The medium was changed 4 h upon transfection. Afterwards, cells were harvested with trypsin, collected in DMEM, and centrifuged at 500 xg and 4°C for 5 min. Cells were washed in 1x PBS and centrifuged as before. Cell pellets were subsequently used for RNA isolation, RNA immunoprecipitation, or cell fractionation as described below.

3.3.4 RNAi knockdown of hnRNP L in HeLa cells

The hnRNP L knockdown was performed by Silke Schreiner. In short, HeLa cells were seeded one day before transfection in 10 cm culture dishes to be 30% confluent on the next day. SiRNA duplexes (hnRNP L and luciferase, Table 2.1) were transfected using Lipofectamine 2000 (Thermo Scientific) at a final concentration of 30 nM according to the manufacturer‘s instructions. Four days after transfection, total RNA was isolated using TRIzol and RNeasy columns (QIAGEN). RNA samples were provided for subsequent RT-PCR analysis by Silke Schreiner. Total RNA was reverse-transcribed using the qScript Flex kit (Quantabio) with oligo(dT) primers, followed by PCR with the primers against hnRNP L alternative splicing targets.

3.3.5 Co-transfection of *CD45* minigene and antisense circRNA in HeLa cells

HeLa cells were seeded in 12-well plate format (10^5 per well) one day before transfection. Transfections were performed with *CD45* minigene and antisense circRNA variants (1 µg each) using Lipofectamine 2000 transfection reagent, according to the manufacturer's instructions. After 24 h or a time course (1 – 4 days), RNA was isolated as described below. In the actinomycin D-experiment, cells were treated with 10 µg/ml actinomycin D 30 min prior to transfections and harvested after 4 h for RNA isolation.

3.3.6 DG75 cells

DG75 cells were grown in RPMI medium (Invitrogen) supplemented with 10% (v/v) FBS, 2 mM L-glutamine, 1 mM sodium pyruvate, and 50 mM β-mercaptoethanol. Cells were grown in 75 cm^2 culture bottles with filter (Greiner Bio-One) and split every 2 – 3 days.

3.3.7 Electroporation of antisense circRNA in DG75 cells

DG75 cells were split one day prior to transfection. 2×10^6 cells per variant were transfected using Nucleofector™ kit V (Lonza). Reactions were performed according to the manufacturer's protocol, namely, 2×10^6 cells were resuspended in 100 µl of Nucleofector solution, supplemented with 3 µg of *in vitro*-produced circRNA or, as a control, 2 µg GFP plasmid, and run on Nucleofector™ 2b device (Lonza) with T-15 program. Then cells were transferred onto 12-well plates and left in 1.5 ml media. After 24 h, cells were harvested and RNA was isolated as described below. In a time course experiment, cells were harvested after 6, 12, and 24 h.

3.4 Working with RNA and characterization of designer circRNAs

3.4.1 Total RNA isolation

Total RNA was collected in TRIzol (Ambion) and isolated with the RNEasy kit or isolated with Norgen total RNA purification kit (Norgen Biotek) according to the manufacturer's instructions. To eliminate the plasmid DNA after RNA isolation with RNeasy kit, the samples were then treated with 5 µl of RNase-free RQ1 DNase according to the manufacturer's protocol. Subsequently, RNA was phenolized by adding one volume of phenol/chloroform, vortexed using a vortex mixer and centrifuged for 5 min at 19,000 xg. The upper aqueous phase was transferred to a new reaction tube and mixed with 2.5 volumes of ethanol, 0.1 volumes of 3 M sodium acetate (pH 5.2), and 1 µl glycogen. The samples were precipitated at -80°C for at least 20 min and centrifuged for 30 min at 19,000 xg and 4°C. The pellet was twice washed with 75% EtOH and centrifuged for 5 min as before. The pellet was dissolved in DMPC-treated ddH_2O. If the Norgen total RNA purification kit was used, RNA samples were on-column treated with 2 µl of TURBO DNase in 100 µl of 1x TURBO DNase buffer (Invitrogen) for 30 min prior to a washing step. RNA concentration was measured on NanoDrop1000 spectrophotometer (Thermo Scientific).

3.4.2 RT-PCR and agarose gel electrophoresis

For the circular and precursor RNA detection in total RNA, semi-quantitative RT-PCR was performed, where 1 µg of total RNA was reverse-transcribed with qScript cDNA synthesis kit (Quantabio). For alternative splicing detection of hnRNP L target genes, qScript Flex kit with oligo(dT) primers was used. All primers for PCR reactions were designed to anneal at 58°C using primer design program primer 3. For primer sequences, see Table 2.2. For the detection of alternative splicing events, the primers were chosen in a way to bind the

surrounding exons. For the circRNA detection, divergent pairs of primers were designed. The PCR was done in 25 µl reactions with 2 µl of RT reaction in 1x *Taq* PCR buffer, supplemented with 400 µl dNTPs (each), 2 mM $MgCl_2$, 800 µM primers (each), and 0.5 µl of *Taq* DNA polymerase (expressed and purified by Silke Schreiner). The following amplification profile was applied: denaturation at 95°C (2 min), 30 or 25 amplification cycles (30 sec at 95°C, 30 sec at 58°C, and 30 sec at 72°C), and a final elongation step (7 min at 72°C). The number of PCR cycles was set to 30 for the alternative splicing RT-PCR assays and reduced to 25 for the detection of transfected or expressed circRNAs. Afterwards, PCR reactions were mixed with loading buffer containing 30% glycerol and 0,025% bromphenol blue in 6X TBE buffer (1X TBE: 89 mM Tris, 89 mM boric acid, and 2 mM EDTA) and loaded on 2% or 2.5% agarose gel. Agarose was melted in 1X TBE, cooled down, and supplemented with ethidium bromide (Roth, final concentration 0.5 µg/ml). GeneRuler DNA ladder mix (Fermentas) or GeneRuler Low Range DNA ladder (Fermentas) were used as markers. Gels were run at 120 V in 1X TBE and documented with SynGene Genetools program on the gel documentation system (SynGene). For RT-PCR assays for detection of alternative splicing, the percentage of mRNA forms was quantified as relative to the sum of both PCR products (both splice variants) using the ImageJ software. For the detection of *CD45* splice forms, primers flanking alternatively spliced exons were used. Skipping/inclusion of individual exons was detected with primers located in the corresponding flanking exons.

3.4.3 Northern blot

The detection of tricRNA by digoxigenin (DIG) Northern blot was done according to Schneider *et al*. (2018), as described below. Pre-denatured total RNA and DIG-labeled DNA ladder (DIG VIII, Roche) were separated on an 8% denaturing polyacrylamide gel, transferred to a nylon membrane (Amersham Hybond-N+, GE Healthcare) for 1 h, at 3 mA/cm^2 using Trans-Blot semi-dry transfer cell (Biorad), cross-linked at 120 mJ/cm^2 at 254 nm in BLX 254 UV-crosslinker (Biolink) and pre-hybridized with the NorthernMax hybridization buffer (Ambion) at 68°C for 1 h. Hybridization with the riboprobe was done at 68°C overnight with constant rotation using HB-1000 hybridization oven (UVP). The DIG-labeled riboprobe directed against the whole circRNA sequence (107 nt) was prepared by *in vitro* transcription with DIG RNA labeling mix (Roche) according to the manufacturer's instructions, treated with RQ1 DNase, and analyzed on the 2100 Bioanalyzer (Agilent). After hybridization, the membrane was washed with 2X SSC [30 mM sodium citrate pH 7.0, 0.1% (w/v) SDS, and 300 mM NaCl] and 0.5X SSC. The membrane was blocked for 1 h with a DIG-blocking solution [2% (w/v) blocking reagent (Roche) in 100 mM maleic acid buffer pH 7.5]. After that, the membrane was incubated with anti-DIG-Fab (Roche) at a final dilution of 1:10,000 for 1 h. The excess antibody was washed with DIG-washing buffer [0.3% (v/v) Tween-20 in 100 mM maleic acid buffer pH 7.5]. Northern blots were developed using the

DIG-detection system, namely 0.5% CDP-star substrate solution (Roche) in DIG-detection buffer (100 mM Tris-HCl pH 9.5 and 100 mM NaCl). The membranes were exposed to Amersham Hyperfilm ECL (GE Healthcare) films for various time intervals. The films were developed on Agfa Curix 60 Processing Machine (AGFA).

3.4.4 E-Gel system

Total RNA integrity and visualization of circRNA expression were accessed as the following. Total RNA pre-denatured at 70°C for 2 min was run in 2% E-Gel EX agarose gel (Invitrogen) on the E-Gel iBase (Invitrogen). Riboruler High Range RNA ladder or Riboruler Low Range RNA ladder (Thermo Scientific) was used as a reference standard. Gels were documented with SynGene Genetools program on G:Box gel documentation system (Syngene).

3.4.5 RNase R treatment of total RNA samples

Total RNA from HeLa cells (5 µg) was treated with or without 2.5 U/µg of RNase R (Epicentre) for 20 min at 37 °C. RNA was phenolized, ethanol-precipitated and diluted in 20 µl of DMPC-water, 2 µl were subsequently used for reverse transcription. PCR with primers against circRNAs was performed with 30 cycles.

To confirm the circular configuration of circRNA expressed from Tornado constructs, 4 µg of total RNA from HeLa cells after Tornado transfections were treated with or without RNase R for 35 min at 37°C. Total reaction volume supplemented with 2X formamide RNA loading buffer (0.5X TBE, 40% formamide, and 0.1% bromphenol blue) was loaded onto 4% E-Gel.

3.4.6 Denaturing urea polyacrylamide gel electrophoresis

Denaturing urea polyacrylamide gel electrophoresis (PAGE) was used for visualization of the expressed circRNAs in total RNA samples and for *in vitro*-produced transcripts. After transfection of HeLa cells with Tornado constructs, 3 µg of isolated total RNA was dissolved in formamide RNA loading buffer and denatured for 2 min at 95°C. The gels of different polyacrylamide (PAA) percentages were prepared by mixing the acrylamide gel solution [20% acrylamide (19:1 acrylamide/bisacrylamide) and 50% (w/v) urea in 1X TBE buffer] with the buffer solution [50% (w/v) urea in 1X TBE]. Gels were polymerized by adding 100 µl of 10% (w/v) ammonium persulfate (APS) and 10 µl of tetramethylethylenediamine (TEMED) per 10 ml of the PAA solution. Denaturing PAA gels were cast using the Mini PROTEAN electrophoresis system (Biorad) and run in Mini PROTEAN electrophoresis chambers (Biorad) in 1X TBE running buffer and 300 V for 15 min (pre-run) and 60 min after loading the samples. Riboruler High Range RNA Ladder or Riboruler Low Range RNA Ladder was used as a reference standard. Gels were stained with ethidium bromide and documented with SynGene Genetools program on G:Box gel documentation system.

3.4.7 In-gel Broccoli aptamer imaging with DFHBI

Total pre-denatured RNA (3 or 4 µg) obtained from HeLa cells transfected with Tornado CA-SELEX X4 Broccoli construct was separated using TBE-urea gels of two different percentages. Riboruler High Range or Low Range RNA ladder was used as a reference standard. Gels were washed with water and stained with the DFHBI staining solution (10 µM DFHBI, 100 mM KCl, 1 mM $MgCl_2$ in 40 mM HEPES pH 7.4) at room temperature for 30 min, as described by Filonov & Jaffrey (2016). Gels were imaged using the INTAS Imager Transilluminator ChemiDoc MP (Bio-Rad) with 477 nm excitation and 535 nm emission. Gels were washed with water and stained with SYBR Gold solution (Roche) diluted in 1X PBS buffer. Total RNA bands were then imaged in UV light using the gel documentation system.

3.4.8 RNA immunoprecipitation and Western blot

Cell pellets were lysed in RIPA buffer (50 mM Tris-HCl pH 7.4, 150 mM NaCl, 5 mM EDTA, 1% NP-40, and 0.1% SDS), filtered through a 0.45 µm syringe membrane-filter and pre-conditioned with 15 µl of Protein-G Dynabeads (Thermo Scientific) at 4°C for 15 min. Antibody binding was performed at 4 °C overnight. Monoclonal mouse 4D11 anti-hnRNP L and polyclonal anti-IMP3 antibody (Millipore), as well as anti-FLAG antibody (Sigma-Aldrich) were used. Bead capturing was carried out with Protein-G Dynabeads for IMP3 antibody and Protein-A Dynabeads (Thermo Scientific) for hnRNP L and FLAG at 4 °C for 1 h. Protein-RNA complexes were washed with 1X150/2X600/1X300/1X150 mM NaCl in 50 mM Tris-HCl (pH 7.4) supplemented with 0.05% Tween-20. RNA from the input and immunoprecipitated (IP) fractions was extracted with TRIzol, separated in Phase Lock Gel tubes (5Prime), followed by ethanol precipitation and reverse transcription (qScript cDNA Synthesis kit). Relative RNA amounts were assayed by semi-quantitative PCR and qPCR. The real-time PCR was carried out in triplicates using Luna Universal qPCR Reaction Mix and the Realplex Mastercycler. The fraction of bound target RNAs in RIP assays was calculated with each target normalized to the corresponding input fraction.

For Western blot analysis after RNA immunoprecipitation (RIP) experiment, input samples lysed in RIPA buffer were resuspended in 2X SDS loading buffer (100 mM Tris-HCl pH 6.8, 4% SDS, 0.2% bromphenol blue). IP samples (protein on beads) were supplemented with 2X SDS loading dye on magnetic stand. PeqGOLD Protein-Marker IV (Peqlab) was used as a molecular weight standard. Proteins were separated on 12 % SDS gel and transferred onto a nitrocellulose membrane (Bio-Rad). The gel, nitrocellulose membrane, and blotting paper were equilibrated for 2 min in transfer buffer (25 mM Tris, 190 mM glycine, 20% methanol). Transfer was performed with 25 V and 1.3 A for 30 min using Trans-Blot Turbo transfer system (Biorad). Then, the membrane was washed twice with PBS-T (0.1% Tween 20 in 1X PBS). Membranes were blocked with 5% (w/v) milk powder (Roth) in PBS supplemented with 0.05% Tween for 60 min. Subsequently, membranes were probed with a 1:10,000 dilution of

primary mouse anti-hnRNP L (4D11), rabbit anti-IMP3 or mouse anti-GAPDH antibody (Sigma-Aldrich) for 60 min at room temperature in 5% milk in PBS-T buffer, followed by incubation with the secondary antibody for 60 min at room temperature: anti-mouse-IgG-HRP (Sigma-Aldrich) for hnRNP L and GAPDH, anti-rabbit-IgG-HRP (Sigma-Aldrich) for IMP3 Western blot. After extensive washing, the blots were incubated with 1 ml of ECL Western blotting substrate (Roche) and visualised on Amersham Hyperfilm ECL films.

3.4.9 Quantitative real-time PCR

For reverse transcription, 1 µg of total RNA with the qScript cDNA synthesis kit was used. Real-time PCR reaction was carried out using the Luna qPCR reaction mix (New England Biolabs) according to the manufacturer's instructions. The qPCR reaction was carried out in Realplex Mastercycler (Eppendorf). The qPCR primers were previously tested for approximately 100% amplification efficiency. The reactions were performed in triplicates. Average cycle threshold (Ct) values were used for calculations with ΔΔCt method. For normalization, the Ct values of the housekeeping genes *ACTB* and *U6* were used.

3.4.10 Cell fractionation

Cytoplasmic and nuclear extracts were isolated from 10 µl packed cell volume (PCV) of HeLa cells transfected with circRNA expression constructs. The NE-PER nuclear and cytoplasmic extraction reagents (Thermo Scientific) with the protease inhibitor cocktail (Thermo Scientific) were used according to the manufacturer's instructions. Cytoplasmic and nuclear extracts were lysed with TRIzol-LC (Ambion). RNA was isolated with the RNeasy kit. Presence of individual circRNAs was analysed by RT-PCR with circRNA-specific primers. Protein distribution between the cytoplasmic and the nuclear fractions was analysed by Western blot. The intensities of the bands corresponding to hnRNP L were quantified by densitometry using ImageJ software. HnRNP L content in each individual fraction was quantified as the per cent of total: nuclear and cytoplasmic hnRNP L.

3.4.11 Determination of absolute concentration of expressed circRNA

HeLa cells were transfected with the Tornado CA-SELEX X4 and CA-SELEX X4 Broccoli constructs. Total RNA was isolated with the Norgen total RNA purification kit and on-column treated with TURBO DNase according to the manufacturer's instructions. Total RNA samples were analyzed on the 2100 Bioanalyzer. *CA-SELEX X4* and *CA-SELEX X4 Broccoli* circRNAs were detected using the Small RNA and Nano RNA kits, respectively. Electropherograms were analyzed using the Agilent 2100 Expert B.02.08 software. The individual peaks, corresponding to circRNAs, were manually integrated by setting the integration borders between 190 and 209 nts for *CA-SELEX X4* and between 254 and 380 nt for *CA-SELEX X4 Broccoli* circRNAs. The software estimates RNA concentration by comparing peak areas of a ladder with peak areas of the RNA of interest. The estimated

circRNA/total ratio was used for further calculations. Cell concentration and average cell volume was measured using Moxi Z mini automated cell counter (ORFLO Technologies). Total RNA concentration was measured on the Nanodrop1000 spectrophotometer. The circRNA content was quantified using the circRNA/total RNA ratio. The total circRNA amount was divided through the number of cells to calculate the absolute amount of circRNA per cell. Absolute circRNA concentrations and the numbers of circRNA per cell were also measured by real-time PCR. HeLa cells were in triplicates transfected with the Tornado CA-SELEX X4 or CA-SELEX X4 Broccoli constructs. For absolute quantification, an external calibration curve based on *in vitro*-produced circRNA standards was used. Knowing the copy number of the standard circRNA, the precise number of molecules added to the RT reaction could be calculated after the subsequent real-time PCR runs, thus providing a standard for specific circRNA quantification. CircRNA standards were prepared as described for antisense circRNA in Chapter 3.2.5. For the RT reaction, 50 ng of the circRNA standards and 100 ng of mock RNA were used. RNA was reverse-transcribed with the qScript cDNA synthesis kit. 10% of the RT reaction, which is equivalent to 5 ng and $1.09x10^{11}$ and $9.09x10^{10}$ copies (*CA-SELEX X4* and *CA-SELEX X4 Broccoli*, respectively), was used for the qPCR. For the standard curve, the RT reaction was diluted in 10-fold dilution steps, making five dilutions. The real-time PCR reactions were carried out using the Luna Universal qPCR kit according to the manufacturer's instructions.

A standard curve was drawn by plotting the threshold cycle (Ct) against the natural log of the number of molecules. The absolute copy number of the expressed circRNA, as well as the copy number of the standards used for the calibration curve, was quantified on NEB Bio Calculator. The number of molecules was converted into pg on DNA/RNA copy number calculator (http://endmemo.com/bio/dnacopynum.php). The circRNA intracellular concentration was calculated on Conversion: weight – moles program (http://molbiol.edu.ru/eng/scripts/01_07.html), where the average cell volume, measured by a Moxi Z mini automated cell counter, was considered.

3.4.12 Microscopy and image processing

One day after transfection, transfected and mock control HeLa cells were treated with trypsin, seeded on the sterilized coverslip and left in the CO_2 incubator for 24 h. Cells were washed with PBS three times, fixed by incubating with 1 ml 4% formaldehyde in PBS for 15 min, and washed three times with cold PBS for 10 min. Cells were imaged in 40 µM DFHBI and 5 µg/mL Hoechst in PBS buffer. Coverslips were mounted on an objective slide in one drop of ProLong Diamond Antifade (Invitrogen), sealed with nail polish, and stored at -20°C. An Axioskop 20 microscope and image processing software (Zeiss) were used for imaging. Broccoli aptamer was imaged with the GFP filter and Hoechst-stained nuclei were imaged with the DAPI filter. Exposure times: 500 ms – 1 s for DFHBI and ~50 ms for Hoechst.

4. Results

4.1 Repetitive elements contribute to circRNA biogenesis

To establish a circRNA expression system, we first used a vector based on *Plt-circR4* circRNA with *Plt-circR4* splice sites and flanking intron fragments. In platelets, circRNA *Plt-circR4* is present exclusively in the circular form (Preußer *et al*., 2018). If *Plt-circR4* circularization protein factors are present in a chosen cell line, or if backsplicing of *Plt-circR4* is largely controlled by the flanking sequences, *Plt-circR4*-based expression system may be successfully implemented for circRNA expression. *Plt-circR4* backsplicing may then be driven by short flanking inverted repeats, comprising only 28 nt both up- and downstream. Taking this into account, Marie Mosbach and Dr. Christian Preusser designed a vector for circRNA expression, which contains the original *Plt-circR4* exon that can be substituted with another sequence, flanked with the *Plt-circR4* splice sites and intronic sequences with inverted repeats (Fig. 4.1A, top). However, ectopic circRNA expression in human cell lines achieved only moderate circularization, with the precursor RNA as the main outcome (data not shown). In other words, the circularization efficiency was relatively low in comparison to the endogenous *Plt-circR4*, where no linear form is present. In order to improve the outcome of the backsplicing reaction, additional two, four, and nine upstream and downstream inverted repeats were cloned into the original vector, thereby increasing the complementary region of the pre-mRNA from ~78 bp to ~133, 205, and 427 bp, respectively (partial secondary structures are shown in Fig. 4.1A, bottom). As a test sequence, we cloned in an hnRNP L intronic sequence that forms a circRNA of 572 nt in the *Plt-circR4* backbone (Plt-circR4-control). In order to compare circularization efficiencies, Plt-circR4-control constructs with one, three, five, and ten copies of inverted repeats were transfected in HeLa cells and the levels of the circular and precursor transcripts were analyzed by RT-PCR with the corresponding primer pairs (Fig. 4.1B). We observed increasing amounts of circRNA upon the oligomerization of the inverted repeat region. Conversely, the level of the linear product dropped dramatically and was completely gone for the construct with ten inverted repeats. Both of these observations are consistent with the RT-qPCR data. As shown in Fig. 4.1C, the increment of inverted repeats to three, five, and ten increased the circRNA expression to 4-, 13-, and 20-fold, respectively, when normalized to one inverted repeat variant. Notably, the pre-mRNA levels decreased dramatically, reaching only 6%, 0.09%, and 0.07% of the initial vector system. These data indicate the importance of the flanking regions for RNA circularization in this particular case of the *Plt-circR4*-based circRNA expression vector.

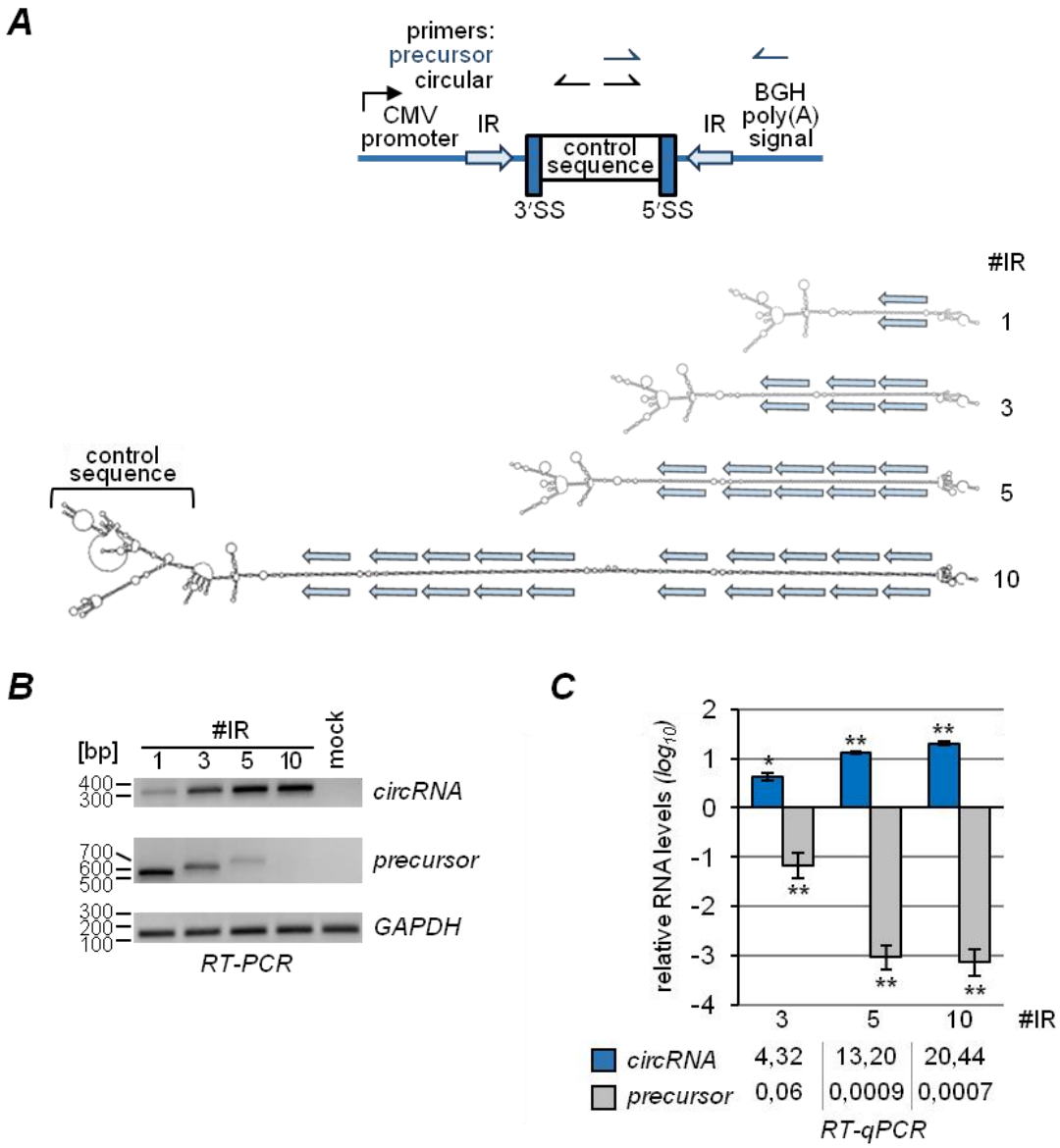

Figure 4.1 Expression of circRNA from the Plt-circR4 vector.

(A) Schematic of the Plt-circR4-control vector (top) and secondary structures of RNAs, transcribed from the Plt-circR4 vector with the different number of inverted repeats (bottom). 3′ and 5′ splice sites (SS) are shown in dark blue. The inverted repeats (IR) are shown as blue arrows. PCR primer binding sites for linear and circular RNA detection are shown in blue and black, respectively. The number of inverted repeats (one, three, five, and ten) is indicated as #IR, where blue arrows represent their positions. For the first three vectors (one, three, and five inverted repeats), the secondary structure of an empty vector variant was analyzed. For ten inverted repeats, Plt-circR4-X10-control sequence is shown.

(B, C) RT-(q)PCR detection of circRNA and precursor upon transfections of Plt-circR4-control constructs in HeLa cells. HeLa cells were transfected with Plt-circR4-control with one, three, five, and ten inverted repeats (designated as #IR). RNA was isolated 24 h after transfection and used for RT-PCR validation with the primers for circular and precursor *Plt-circR4-control* RNA; *GAPDH* was used as a control ***(B)***. Relative amounts of the circRNA and precursor RNA were analyzed by RT-qPCR [***(C)***, normalized to *ACTB* and *U6* RNA]. Values are plotted as $\log_{10}$ of fold changes relative to one inverted repeat variant. The fold change is shown below. Error bars denote standard deviations (n = 3; ∗ = $p < 0.05$; ∗∗ = $p < 0.01$).

4.2 A tRNA-based construct optimized for circRNA expression

Next, we focused on another available circRNA expression system that can be used for the ectopic expression of designer circRNA. Previously, a circRNA expression system based on the tRNA backbone was described (Lu *et al*., 2015; Noto *et al*., 2017). As tRNA intronic circRNA (tricRNA) is also formed endogenously, it utilizes endogenous tRNA maturation mechanisms when expressed by constructs for circRNA expression (reviewed by Schmidt & Matera, 2020). To assay the circRNA expression from the tricRNA vector and its potential application for protein sponging, we utilized the vector introduced by Lu *et al*. (2015). This vector with the tRNA backbone and inserted Broccoli aptamer was used for cloning of one copy of the 20-nt long SELEX-derived hnRNP L-specific high-affinity binding sequence (5′-ATACATGACACACACACGCA-3′; Hui *et al*., 2005; Fig. 4.2A). To confirm the circular configuration of the expressed *CA-SELEX* tricRNA, HeLa cells were transfected with the corresponding vector; total RNA from these cells was subjected to RNase R treatment, and used for RT-PCR with the primers specific to circular and precursor expressed tricRNA, as well as the endogenous circRNA control *CAMSAP1* (Fig. 4.2B). Partial resistance of the linear precursor *CA-SELEX* to RNase R treatment can be explained by tRNA modifications and its extensive secondary structure. Total RNA and the RNA sample after RNase R treatment were also assayed by Northern blot with a riboprobe against the circRNA backsplice junction covering the complete sequence (Fig. 4.2C). Surprisingly, we detected several bands, which presumably correspond to precursor molecules on different processing steps of expressed tricRNA. After RNase R treatment, two precursor bands vanished, and the circRNA band remained. Next, we detected the expressed RNA in fixed cells using fluorescence imaging. Due to the presence of the Broccoli aptamer sequence in this vector, tricRNAs, as well as its linear precursor RNAs, were visualized with the GFP filter in fixed cells transfected with CA-SELEX vector displaying both nuclear and cytoplasmic localization (Fig. 4.2D).

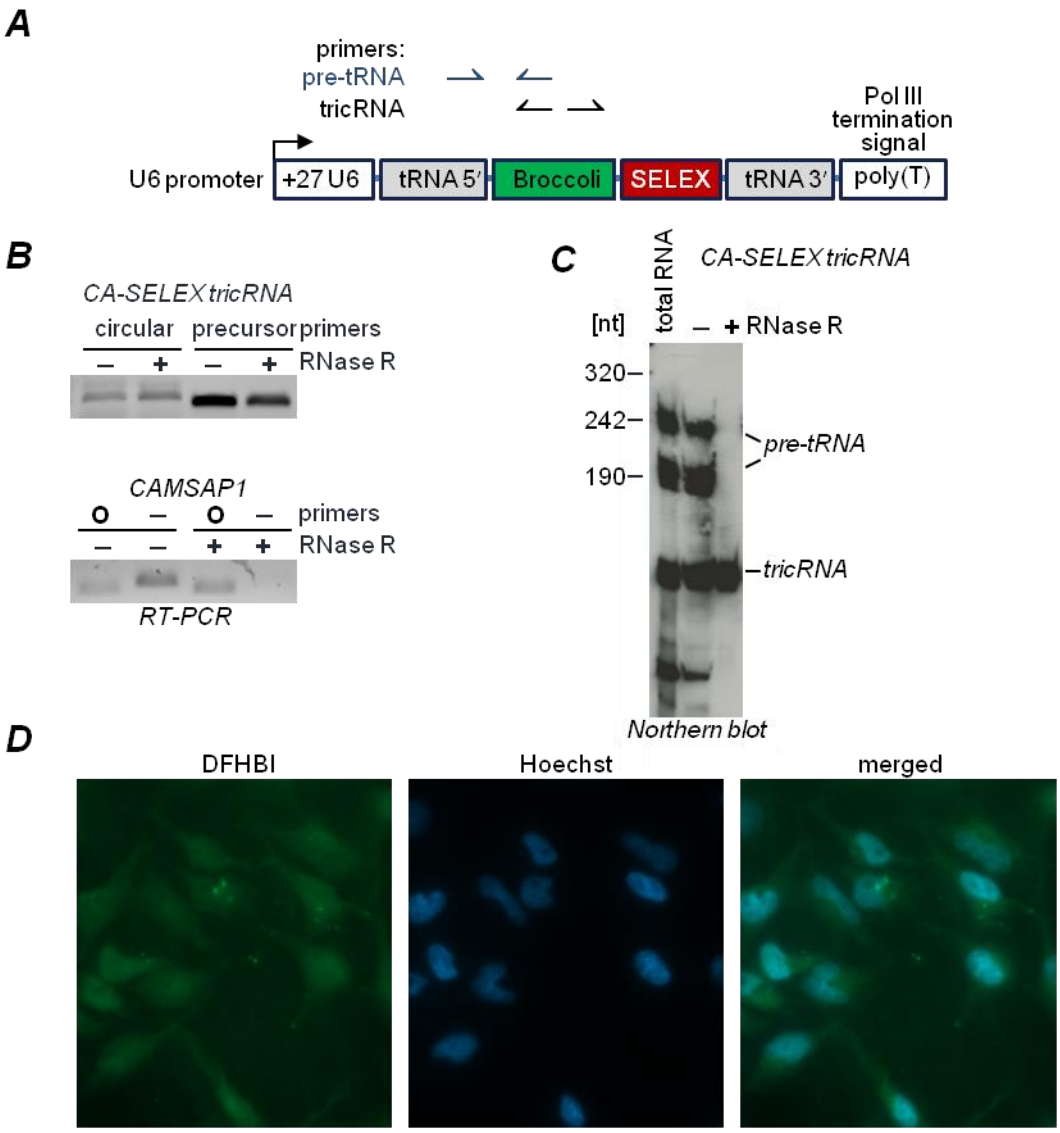

Figure 4.2 Expression of tricRNAs with high affinity to hnRNP L in HeLa cells.
(A) Schematic of tricRNA expression construct with one CA-SELEX sequence. PCR primer binding sites for linear and circular PCR products are shown in blue and black, respectively. The vector includes U6 promoter, the first 27 nucleotides of U6, tRNA sequences (5′ and 3′ tRNA), the SELEX sequence (5′-ATACATGACACACACACGCA-3′; Hui *et al*., 2005), and the Pol III termination signal.
(B) RT-PCR tricRNA detection after RNase R treatment. HeLa cells were transfected with CA-SELEX tricRNA construct and total RNA was isolated after 24 h. Total RNA samples (5 µg) were treated with (+) or without (–) RNase R. 20% of the reaction was used for RT-PCR analysis with tricRNA-specific primers (above) and endogenous circRNA *CAMSAP1* (below, used as a control for RNase R digestion).
(C) Detection of *CA-SELEX* tricRNA by Northern blot. RNA samples (2 µg each) were treated with (+) or without (–) RNase R. For comparison, the same amount of total RNA after transfection was loaded (total RNA). The DIG-labelled RNA probes hybridize across the splice junction and span the whole sequence. The only band remaining after RNase R treatment was identified as the *CA-SELEX* tricRNA (107 nt). Other bands correspond to pre-tRNA (expected at 180 and 238 nt).
(D) Detection of Broccoli aptamer as a part of *CA-SELEX* tricRNA in HeLa cells. Broccoli staining in fixed cells was performed two days after transfection of CA-SELEX tricRNA construct. HeLa cells were stained with DFHBI and Hoechst and imaged by fluorescence microscopy.

Next, we addressed the hnRNP L-binding efficiency of the expressed *CA-SELEX* tricRNA by RNA immunoprecipitation (RIP). Total RNA from HeLa cells after transfection was immunoprecipitated with hnRNP L and FLAG antibody. As a control, transfection of the empty vector construct without the CA-SELEX sequence was used. *CA-SELEX* circular and precursor RNA co-immunoprecipitation was determined by RT-PCR (Fig. 4.3, top). We detected efficient binding of the pre-tRNA to hnRNP L and much weaker binding of tricRNA. This is consistent with the observations from Fig. 4.2B, where high expression of the pre-tRNA relative to tricRNA was demonstrated by RT-PCR. Western blot with hnRNP L and GAPDH antibodies (negative control) for input and immunoprecipitated fractions confirmed efficient hnRNP L pulldown (Fig 4.3, bottom).

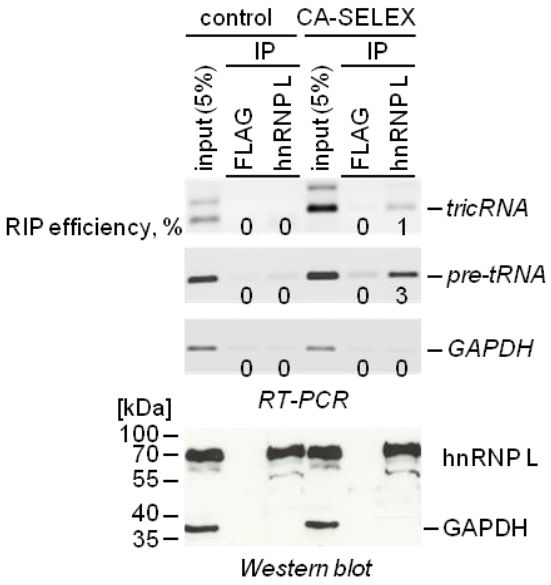

Figure 4.3 *CA-SELEX* tricRNA binds hnRNP L *in vivo*.
HeLa cells were transfected with CA-SELEX tricRNA expression plasmid or control construct (Broccoli tricRNA). RNA immunoprecipitation was performed with HeLa cell lysates prepared 24 h post-transfection, using antibodies against hnRNP L or FLAG (control). RNA was isolated and used for RT-PCR with the primers against tricRNA, pre-tRNA and *GAPDH* (upper panel). For comparison, 5% of the input was analyzed. RIP efficiency was quantified by densitometry and shown below each lane. Input and IP samples were analyzed by Western blot with antibodies against hnRNP L and GAPDH (lower panel).

In sum, utilizing the tricRNA expression system for sponging of hnRNP L, we detected abundant and multiple precursors, which partly remain after RNase R treatment. These precursors might affect the results and complicate the result interpretation. However, expressed *CA-SELEX* tricRNA containing a single SELEX sequence with high affinity to hnRNP L was detected to bind the target protein at low efficiency.

4.3 Designer PIE circRNAs act as hnRNP L sponges

In agreement with the previous observations, we focused on the circRNA protein sponge design. For this, we used the PIE expression system (Wesselhoeft *et al*., 2018), where several previously introduced 20-nt long CA-rich SELEX sequences were incorporated.

Based on the results described above, we expected the efficiency of hnRNP L sponging to be higher when multiple copies of the 20-nt long SELEX sequence are introduced. Therefore we cloned 4, 8, 16, and 32 SELEX repeats separated by ATAT linkers, into the PIE vector, transcribed the RNA *in vitro*, and circularized the transcripts (Fig. 4.4A). The circRNA fractions were further enriched with RNase R treatment (Fig. 4.4B). As a negative control, we used a vector fragment sequence. A CA-repeat sequence, $(CA)_{100}$, which binds hnRNP L with high affinity (Schreiner *et al*., *in press*) was used as a positive control. Both control constructs were designed and generated by Silke Schreiner.

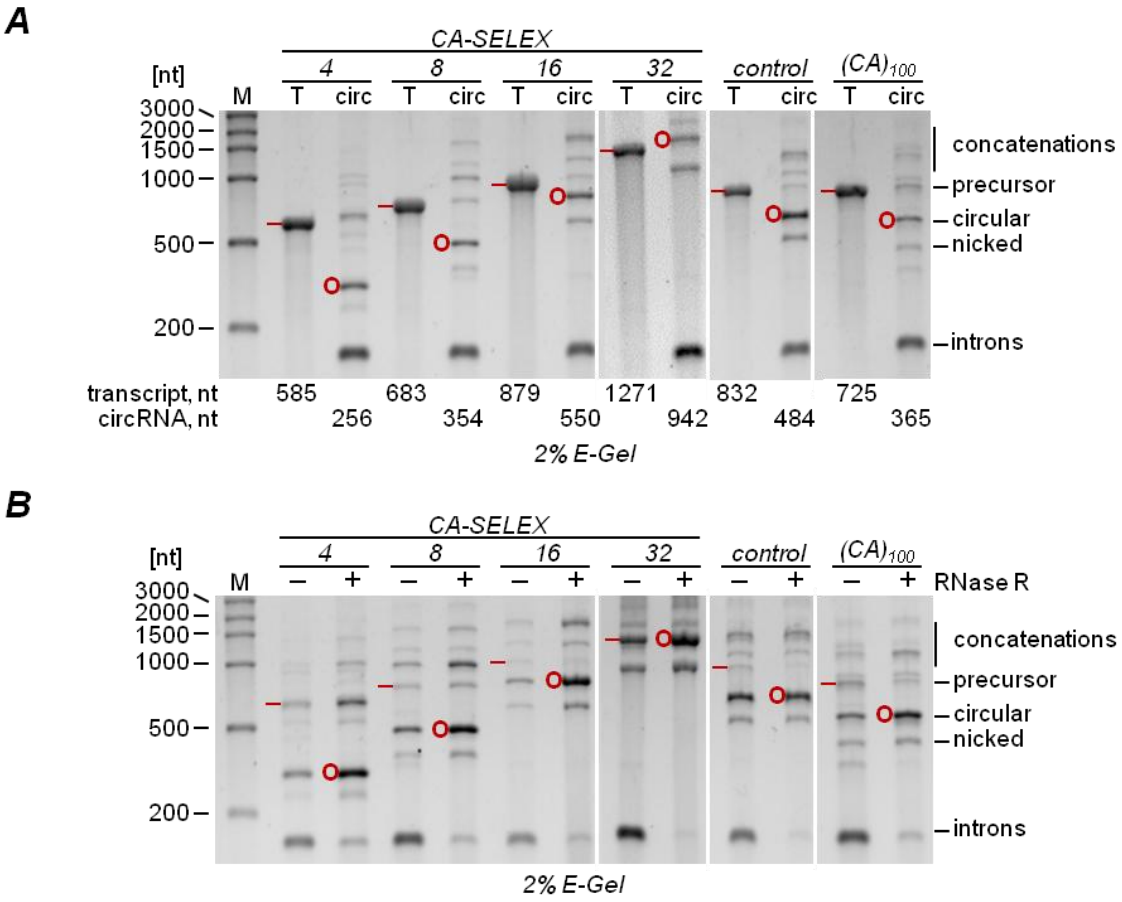

Figure 4.4 Synthesis and purification of permuted intron-exon (PIE) circRNA.
(A) PIE RNA circularization. E-Gel shows the linear transcripts (designated "T") and RNA after splicing reaction (designated "circ"). RNA was *in vitro* transcribed from PIE constructs containing 4, 8, 16, 32 CA-SELEX sequences, negative or positive control (*control* and $(CA)_{100}$, respectively). These precursor RNAs were subjected to *in vitro* PIE-mediated processing to obtain circRNAs. The sizes of the precursor and circRNA are shown below. Linear and circular RNA species are marked in red. The products of the splicing reactions were assigned as described by Wesselhoeft *et al*. (2018) and shown on the right. *M*, marker (HR RNA ladder).
(B) Purification of the circRNA reactions by RNase R. E-Gel shows the splice reactions with (+) and without (–) RNase R treatment. The remaining precursor and enriched circRNA bands are marked in red. *M*, marker (HR RNA ladder).

The main output of the circularization reactions was circRNA. However, when the reactions were separated on an E-Gel, many additional bands were detected. According to Wesselhoeft *et al*. (2018), these bands were assigned as circular and linear concatenations,

a linear precursor molecule, nicked circle, splicing intermediates, and excised introns. RNase R did not fully digest *Anabaena* introns, circRNA concatemers, and nicked circRNA (Fig 4.5B), which is also consistent with the previous observations on PIE circRNA preparation (Wesselhoeft *et al*., 2019).

To maximize the effects of the functional designer circRNA and to avoid innate cellular immune responses, it was previously suggested to purify PIE circRNA reactions by HPLC (high-performance liquid chromatography, Wesselhoeft *et al*., 2018). Therefore, both circular and linear RNA samples (used as a control) were purified by HPLC. CircRNA fractions (A15 – B2) were collected, visualized by the E-Gel system, and combined for subsequent transfection of HeLa cells (Fig. 4.5A). As a control, corresponding linear transcripts were used (Fig 4.5B, fractions A11 – B1).

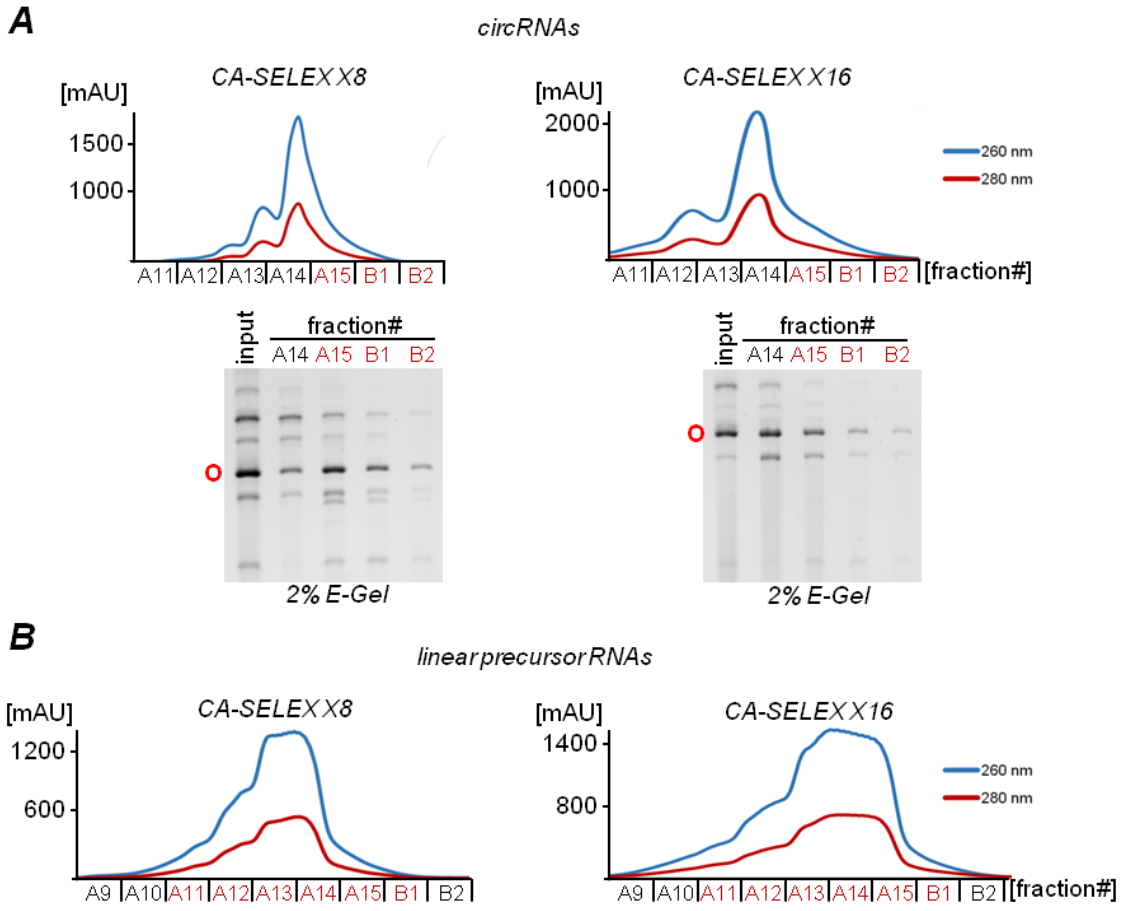

Figure 4.5 HPLC purification of circRNA obtained from PIE splicing reactions.
(A) HPLC purification of *CA-SELEX X8* and *CA-SELEX X16* PIE circRNA. Top: HPLC chromatograms of splicing reactions. Bottom: E-Gel with purified fractions. RNA was detected by UV absorbance; mAU designates milli-absorbance units. Individual circRNA-containing fractions were collected, precipitated with ethanol, and separated on a precast E-Gel. Each lane represents 5% of the collected fraction. The bands corresponding to circRNA are marked in red. Fractions A15 – B2 (marked in red) were collected and used for transfection of HeLa cells..
(B) Chromatograms of linear PIE transcripts from CA-SELEX X8 and CA-SELEX X16 PIE constructs. Precursor PIE RNAs were separated by size exclusion chromatography. Fractions A11 – B1 (marked in red) were combined, precipitated with ethanol, and used for transfection in HeLa cells as linear controls for *CA-SELEX X8* and *CA-SELEX X16* circRNA.

Therefore, we designed and generated PIE circRNA for hnRNP L sponging, and validated circRNA integrity and purity before proceeding to transfection experiments.

4.3.1 Binding of hnRNP L by transfected PIE circRNAs

To find out if the PIE designer circRNAs with high-affinity hnRNP L-binding sequences are physically associated with this protein, we performed a RIP-PCR assay (Fig. 4.6). In short, we used cell lysates from HeLa cells transfected with purified *SELEX X16* or $(CA)_{100}$ PIE circRNAs. To assess nonspecific interactions that may occur in RIP, we carried out a control experiment with PIE circRNA containing a vector fragment (Fig. 4.6, "*control*"). To access their integrity, purified circRNA samples were loaded on a gel prior to transfection (Fig. 4.6A). Cell lysates from these variants were probed with hnRNP L or FLAG antibodies. The lysates were subsequently precipitated with Protein-A-coupled beads. RNA from the input and immunoprecipitated fractions was assayed by RT-PCR with the circRNA-specific and *GAPDH* (negative control) primers (Fig. 4.6B&C). HnRNP L and GAPDH (negative control) protein levels were monitored by Western blot (Fig. 4.6D). By testing the *control* circRNA we confirmed that hnRNP L protein was not associated with the control sequence. Overall, we conclude, that the *CA-SELEX X16* circRNA binds hnRNP L *in vivo* with high specificity and efficiency comparable to $(CA)_{100}$ circRNA.

4.3.2 PIE circRNA sponges affect alternative splicing

HnRNP L is involved in the regulation of multiple alternative splicing events (Hung *et al*., 2008). Transfection of the hnRNP L sponges might affect hnRNP L function and, therefore, splicing of hnRNP L target genes. To analyze alternative splicing of the hnRNP L targets, linear or circular RNAs generated by the PIE system were transfected in HeLa cells. Total RNA was harvested at different time points (Fig. 4.7) and used for RT-PCR assays with the gene-specific primers. HnRNP L target genes assessed here had previously been identified in a combined RNAi and microarray analysis (Hung *et al*., 2008). In hnRNP L knockdown experiments, *BPTF* (*FALZ*) and *TJP1* demonstrated hnRNP L-dependent alternative splicing patterns. Specifically, exon 20 of *TJP1* and exon 18a of *BPTF* exhibited high inclusion ratio, when assayed by RT-PCR and quantified by densitometry (Hung *et al*., 2008). For these two genes, hnRNP L acts as a splicing repressor and inhibits exon inclusion. Here, in a time-course experiment, significant effects on *BPTF* alternative splicing were detected 8 and 24 h after *CA-SELEX* PIE circRNA transfection, where exon inclusion increased from 3% (*control*) to 11 – 14% after 8 h, reaching 14 – 16% after 24 h (Fig. 4.7). For both time points, $(CA)_{100}$ positive control circRNA had the maximal effect on exon inclusion: 17% and 32% after 8 and 24 h, respectively. In the case of linear PIE RNA, no effect on alternative splicing of *TJP1* was detected.

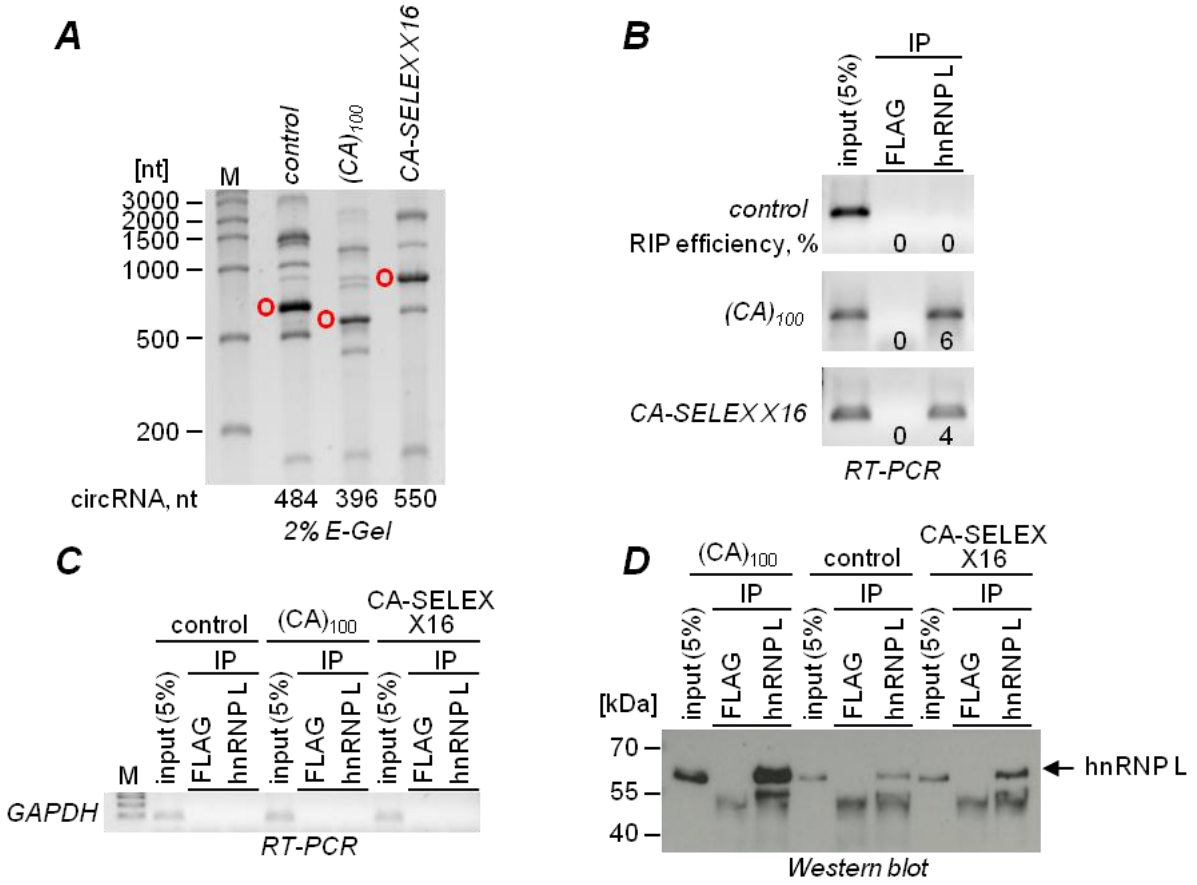

Figure 4.6 *In vivo* binding of hnRNP L to *CA-SELEX X16* circRNA.
(A) PIE circRNA used for transfection. CircRNAs obtained from control, $(CA)_{100}$, and CA-SELEX X16 PIE constructs were purified by RNase R and HPLC, loaded on an E-Gel, and subsequently used for transfections in HeLa cells. Bands corresponding to circRNAs are marked in red. *M*, marker (HR RNA ladder).
(B) HnRNP L sponging by PIE $(CA)_{100}$ and *CA-SELEX X16* circRNA *in vivo.* Immunoprecipitations were performed from HeLa cells transiently transfected with the negative control (*control*), $(CA)_{100}$ or *CA-SELEX X16* circRNA. Cell lysates were prepared 24 h post-transfection and used for immunoprecipitation reactions with anti-hnRNP L or -FLAG antibodies. RNA was isolated from input and IP samples and used for RT-PCR with gene-specific primers against *control*, $(CA)_{100}$, and *CA-SELEX X16* circRNAs. RIP efficiency was quantified by densitometry and shown below each lane.
(C) RT-PCR with the primers against *GAPDH* after the RIP experiment. RNA from each IP and input reaction was used for RT-PCR with *GAPDH* primers, to serve as an IP negative control. *M*, marker (DNA Ladder Mix).
(D) HnRNP L protein content in input and IP fractions after the RIP experiment. Input and IP samples were analyzed by Western blot with antibodies against hnRNP L.

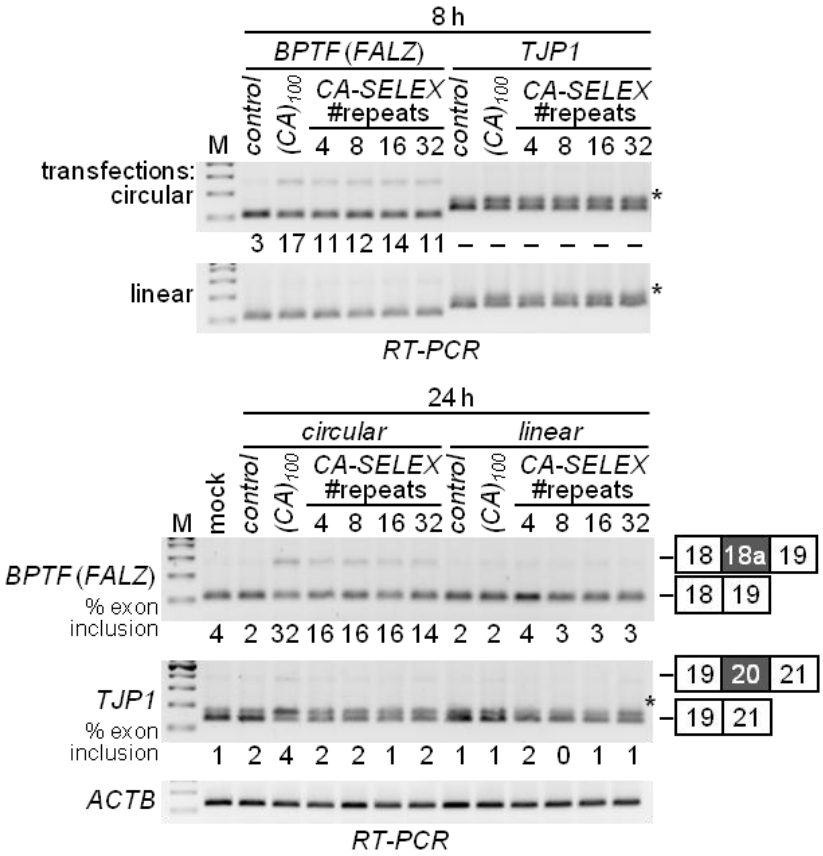

Figure 4.7 Transfected *CA-SELEX* linear and circRNA alter alternative splicing of hnRNP L target genes.
Total RNA was prepared after HeLa cells were transfected with PIE construct-derived RNA for 8 and 24 h (top and bottom, respectively). Isolated RNA was used for RT-PCR with primers against *BPTF* (*FALZ*) and *TJP1*. *ACTB* was used as a loading control. For *TJP1*, the additional minor band (asterisk) represents a mispriming RT-PCR product. The mock sample corresponds to a mock transfection; *control* circRNA transfection is marked as *control*. The effect of PIE *CA-SELEX* RNA transfection on alternative splicing of *BPTF* (*FALZ*) and *TJP1* was calculated as a percentage of exon inclusion and listed below the corresponding lanes. After 8 h, no PCR products corresponding to exon inclusion of *TJP1* was detected (marked as dash). Positions of PCR products corresponding to alternatively spliced mRNAs are schematically shown on the right (bottom panel). *M*, marker (DNA Ladder Mix).

To investigate the characteristics of PIE designer circRNAs further, we performed another time-course experiment including the additional time points 4 and 48 h. As demonstrated in Fig. 4.8, 4 and 48 h after transfection, only moderate effects on alternative splicing of the chosen mRNAs were detected. Additionally, alternative splicing of the hnRNP L target gene *DAF*, was checked by RT-PCR. In the case of *DAF* intron 7, hnRNP L acts as a splicing activator, promoting the efficient removal of the intron. When *CA-SELEX* or $(CA)_{100}$ circRNAs are transfected in HeLa cells, they bind hnRNP L and cause *DAF* intron 7 retention. However, the effect of *CA-SELEX* circRNA sponges was less prominent when compared to $(CA)_{100}$, or in comparison to hnRNP L knockdown experiments (Hung *et al*., 2008). Similar to the previous experiments, the maximal effect on alternative splicing was reached 24 h after transfection. Increasing the number of SELEX sequences did not change the effect on

alternative splicing. This indicates that four SELEX sequences, forming a CA-rich RNA stretch of 92 nt, are sufficient for partial restraining hnRNP L from binding to its target pre-mRNAs. Besides, transfected PIE circRNAs were detected in total RNA by RT-PCR with the circRNA-specific primers. As shown in Fig. 4.8B, we observed a relatively constant level of the PIE circRNAs 4 – 48 hours after transfection.

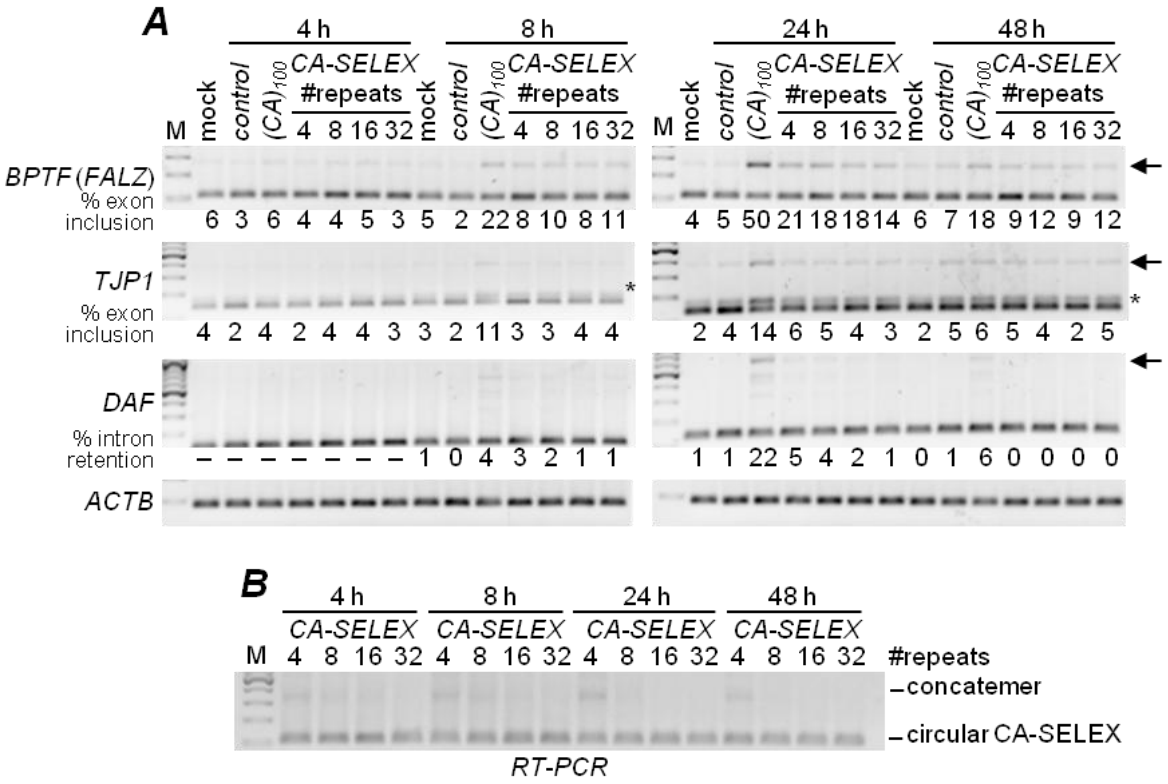

Figure 4.8 *CA-SELEX* PIE circRNAs modulate splicing in a time-course experiment.
HeLa cells were transfected with the *control*, $(CA)_{100}$, and *CA-SELEX* (*X4/8/16/32*) PIE circRNAs. Total RNA was isolated 4, 8, 24, and 48 h post-transfection and used for RT-PCR.
(A) Detection of exon inclusion and intron retention cases upon transfections of PIE hnRNP L sponges. RT-PCR was performed with primers against *BPTF* (*FALZ*), *TJP1*, *DAF*, as well as *ACTB* (used as a loading control). For *TJP1*, an asterisk marks the mispriming RT-PCR product. The mock sample corresponds to a mock transfection, *control* PIE circRNA transfection is marked as *control*. The percentages of exon inclusion or intron retention are listed below each lane. After 4 h, no PCR products corresponding to intron retention of *DAF* was detected (marked as dash). *M*, marker (DNA Ladder Mix).
(B) Detection of transfected circular *CA-SELEX* (*X4/8/16/32*) PIE RNA. After the time-course experiment, transfected *CA-SELEX* PIE circRNAs were detected by RT-PCR with gene-specific primers. The additional upper band (concatemer) represents a rolling-circle RT-PCR by-product of *CA-SELEX X4* circRNA. Positions of the respective PCR products are shown on the right. *M*, marker (DNA Ladder Mix).

Interestingly, exon inclusion ratios for both *BPTF* and *TJP1* vary between these two time-course experiments. We suppose that the main source of this difference comes from biological variations, such as differences in PIE circRNA transfection efficiencies or dependencies on cell cycle states.

In summary, we implicated the PIE system for production of designer circRNA for specific protein sponge function, where we compared CA repeats with the CA-rich SELEX sequence and their binding to the target protein. HnRNP L sponges with SELEX sequences affect the alternative splicing of hnRNP L target genes to a lesser extent in comparison to the positive control *(CA)$_{100}$* circRNA. However, the SELEX sequence is expected to be more specific and cause less off-target effects than CA-repeats alone.

4.4 Expressed Tornado circRNA with protein sponge function

To further pursue the aim of protein sponge design, we applied another vector-based circRNA expression system developed by Litke and Jaffrey (2019). This system is based on the Tornado expression cassette and relies on ribozyme activity of the transcript and ligation of tRNA intron by the endogenous RtcB protein. The Tornado system was shown to generate higher levels of circular RNA than any other expression system developed so far. As this system is more suitable for expression of short circRNAs, we incorporated two and four SELEX sequences as well as $(CA)_{20}$ in the Tornado vector, as schematically shown in Fig. 4.9A. One of the SELEX X4 constructs also contains an F30 arm for proper folding of the Broccoli aptamer, which provides direct RNA detection by fluorescence imaging. Additionally, secondary structure prediction for these circRNAs showed the accessibility of the hnRNP L binding sites, as they were not detected to form any stable secondary structures (Fig. 4.9B). Next, we assayed the expression of the circRNA containing four SELEX repeats in HeLa cells upon transfection of the Tornado constructs in a time-course experiment. As shown in Fig. 4.10, *CA-SELEX X4* and *CA-SELEX X4* Broccoli circRNAs were stably expressed. They were detected by both RT-PCR (Fig. 4.10A&B) and analysis of total RNA by gel electrophoresis (Fig. 4.10D&E). Notably, when detected by RT-PCR, circRNA remained stable for at least four days, while the linear precursor RNA was detectable at comparatively low levels due to its rapid processing (Fig. 4.10A&B). Next, total RNA obtained from CA-SELEX X4 transfection was separated on a SYBR Gold-stained E-Gel (Fig. 4.10D). Here, we could visualize the abundant endogenous RNAs such as tRNA, 5S and 5.8S RNA. In samples transfected with CA-SELEX X4 construct, an additional band of near equal intensity to 5S was detected. This band was identified as the Tornado circRNA. For *CA-SELEX X4 Broccoli* circRNA, we analyzed the mobility of the circRNA band (described below) and stained the total RNA gel with DFHBI to detect the Broccoli-containing transcripts (Fig. 4.10E). Comparing these samples to mock transfection, we demonstrated that the specific bands originate from the Tornado expression system. In addition, we tested expression of the *(CA)$_{20}$* and *CA-SELEX X2* by RT-PCR two days after transfection, where no linear precursor was detected (Fig. 4.10C).

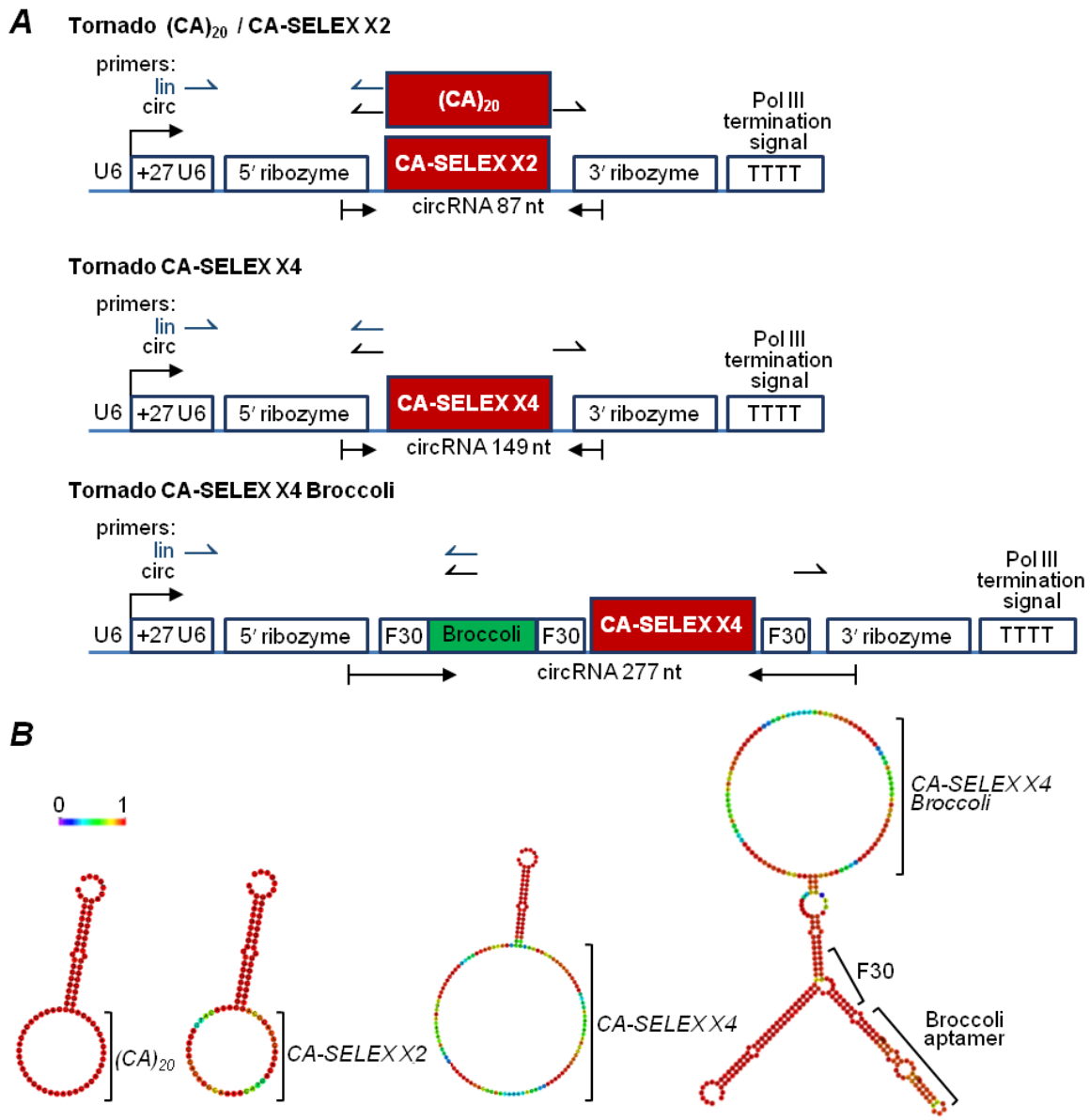

Figure 4.9 Tornado CA-SELEX constructs.

(A) Schematic of $(CA)_{20}$, CA-SELEX X2, CA-SELEX X4, and CA-SELEX X4 Broccoli constructs. Pol III transcription is driven by U6 promotor with the first 27 nucleotides of U6. The circularizing sequences are flanked by Twister ribozymes (5′ and 3′ ribozymes). The Tornado circRNA expression cassette ends with the Pol III termination site (T-stretch). CA-SELEX X4 Broccoli construct in addition contains the Broccoli aptamer sequence and three short sequences named F30. CA-SELEX sequence is a CA-rich SELEX-derived hnRNP L binding sequence (5′-ATACATGACACACACACGCA-3′; Hui *et al.*, 2005).

(B) Predicted Tornado circRNA secondary structures. HnRNP L binding sequences, as well as the F30 3-way junction, and the Broccoli aptamer sequence, are marked. The color code denotes the probability of base-pairing from zero to one (from violet to red, respectively). For unpaired regions the color denotes the probability of being unpaired.

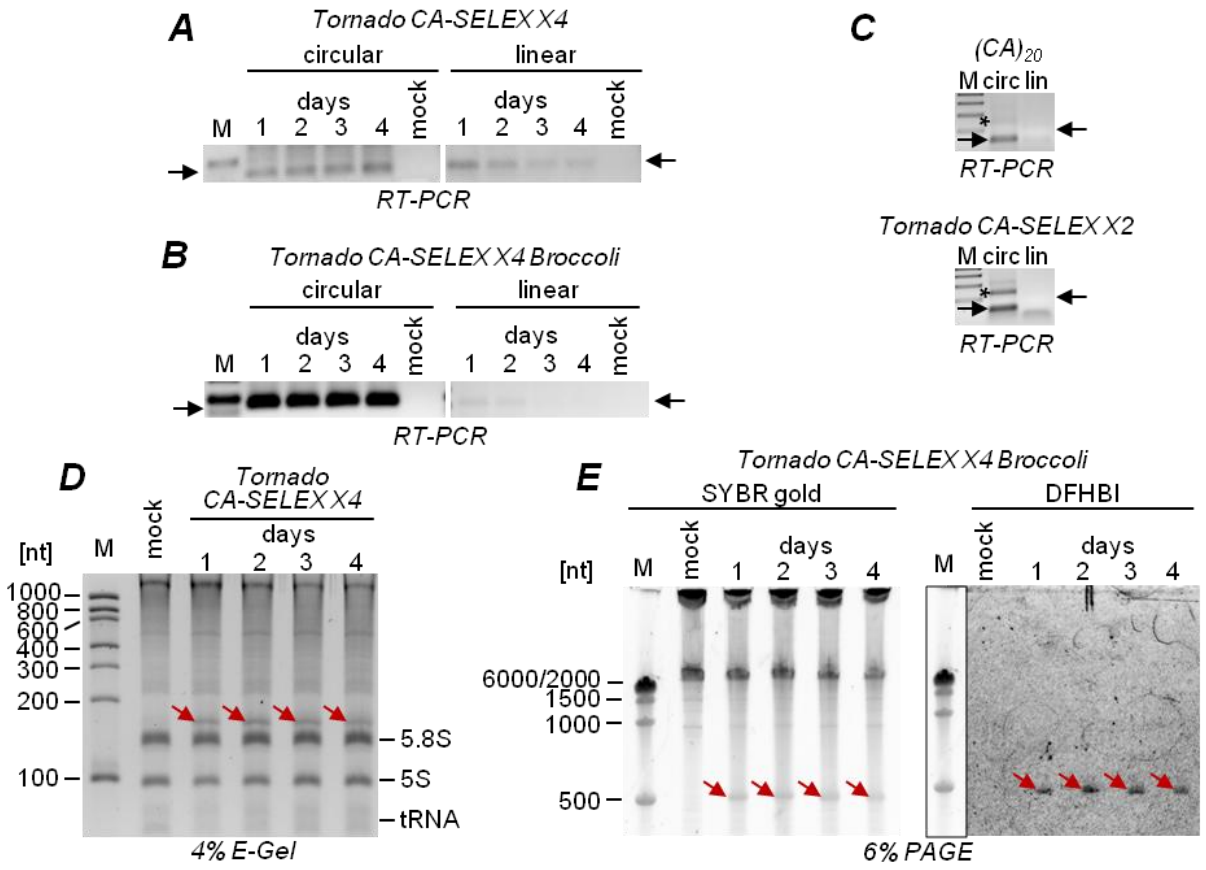

Figure 4.10 Analysis of expression and stability of Tornado circRNAs.
RNA from HeLa cells after transient transfection with $(CA)_{20}$, CA-SELEX X2, CA-SELEX X4, or CA-SELEX X4 Broccoli constructs was harvested two days post-transfection or in a time-course experiment and compared to mock transfection.
(A, B, C) Detection of Tornado circular and precursor linear RNA by RT-PCR. Total RNA after transfection was used for the detection of the linear and circular RNA by RT-PCR with circRNA-specific primers. The expected PCR products are shown by arrows. The additional upper band (concatemer) represents a rolling-circle RT-PCR by-product ***(C)***. *M*, marker (LR DNA Ladder).
(D, E) Direct visualization of expressed Tornado circRNA in total RNA samples. Total RNA (3 µg) from the time-course experiment was visualized either by E-Gel electrophoresis ***(D)***, or by 6% polyacrylamide gel electrophoresis ***(E)***. For direct in-gel detection of Broccoli-tagged circRNA, the 6% polyacrylamide gel was additionally stained with DFHBI (***E***, right panel), and then stained with SYBR Gold to reveal total RNA (***E***, left panel). Bands corresponding to circRNA are marked by arrows. The experiment shown in ***(E)*** was performed by Anna Wilmen. *M*, marker (LR ***(D)*** and HR ***(E)*** RNA ladder).

Thus, the Tornado system implemented for circRNA production provides high levels of the expressed circRNA that are similar to the most abundant endogenous RNAs.

In order to confirm the circular configuration of the expressed RNA, we first applied RNase R treatment on total RNA samples after transfection of Tornado constructs (Fig. 4.11A). A band remaining after RNase R treatment corresponds to RNase R-resistant RNA molecule, such as circRNA. For *CA-SELEX X4*, the circRNA band runs very close to the 5.8S rRNA, which is partly resistant to RNase R treatment, so that the circRNA band is hardly distinguishable from the 5.8S rRNA. An additional band was observed in total RNA from HeLa cells transfected with CA-SELEX X4 Broccoli Tornado construct, this band was absent from mock

RNA and resistant to RNase R. Next, we tested the characteristic change in mobility of the circRNA in gels with different polyacrylamide concentrations. In the case of *CA-SELEX X4 Broccoli* circRNA, a prominent band that migrates anomalously on denaturing polyacrylamide gels, running at ~500 nt in a 6% gel, and ~600 nt in a 9% gel, was detected (Fig. 4.11B). *$(CA)_{20}$* and *CA-SELEX X2* circRNAs were assayed similarly (Fig. 4.11C), showing a migration pattern of <100 nt in 12% gel, and >100 nt in 15% gel. Therefore, we validated the circular configuration of the transcripts expressed from the Tornado constructs and assessed their stable expression in HeLa cells.

We next estimated intracellular concentrations of the expressed Tornado circRNAs, using RT-qPCR and *in vitro*-produced circRNA standards for absolute quantification (Fig. 4.12). As circRNAs are resistant to exoribonucleases, they can potentially reach exceptionally high concentrations in cells, which coincides with our observations on direct circRNA visualization in total RNA on gels. First, we produced circRNAs *in vitro*, which could be detected with the original circRNA-specific primers (Fig. 4.12A). Then, we used these circRNAs in RT-qPCR assays for creating a standard curve. In parallel, we assayed the RNA from Tornado-transfected cells. The number of cells was measured and considered for absolute calculations. All three biological replicates demonstrated the micromolar range of circRNA intracellular concentration (Fig 4.12B).

Furthermore, the *CA-SELEX X4* and *CA-SELEX X4 Broccoli* circRNA concentrations were estimated by Bioanalyzer, which yielded similar values in the micromolar range (Fig. 4.12C&D). In sum, we demonstrated remarkably high expression levels of the designer circRNAs. Their high abundance argues for target protein saturation and supports potential applications of circRNAs as protein sponges for various protein targets.

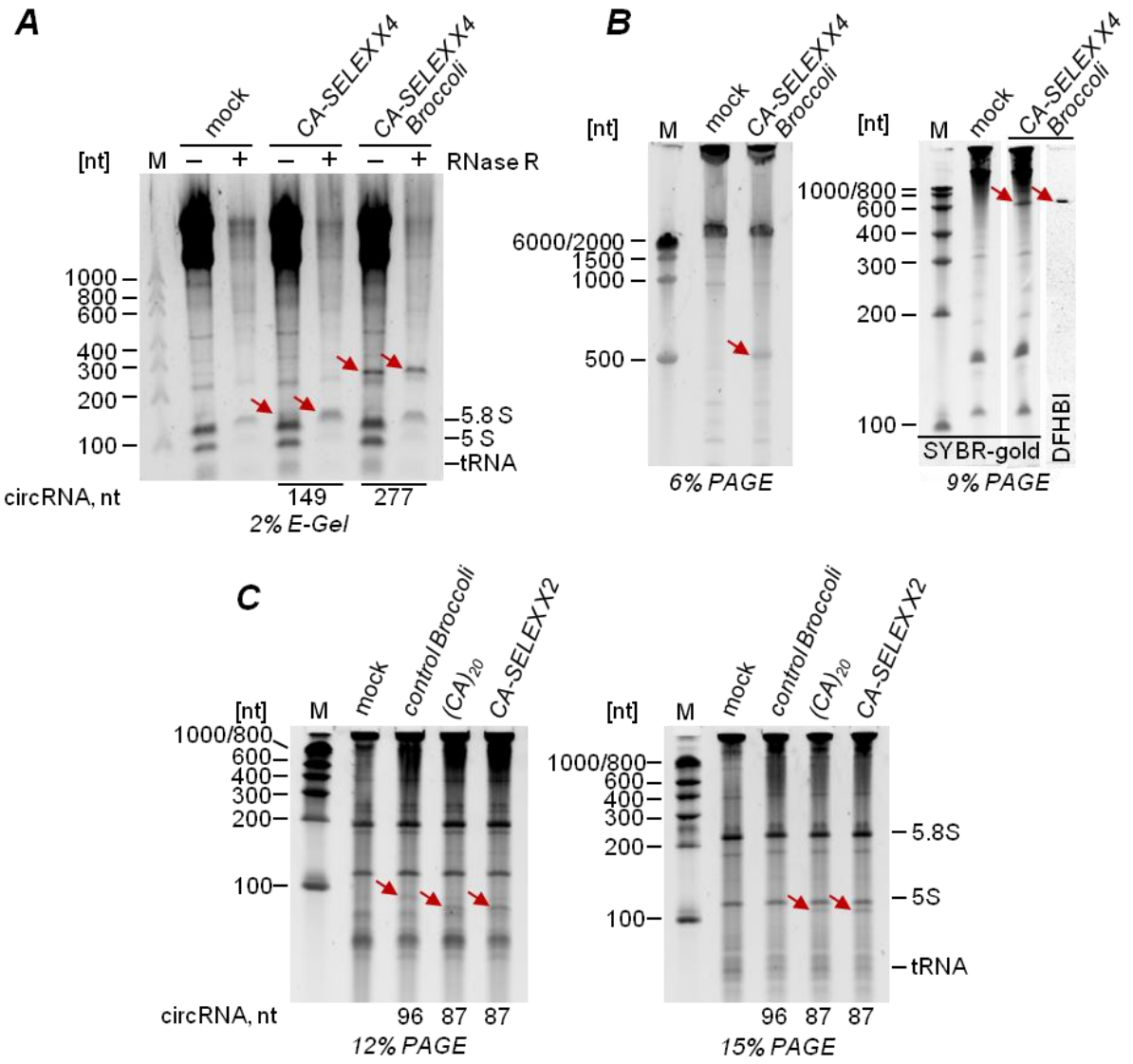

Figure 4.11 Detection of circRNA upon transient transfection of Tornado constructs.
(A) RNase R treatment of total RNA after Tornado transfections. Total RNA was isolated from HeLa cells after mock, CA-SELEX X4, or CA-SELEX X4 Broccoli Tornado transfections. RNA was treated with (+) or without (–) RNase R and loaded on an E-Gel. Each lane corresponds to 4 µg of total RNA. CircRNAs remaining after RNase R digestion are marked by arrows, and their sizes are shown below. Ribosomal 5S and 5.8S RNA, and tRNA are marked. *M*, marker (LR RNA ladder).
(B) Detection of expressed *CA-SELEX X4 Broccoli* circRNA. HeLa cells were transfected with CA-SELEX X4 Broccoli construct. Two days after transfection, total RNA was isolated. 4 µg of total RNA was analyzed on denaturing polyacrylamide gel (6% and 9%). For direct in-gel detection of Broccoli-tagged circRNA, the 9% polyacrylamide gel was additionally stained with DFHBI (right panel), and then with SYBR Gold to reveal total RNA (left panel). Bands corresponding to circRNA are marked by arrows. Mock transfection was used as a negative control. *M*, markers, HR (left) and LR (right) RNA ladder.
(C) Detection of expressed *$(CA)_{20}$* and *CA-SELEX X2* Tornado circRNA. Following transfection of control Broccoli, $(CA)_{20}$, and CA-SELEX X2 Tornado constructs, total RNA (3 µg each) was visualized by denaturing polyacrylamide electrophoresis (12% and 15%). Bands corresponding to circRNAs are marked by arrows, circRNA sizes are given below. Ribosomal 5S and 5.8S RNAs, and tRNA are marked on the right. *M*, marker (LR RNA ladder).

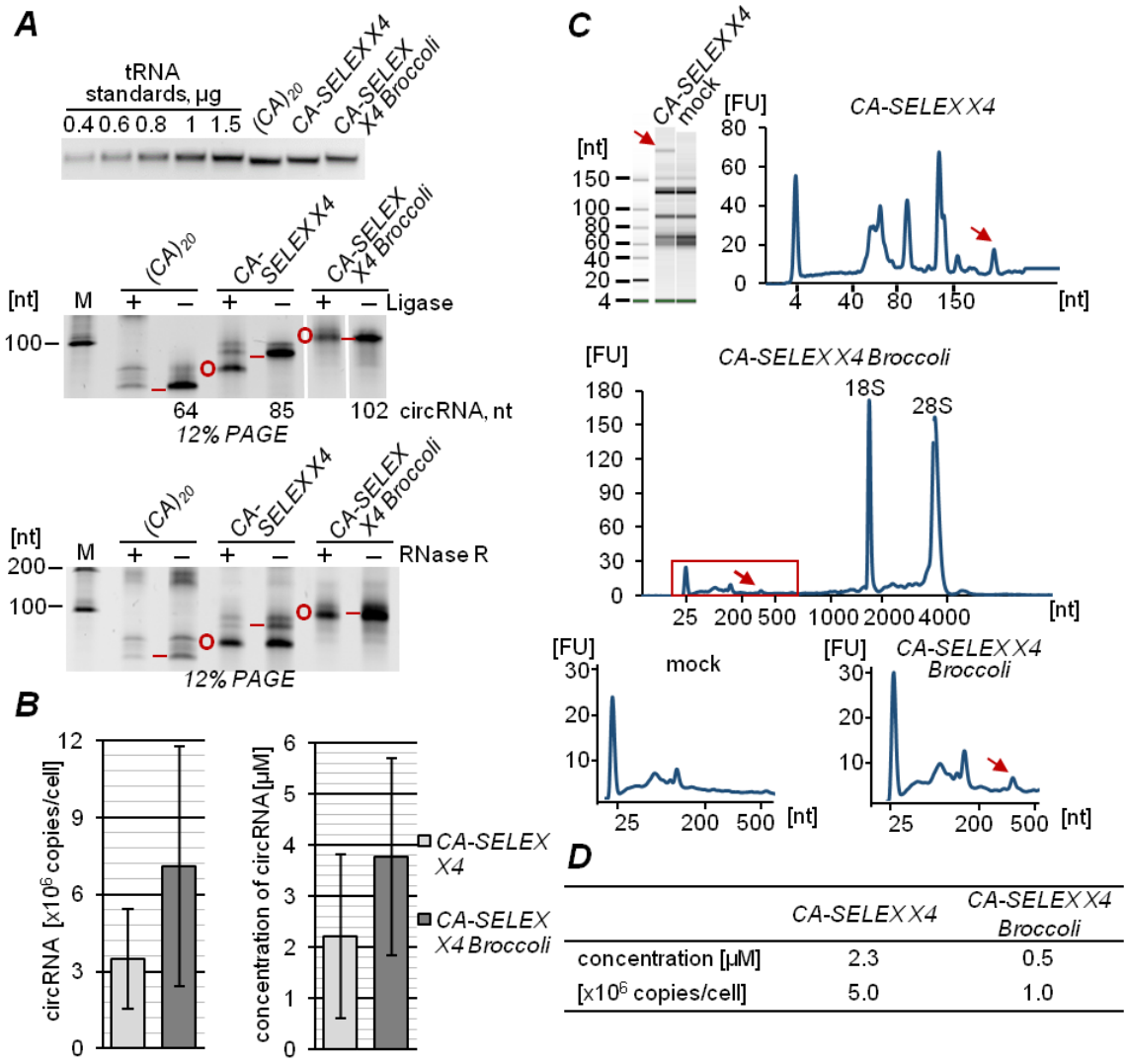

	CA-SELEX X4	CA-SELEX X4 Broccoli
concentration [µM]	2.3	0.5
[x10^6 copies/cell]	5.0	1.0

Figure 4.12 Absolute quantification of Tornado circRNA expressed in HeLa cells.
(A) *In vitro* preparation of standard circRNAs for absolute quantification by RT-qPCR. RNA was *in vitro* transcribed from the corresponding synthetic annealed oligonucleotides. The quality of the transcripts and, additionally to Qubit measurements, the RNA concentrations were estimated by agarose gel electrophoresis with tRNA standards (upper panel). Transcripts were ligated with RNA ligase and visualized on 12% polyacrylamide gel (middle panel). Ligated RNA was treated with and without (+/–) RNase R and run on 12% polyacrylamide gel (lower panel). *In vitro*-produced $(CA)_{20}$ circRNA formed multiple by-products after the ligation reaction and was not used for absolute quantification of the corresponding Tornado circRNA. *CA-SELEX X4* and *CA-SELEX X4 Broccoli* circRNAs were used for RT and subsequent qPCR in 5 dilutions for plotting a calibration curve for quantification of the corresponding Tornado-expressed circRNAs. *M*, marker (LR RNA ladder).
(B) Absolute quantification of expressed circRNA based on RT-qPCR. Average numbers of circRNA copies per cell (left) and intracellular circRNA concentration (right) were calculated as an average of three biological replicates. Error bars denote standard deviations (n = 3).
(C) Detection of *CA-SELEX X4* and *CA-SELEX X4 Broccoli* circRNA in total RNA by Bioanalyzer. After the transfection of HeLa cells with the Tornado constructs, total RNA was loaded on a Bioanalyzer chip. *CA-SELEX X4* circRNA is marked on the gel and the chromatogram with red arrows. For *CA-SELEX X4 Broccoli*, circRNA is marked with red arrows on the chromatogram (upper panel) and zoomed chromatogram in comparison with mock transfection (lower panel). For absolute quantification, the highlighted peaks were manually integrated and the resulted values were used for further calculations. FU refers to fluorescence units.
(D) Summary of absolute quantification of Tornado circRNAs obtained with Bioanalyzer.

4.4.1 Tornado-expressed circRNAs bind hnRNP L in HeLa cells

Prior to the analysis of hnRNP L target genes, binding of Tornado-expressed circRNAs to hnRNP L protein was assayed by RIP. Similar to the RIP assay described for PIE circRNA transfections, cell lysates were immunoprecipitated with FLAG or hnRNP L antibodies. In addition, IMP3, which is a protein with high affinity to CA-rich sequences (Schneider *et al*., 2019), was used here as a specificity control. In detail, cells were transfected with $(CA)_{100}$ Broccoli and CA-SELEX X4 Broccoli Tornado constructs, corresponding cell lysates were prepared after 48 h and probed with the antibodies. Later RT-(q)PCR assays detected efficient binding of the designer circRNAs to hnRNP L (Fig. 4.13A&B). IMP3 also bound CA-rich circRNAs, although at much lower efficiency than hnRNP L. As shown in Fig. 4.13B, the binding efficiency to IMP3 and hnRNP L counted to 6% vs. 82% for *$(CA)_{100}$ Broccoli* and 9% vs. 24% for *CA-SELEX X4 Broccoli* circRNA (Fig.4.13B). The immunoprecipitated proteins were identified as hnRNP L and IMP3 by Western blot; GAPDH was detected as input and RIP negative control (Fig. 4.13C).

Next, we tested the shorter CA-rich Tornado circRNAs for hnRNP L binding in a similar RIP experiment (Fig. 4.14). Direct interaction of *SELEX X2* and *$(CA)_{20}$* circRNAs with hnRNP L was shown by RT-(q)PCR (Fig. 4.14A&B). *$(CA)_{20}$* Tornado circRNA demonstrated a 10.7% RIP efficiency, whereas *$(CA)_{100}$ Broccoli* was shown to bind hnRNP L with 82% efficiency (Fig. 4.13B). *CA-SELEX X2* circRNA sponged hnRNP L less efficiently, showing only 3.8% binding. *ACTB* mRNA was not detected in RIP samples (Fig. 4.14C), nor was GAPDH protein co-immunoprecipitated with hnRNP L (Fig. 4.14C), confirming the specificity of the RIP experiment. Altogether, this result argues for a direct interaction between hnRNP L and the expressed designer circRNAs. Four hnRNP L-specific SELEX sequences performed very well, demonstrating binding of up to 24%. However, *$(CA)_{100}$ Broccoli* confirmed the best performance in terms of hnRNP L affinity.

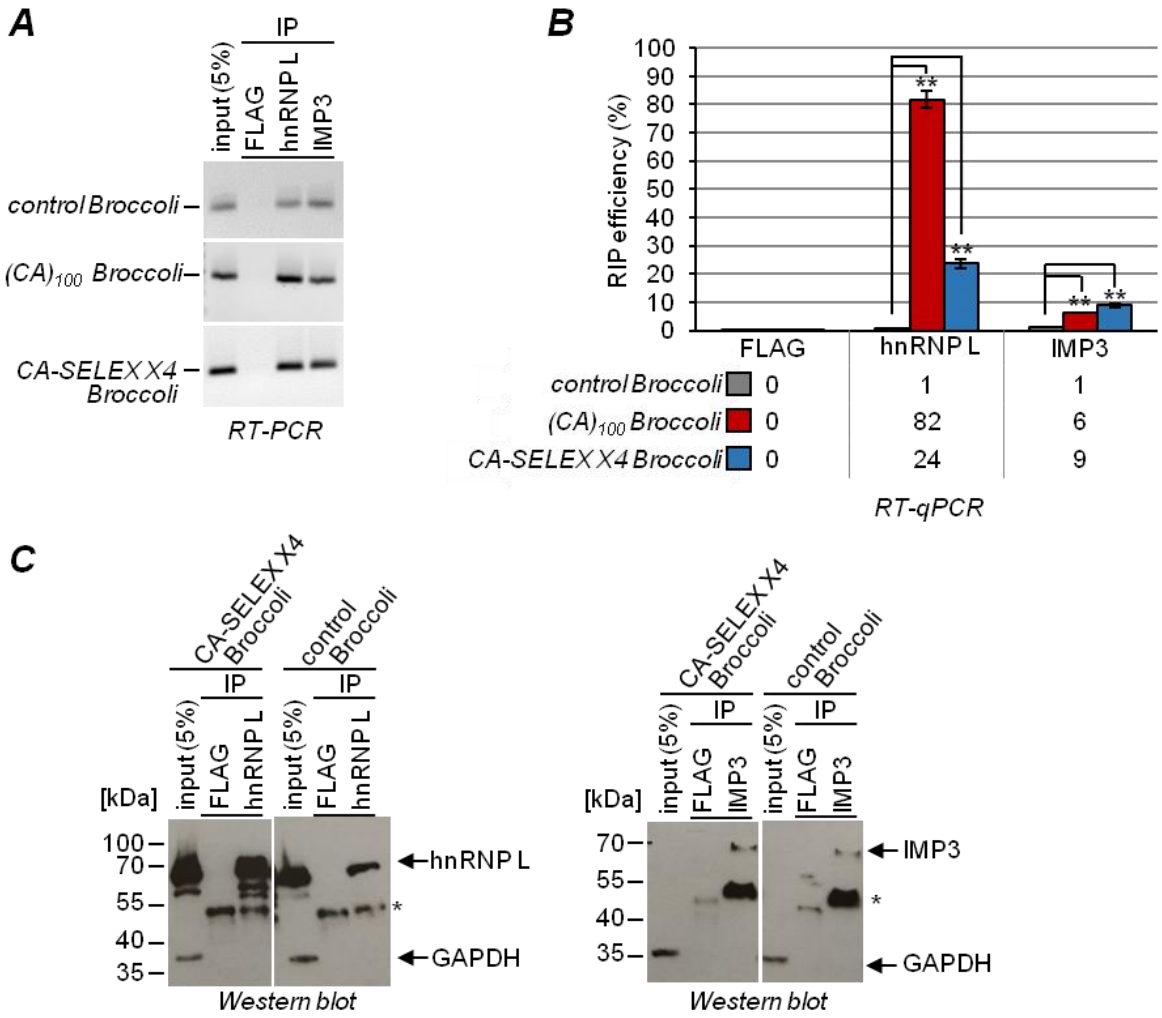

Figure 4.13 HnRNP L binding by Tornado-expressed CA-sponge circRNAs.
(A, B) RT-(q)PCR detection of Tornado circRNA after RNA immunoprecipitation (RIP) experiment. HeLa cells were transfected with the control Broccoli, $(CA)_{100}$ Broccoli, or CA-SELEX X4 Broccoli constructs. Cell lysates were prepared two days after transfection and immunoprecipitated using anti-hnRNP L, -IMP3 (specificity control), or -FLAG (negative control) antibodies. After subsequent RNA isolation from IP and input samples, transfected circRNAs were detected by RT-PCR ***(A)*** and RT-qPCR ***(B)***. RIP efficiency (%) for the corresponding constructs is shown below the qPCR diagram. Error bars represent standard deviations (n = 3; ** = $p < 0.01$).
(C) Western blots demonstrating hnRNP L and IMP3 binding in hnRNP L and IMP3 RIP experiments. Input and IP samples were analyzed by Western blot with antibodies against hnRNP L (left panel), IMP3 (right panel), and GAPDH. IgG heavy chain (~50 kD) is marked with asterisks.

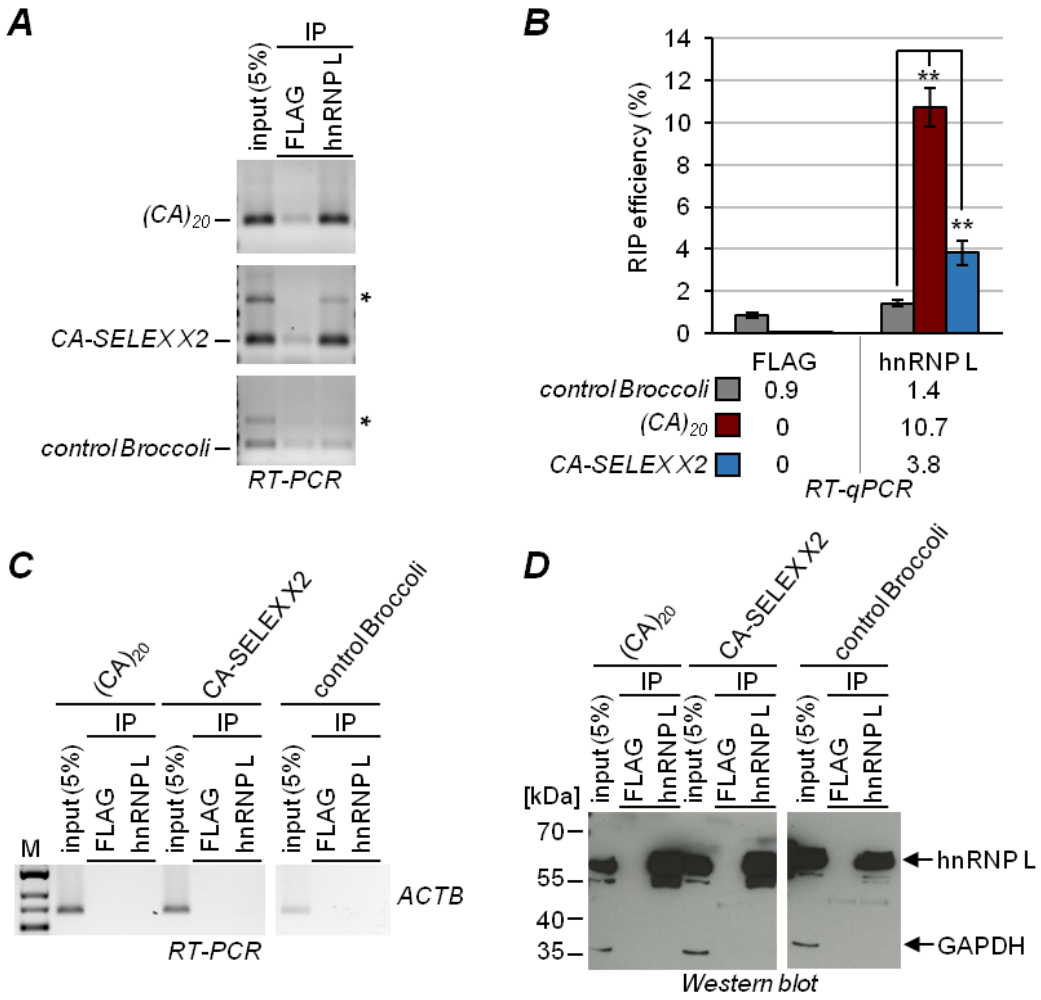

Figure 4.14 Analysis of short Tornado-expressed circRNA hnRNP L sponges by co-immunoprecipitation.

HeLa cells were transfected with the $(CA)_{20}$, CA-SELEX X2, or control Broccoli Tornado constructs. Cell lysates were harvested two days post-transfection and immunoprecipitated using anti-hnRNP L and -FLAG (negative control) antibodies.

(A) RT-PCR detection of the Tornado-expressed circRNA in input and IP samples. The additional bands above (marked with the asterisks) represent rolling-circle RT-PCR products.

(B) RT-qPCR calculations of RIP efficiency for the expressed Tornado circRNAs. FLAG- and hnRNP L-precipitated RNAs were detected by RT-qPCR and their RIP efficiency was plotted (also shown below the diagram, %). CircRNA-derived *Ct* values from the IP samples were normalized to the input, and primer amplification efficiency was considered. Error bars represent standard deviations (n = 3; ** = $p < 0.01$).

(C) RT-PCR specificity control for the RIP experiment. *ACTB* mRNA was amplified by RT-PCR from input and IP samples and used as a negative control for RIP. *M*, marker (DNA Ladder Mix).

(D) Detection of hnRNP L and GAPDH levels after RIP experiment by Western blot. The input and IP samples were analyzed by Western blot with antibodies against hnRNP L and GAPDH.

4.4.2 Designer Tornado circRNAs alter alternative splicing of hnRNP L target genes in HeLa cells

As an initial test for whether hnRNP L sponging by Tornado designer circRNAs affects alternative splicing, we chose the longer circRNAs with four SELEX sequences. Therefore, we assayed splicing of three known hnRNP L targets *BPTF* (*FALZ*), *TJP1, and DAF,* and

compared the effects with hnRNP L knockdown, relative to luciferase control (Fig. 4.15). The effects of both *CA-SELEX X4* and *CA-SELEX X4 Broccoli* circRNAs on alternative splicing were similar, getting close, but not reaching the effect of hnRNP L knockdown. For *BPTF* (*FALZ*) and *TJP1,* an increase of exon inclusion from 19% and 9% to up to 82% and 41%, respectively, was detected. Intron retention for *DAF* mRNA increased from background levels in the control sample to >10% when hnRNP L was sponged with *CA-SELEX X4* circRNA. In general, the maximal effect on alternative splicing was detected two days after transfection of Tornado constructs, which presumably results from a compromise between the endogenous RNA turnover and Tornado circRNA accumulation.

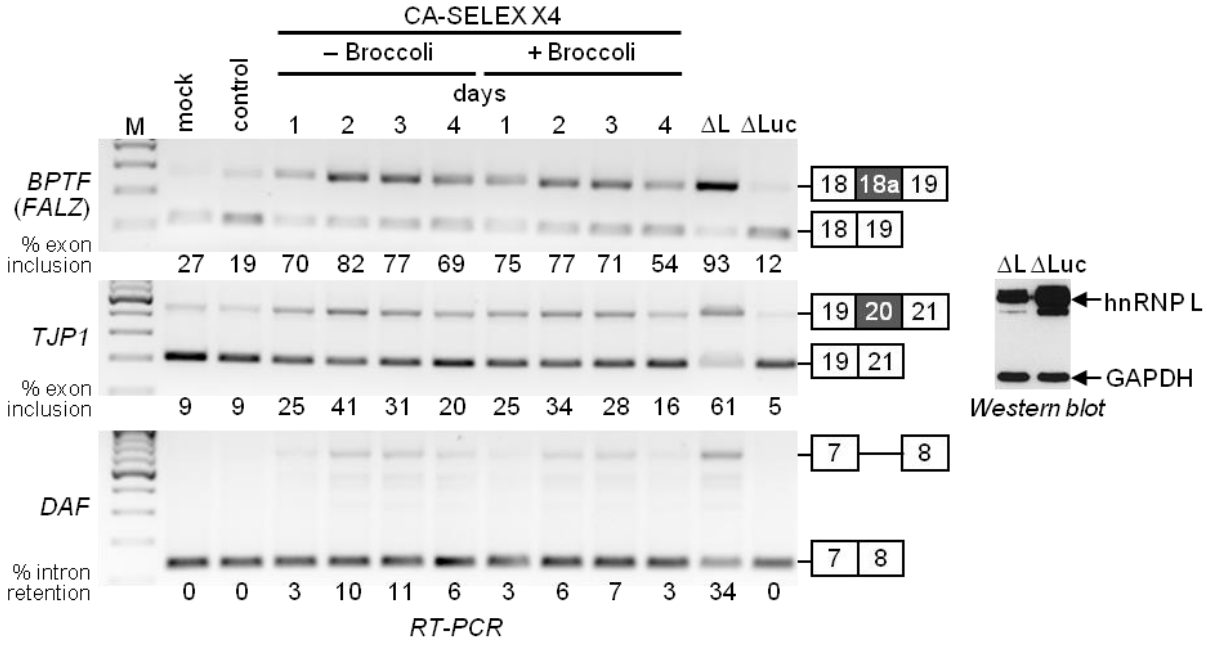

Figure 4.15 Expressed CA-sponges modulate alternative splicing in HeLa cells.
HeLa cells were transfected with control, CA-SELEX X4, or CA-SELEX X4 Broccoli Tornado constructs or subjected to siRNA-mediated knockdown of hnRNP L. RNA from CA-SELEX X4- and CA-SELEX X4 Broccoli-transfected cells was harvested one, two, three, and four days post-transfection. Alternative splicing of endogenous *BPTF* (*FALZ*), *TJP1* mRNA (exon skipping), and *DAF1* (intron retention), as schematically shown on the right, was assayed by semiquantitative RT-PCR. Exon skipping and intron retention are shown as a percentage below. Western blot analysis of relative hnRNP L and GAPDH amounts is presented on the right. ΔL and ΔLuc designate knockdown of hnRNP L and luciferase, respectively. *M*, marker (DNA Ladder Mix).

Next, we additionally included the shorter Tornado circRNA and analyzed a broader range of hnRNP L targets, including the recently discovered ones (Schreiner *et al*., in press; Fig. 4.16). HnRNP L acts as a splicing repressor when bound to CA-rich ISS or ESS sites, hindering the recruitment of spliceosomal components, which in turn leads to exon skipping. When hnRNP L is limiting, its repressor function is minimized, resulting in partial exon inclusion (Fig. 4.16A). Splicing activator function of hnRNP L assumes hnRNP L-driven exon inclusion or intron removal, which is diminished when hnRNP L is bound by circRNA sponges. When hnRNP L regulates exon inclusion, hnRNP L sequestration promotes exon

skipping (Fig. 4.16B). In the case of *DAF* intron 7, hnRNP L acts as a splicing activator, promoting efficient intron splicing. When the designer sponges for sequestration of hnRNP L protein are introduced, hnRNP L cannot promote efficient intron removal and introns are partially retained (Fig. 4.16C). Another example is hnRNP L suppression of multiple exons (Hung *et al*., 2008). In the case of protein sponge expression, *ARGBP2* variable exons 4a and 4b become detectable by RT-PCR (Fig. 4.16D).

Here, we conclude that the CA-rich designer circRNAs reproducibly and strongly affect alternative splicing of a broad range of hnRNP L targets, which include various hnRNP L mechanisms of action. The effects are stable for at least four days upon transfection and comparable with the hnRNP L knockdown effects (Fig. 4.15). We observed strong effects on alternative splicing after expression of each designer circRNAs, ranking in strength consistently for most of the targets in this order: *CA-SELEX X2*, *$(CA)_{20}$*, *CA-SELEX X4 Broccoli*, *CA-SELEX X4*.

4.4.3 Sponge Tornado circRNAs shift nuclear-cytoplasmic hnRNP L distribution

As hnRNP L is known to shuttle between nucleus and cytoplasm (Pinol-Roma *et al*., 1989), with a predominant nuclear localization, we decided to check its nuclear-cytoplasmic distribution in cells expressing the CA-rich circRNAs, and compare it with mock and control Tornado transfections (Fig. 4.17). After transfection of HeLa cells with the $(CA)_{20}$, CA-SELEX X4 Broccoli, control construct, or mock control, cells were fractionated into cytoplasmic and nuclear fractions. Equivalent amounts of these fractions were used for Western blot (Fig. 4.17A) and, after RNA isolation, for the detection of the Tornado circRNA localization by RT-qPCR (Fig. 4.17B). For mock and control construct samples, Western blot demonstrated typical hnRNP L nuclear-cytoplasmic distribution (~80/20%); in contrast, in cells transfected with the designer hnRNP L sponges, this distribution shifted considerably (~50%/50%). Localization of the expressed circRNAs, as well as typically localized in the cytoplasm (*GAPDH*) and nucleus (snoRNA *U78*) RNAs was assessed by RT-qPCR (Fig. 4.17B). As hnRNP L is involved in mRNA transport (Krecic and Swanson, 1999), this cytoplasmic shift may affect many cellular processes. In this case, when designer circRNA were transfected, *GAPDH* demonstrated no definite localization preference, while a control transfection confirmed characteristic cytoplasmic localization of the *GAPDH* mRNA. U78 RNA was used as a control for cell fractionation and demonstrated clear nuclear localization. CircRNAs were either equally distributed between the nucleus and the cytoplasm (*control Broccoli* and *CA-SELEX X4 Broccoli*) or predominantly cytoplasmic [*$(CA)_{20}$*]. In sum, we conclude that hnRNP L localization was dramatically affected by the designer circRNAs.

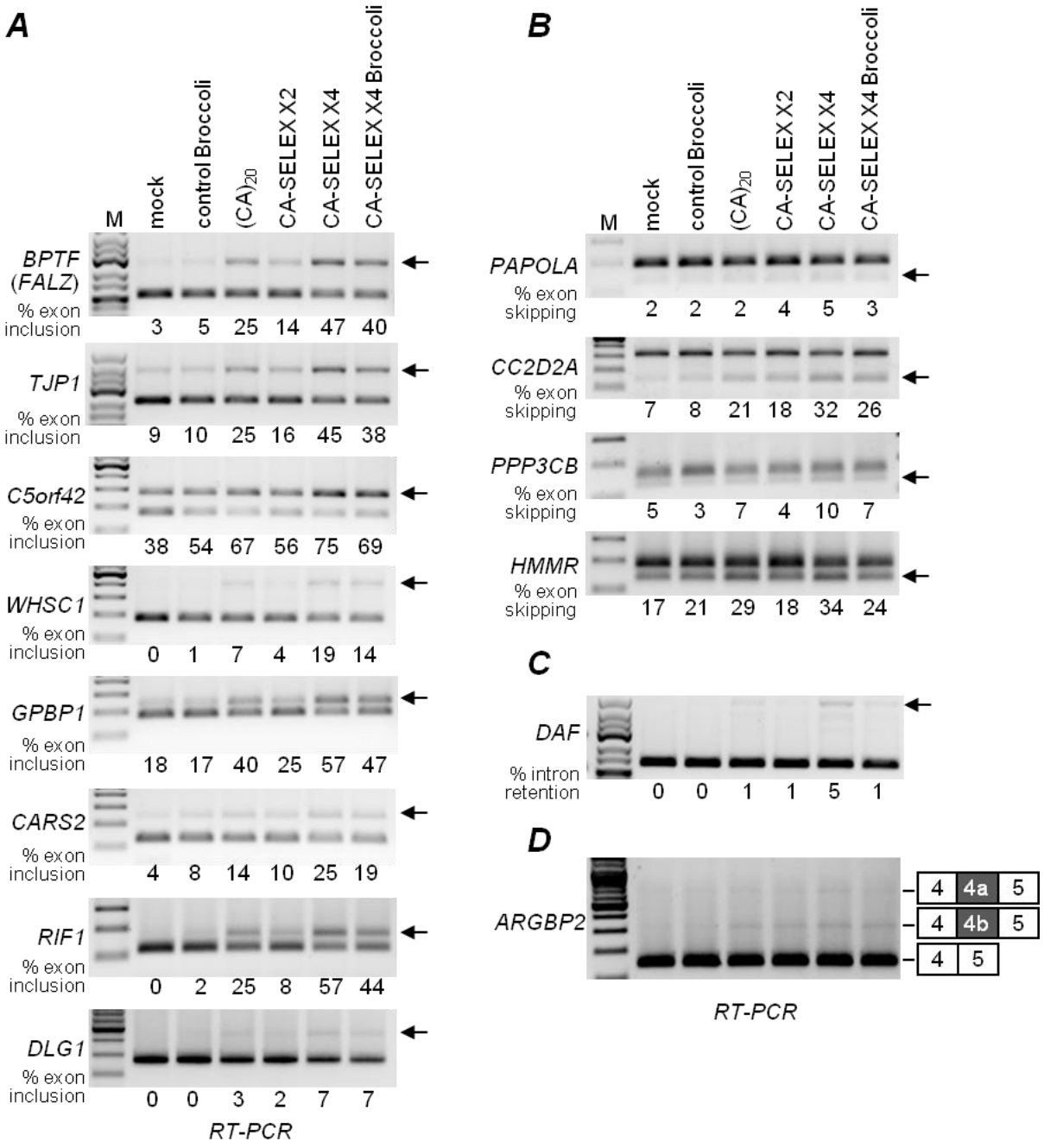

Figure 4.16 Transfected CA-sponge circRNAs affect hnRNP L alternative splicing targets in HeLa cells.

(A, B, C, D) Total RNA was prepared from HeLa cells two days post-transfection. Isolated RNA was used for RT-PCR with primers against hnRNP L alternative splicing targets. The percentages of exon inclusion, exon skipping, and intron retention are listed below the corresponding lanes. Positions of PCR products corresponding to alternatively spliced mRNAs are shown on the right. Alternative splicing was assayed for the mRNAs, where hnRNP L acts as a splicing repressor ***(A)***, splicing activator ***(B)***, or contributes to intron retention ***(C)*** and suppression of multiple exons ***(D)***. *M*, marker (DNA Ladder Mix).

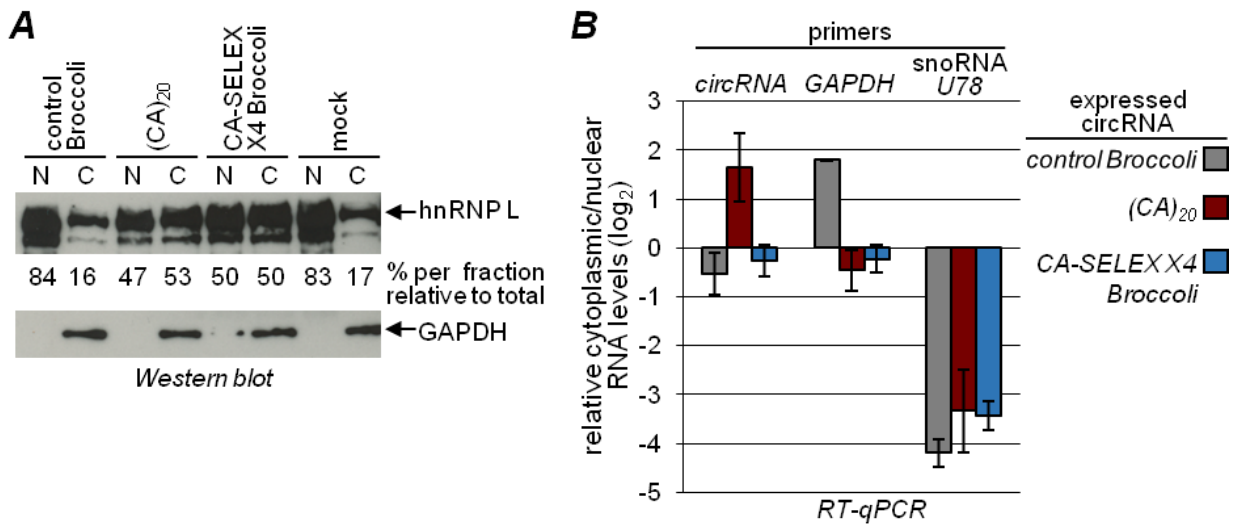

Figure 4.17 Expressed CA-sponge circRNAs shift nuclear-cytoplasmic hnRNP L distribution.
HeLa cells were transfected with the control Broccoli, $(CA)_{20}$, or CA-SELEX X4 Broccoli Tornado constructs, and harvested two days post-transfection. Cell pellets were fractionated into nuclear and cytoplasmic extracts.
(A) Detection of the hnRNP L nuclear/cytoplasmic distribution. Equivalent amounts of the nuclear (N) and cytoplasmic (C) fractions were analyzed by Western blot with antibodies against hnRNP L and GAPDH. Relative amounts of hnRNP L from each fraction were calculated by densitometry.
(B) Analysis of RNA nuclear/cytoplasmic distribution. After fractionation, equivalent RNA amounts from the nuclear and cytoplasmic fractions were assayed by RT-qPCR. The levels of the respective Tornado-expressed circRNAs, as well as *GAPDH* mRNA and snoRNA *U78*, were assayed. The graph represents data obtained from two biological replicates. Whiskers denote the standard deviation of two independent experiments.

4.5 Antisense circRNA for splicing modulation

In addition to developing designer circRNA protein sponges, we addressed the application of antisense circRNAs as splice-switching oligonucleotides with the potential therapeutic application. Therefore, we chose *CD45* as a target for alternative splicing modulation and designed the corresponding circRNAs containing the perfectly complementary antisense region, which comprises 30 or 40 nt (Fig. 4.18A). At first, we focused on alternative splicing of the *CD45* minigene (Preussner *et al*., 2012). The minigene was previously characterized as a model for *CD45* alternative splicing studies, where exons 4, 5, and 6 are alternatively spliced. In addition, the minigene contains the flanking constant exons: fused exons 2 and 3, and exon 7. The intron sequences of *CD45* were shortened to ~100 nucleotides. To determine if the target sites of the *CD45* pre-mRNA expressed from the minigene are sterically available, we assessed its secondary structure, as well as the secondary structures of the antisense circRNAs (Fig. 4.18B, Fig. 4.19). The target sites on the pre-mRNA of the *CD45* minigene were chosen to include unstructured or partially unstructured regions. For most of the circRNAs, the stem region was base-paired, exposing the partially structured antisense region.

Overall, to validate circRNA-driven splicing modulation, the following circRNAs with 40 nt antisense regions were designed:

- *Ex4 ESS* and *Ex6 ESS*, targeting the ESSs in exons 4 and 6, respectively;
- *Ex4 3'SS* and *Ex4 5'SS*, targeting the 20 nt up- and downstream from the corresponding splice sites;
- *Intr4*, targeting intron 4;
- *Ex5*, against the co-repressed exon 5;
- *Ex7*, complementary to a sequence from the constant exon 7;
- *Scrambled*, generated from randomized Ex4 ESS sequence.

The corresponding *cis*-elements targeted by *Ex4 ESS* and *Ex6 ESS* circRNAs were previously characterized by Preussner *et al*. (2012). In addition, shorter versions of the *Ex4 3'SS*, *Ex4 ESS*, *Intr4*, and *Scrambled* were generated, comprising an antisense region of only 30 nt, resulting in a circRNA of 50 nt.

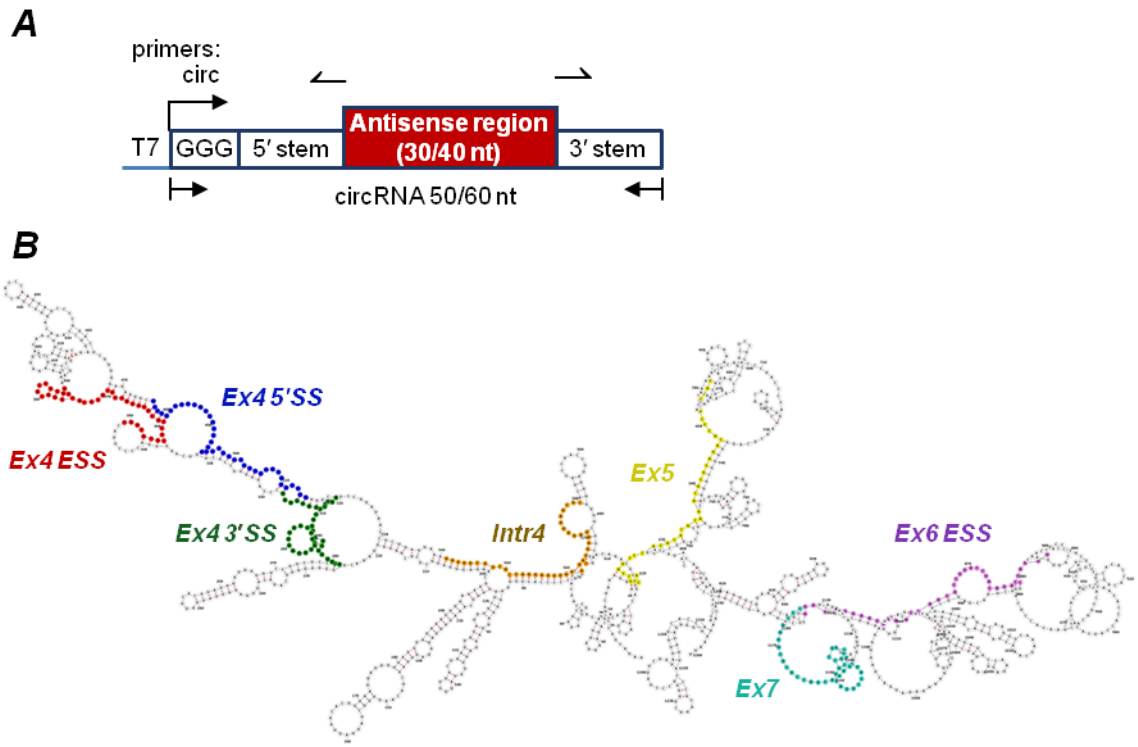

Figure 4.18 Templates for antisense circRNAs and *CD45* minigene target regions.
(A) Schematics of DNA-oligonucleotide templates design for *in vitro* circRNA expression. Transcription is driven by a T7 promoter. The antisense sequence is surrounded by 5′ and 3′ stem regions, each consists of 10 nt. Primers for the detection of circRNA are shown schematically.
(B) Model of secondary structure for the *CD45* minigene transcript. The selective target regions were marked corresponding to the circRNAs with 40-nt long antisense regions targeting *CD45* minigene mRNA.

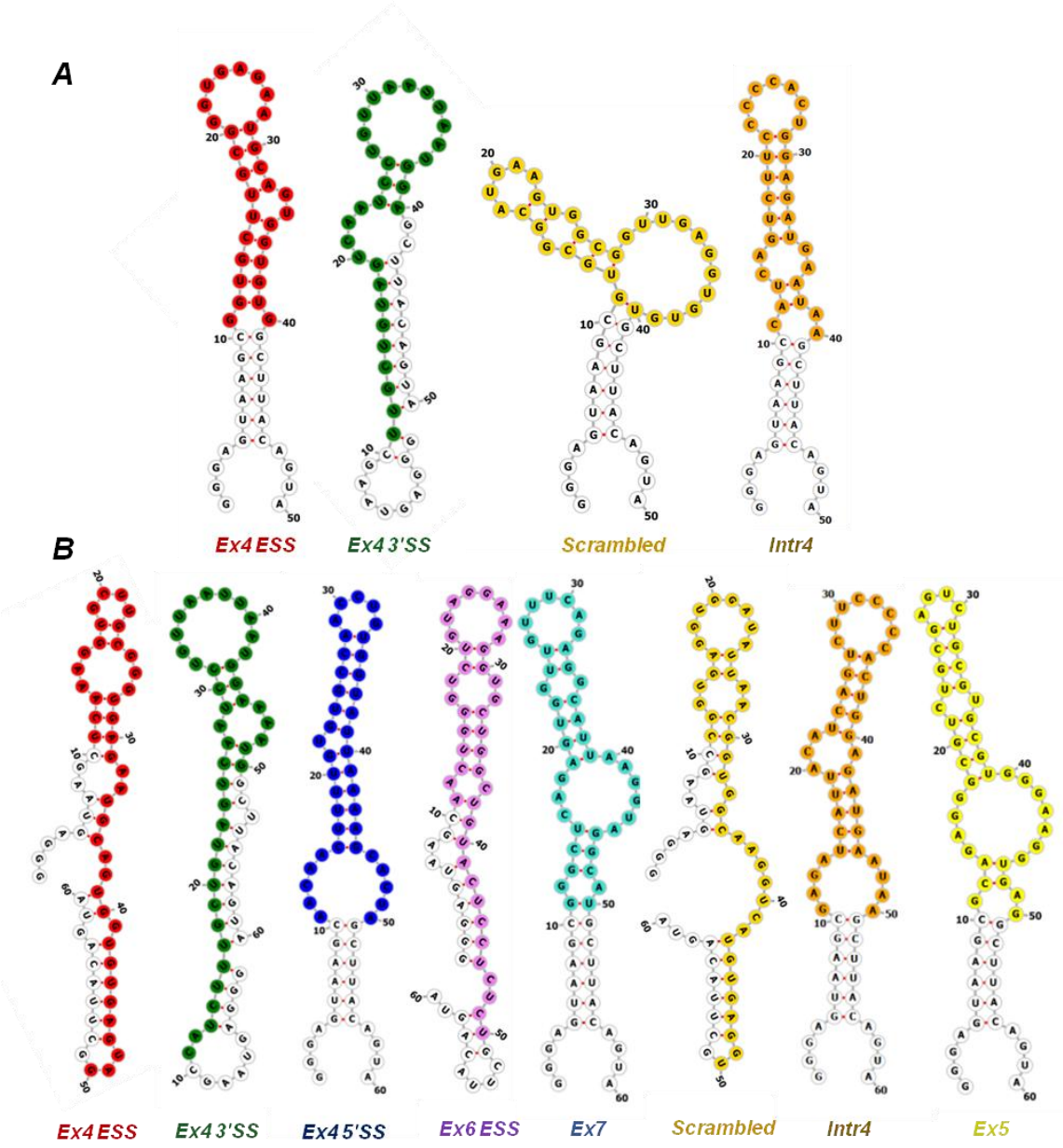

Figure 4.19 Predicted secondary structures of designer antisense circRNAs.
(A, B) CircRNAs secondary structures with the 30- ***(A)*** or 40-nt long ***(B)*** antisense region. CircRNA antisense regions are shown in different colors, corresponding to each particular circRNA variant and target sequence on the secondary structure of the *CD45* minigene transcript. CircRNA stem region identical for each circRNA is shown in white.

Next, we produced the corresponding circRNAs by T7 *in vitro* transcription, ligated them (Fig. 4.20A), and applied RNase R treatment as a circRNA purification step (Fig. 4.20B). Most of the RNA variants produced the single band corresponding to the circRNA already after circularization. In this case, additional RNase R treatment was used as a confirmation of the circular configuration of these RNA species. RNase R digestion revealed a single remaining band for all of the circRNAs with one exception: Multiple circular concatenation products remained for *Ex4 3'SS* (40-nt antisense region). Since the circRNA was visualized as the major band, *Ex4 3'SS* was still used for further experiments.

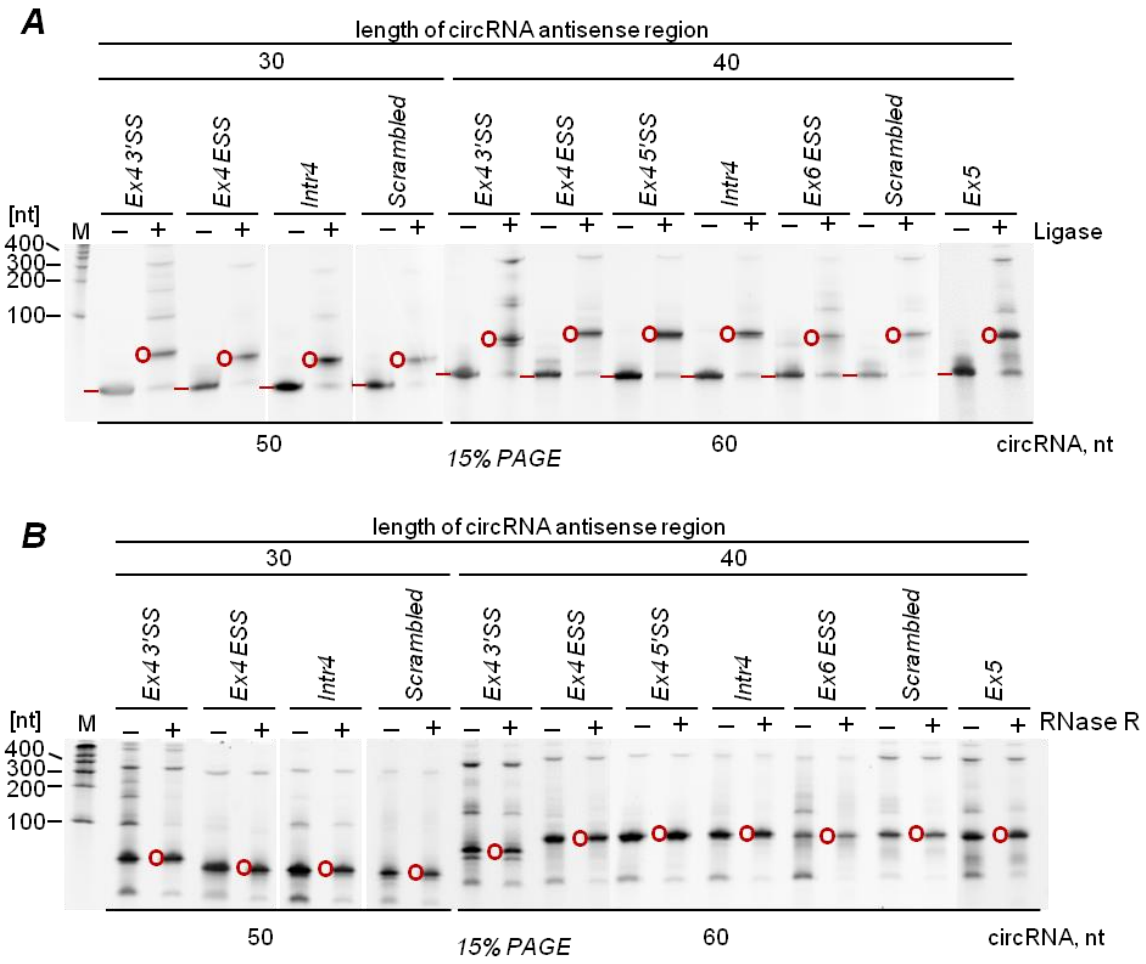

Figure 4.20 Preparation of CD45 antisense circRNAs.
RNAs containing 30- or 40-nt antisense sequences or *Scrambled* RNA were transcribed, ligated *in vitro* (–/+), and subjected to RNase R digestion (–/+). Linear and circular RNA species are marked in red. RNA was analyzed on 15% polyacrylamide gel and visualized with ethidium bromide. *M*, marker (LR RNA ladder).
(A) *In vitro* ligation of circRNAs. After transcription, RNA species were incubated with RNA ligase. The efficiency of the ligation reaction was accessed by polyacrylamide gel electrophoresis.
(B) RNase R treatment of circRNA samples after ligation. Ligated RNA was treated with (+) and without (–) RNase R and visualized by polyacrylamide gel electrophoresis.

4.5.1 Modulation of *CD45* alternative splicing by transfected antisense circRNAs

Next, we transfected the circRNAs and the *CD45* minigene construct in HeLa cells and investigated the splicing pattern of the *CD45* minigene by RT-PCR with primers specific to flanking constant exons spanning the alternatively spliced exons 4, 5, and 6 (ex2/3 – ex7); or with primers surrounding individual alternatively spliced exons (ex2/3 – ex5, ex5 – ex7). HeLa cells represent a convenient model for studying *CD45* alternative splicing modulation as they express both hnRNP L and hnRNP LL, and there is no endogenous *CD45* expression. Therefore, in HeLa cells, *CD45* minigene reproduces the alternative splicing pattern of the endogenous *CD45*, where the alternative splicing of the exons 4, 5, and 6 results in a mixture of R456, R45, R5, and R0 forms (Fig. 4.21, “Plasmid”).

As shown in Fig. 4.21, co-transfections of the designer circRNAs caused dramatic changes in alternative splicing pattern of *CD45* minigene mRNA. Comparing the circRNAs with 30- and 40-nt antisense region, we did not observe any drastic difference on the alternative splicing, so we decided to focus on the 40-nt antisense region for a more in-depth analysis with the additional circRNA variants. Focusing on the longer circRNAs, we compared the changes caused by antisense circRNA to the plasmid transfection alone and scrambled circRNA co-transfections. For *Ex4 3'SS* and the *Ex4 ESS*, similar effects were observed, namely, R45 form decreased, shifting the splicing pattern to the R5 and R0 forms. However, *Ex4 5'SS* circRNA did not show any effect (at least, not detectable by RT-PCR). Transfection of *Ex6 ESS* and *Ex5* circRNAs led to the expression of the R4 form, which was not detectable in control variants. Moreover, *Ex5* circRNA dramatically shifted the splicing pattern of *CD45* to the R4 and R0 forms. Co-transfection of the *Intr4* circRNA did not demonstrate any effects on alternative splicing. However, when compared to scrambled circRNA co-transfection, the *Intr4* variant revealed overall lower levels of *CD45*. When splicing of individual exon 4 was assayed, we observed repression of the targeted exon when the corresponding circRNA was co-transfected. In particular, transfections of *Ex4 ESS* (30 and 40 nt), as well as the *Ex4 3'SS* (40 nt) led to a loss of the exon 4 inclusion form (primer ex2/3 – ex5).

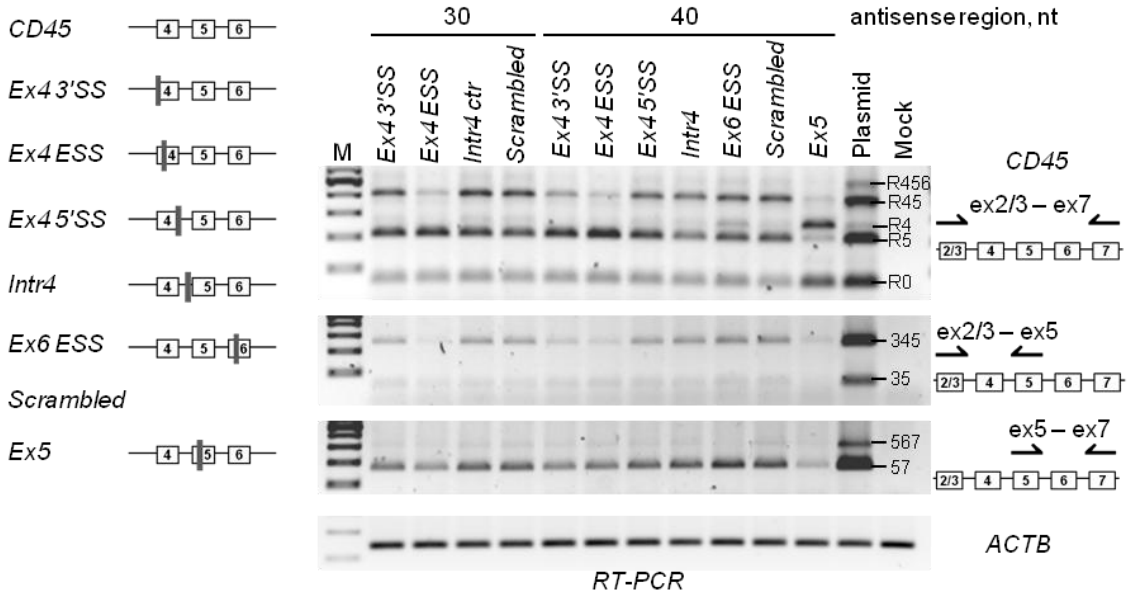

Figure 4.21 Effects of antisense circRNAs on alternative splicing of *CD45* minigene transcript. HeLa cells were co-transfected with *CD45* minigene construct and scrambled or antisense circRNA, as well as with the *CD45* minigene only (Plasmid). RNA from transfected cells was harvested one day post-transfection. Alternative splicing of endogenous *CD45* minigene mRNA was assayed by semiquantitative RT-PCR. Primer pairs (*CD45* ex2/3 – ex7, ex2/3 – ex5, and ex5 – ex7) and PCR products (splice forms R456, R45, R4, R5, and R0), exon 4 inclusion/skipping "345"/"35", and exon 6 inclusion/skipping "57"/"567" are shown on the right. The length of the antisense circRNA region is given above. CircRNA target regions are schematically shown on the left. *M*, marker (DNA Ladder Mix).

Next, we assayed the effects of the antisense circRNAs in a time-course experiment (Fig. 4.22). For that, *Ex4 ESS*, *Ex5*, or *Scrambled* circRNAs were co-transfected in HeLa cells together with the *CD45* minigene construct. Plasmid transfection alone was used as a control. First, we detected the transfected circRNAs by RT-PCR with circRNA-specific primers (Fig. 4.22A). *Ex4 ESS* and *Ex5* circRNAs were identified and remained at a high level one to four days after co-transfection. Then, we examined alternative splicing of the *CD45* minigene by RT-PCR (Fig. 4.22B). For *Ex4 ESS* and *Ex5* circRNAs, the most prominent effects were observed one day after transfection. Already on the second day, the *CD45* expression decreased and the effects were not distinguishable. For instance, in the *Ex5* variant, the characteristic R4 band appeared only on day one; on the second day, the R4 form almost vanished. At the same time, we addressed the question of the circRNA immunogenicity by testing the relative expression of protein kinase R (*PKR*), and interferon beta-1β **(***IFN-1β*) by RT-PCR. PKR is a dsRNA-dependent protein kinase which is activated by dsRNA stretches >33 bp (Husain *et al*., 2012). *PKR* upregulation leads to the shutdown of protein synthesis in a cell, which is a key process of innate immune response to viruses. Previously, *IFN-1β* transcription was shown to be induced when circRNAs with impurities and side products were transfected (Wesselhoeft *et al*., 2019). IFN-1β is a cytokine known to promote antiviral function and act as an immunomodulator in the innate immune response. Here we showed that the antisense circRNA transfections did not induce transcription activation of *PKR* and *IFN-1β* (Fig. 4.22B).

4.5.2 *CD45* alternative splicing alteration by antisense circRNA involves a post-transcriptional mechanism

Since the effects of the antisense circRNAs on *CD45* alternative splicing might originate not only from steric blocking of the sequences required for splicing, we aimed to determine if this observed alternative splicing modulation is a result of post-transcriptional mRNA processing. Therefore, we addressed the *CD45* alternative splicing modulation under conditions of inhibited transcription by blocking *de novo* transcription with actinomycin D. Accordingly, we designed an experiment where the circRNA transfections preceded by actinomycin D treatment in HeLa cells. In short, HeLa cells were treated with actinomycin D, or left untreated; 30 min later, the *CD45* construct and circRNAs *Ex4 ESS*, *Ex5*, *Scrambled*, or *CD45* construct alone, were transfected in actinomycin D-treated and untreated cells; four hours later, the cells were harvested. Surprisingly, we found that the application of *Ex4 ESS* and *Ex5* circRNAs demonstrated characteristic repression of the R45 form and upregulation of the R4 form, respectively (Fig. 4.23, top panel). Therefore, we observed effects of antisense circRNAs which originate post-transcriptionally. Transcription inhibition was proven by assessing the levels of short-living mRNAs *FOXO3*, *ZNF260*, and *MYC* (half-life time <1 h, Lugowski *et al*., 2018) by RT-PCR, which were found to be substantially reduced in

actinomycin D-treated in comparison to untreated cells (Fig. 4.23, bottom panels), while *ACTB* levels remained constant (half-life time >24 h).

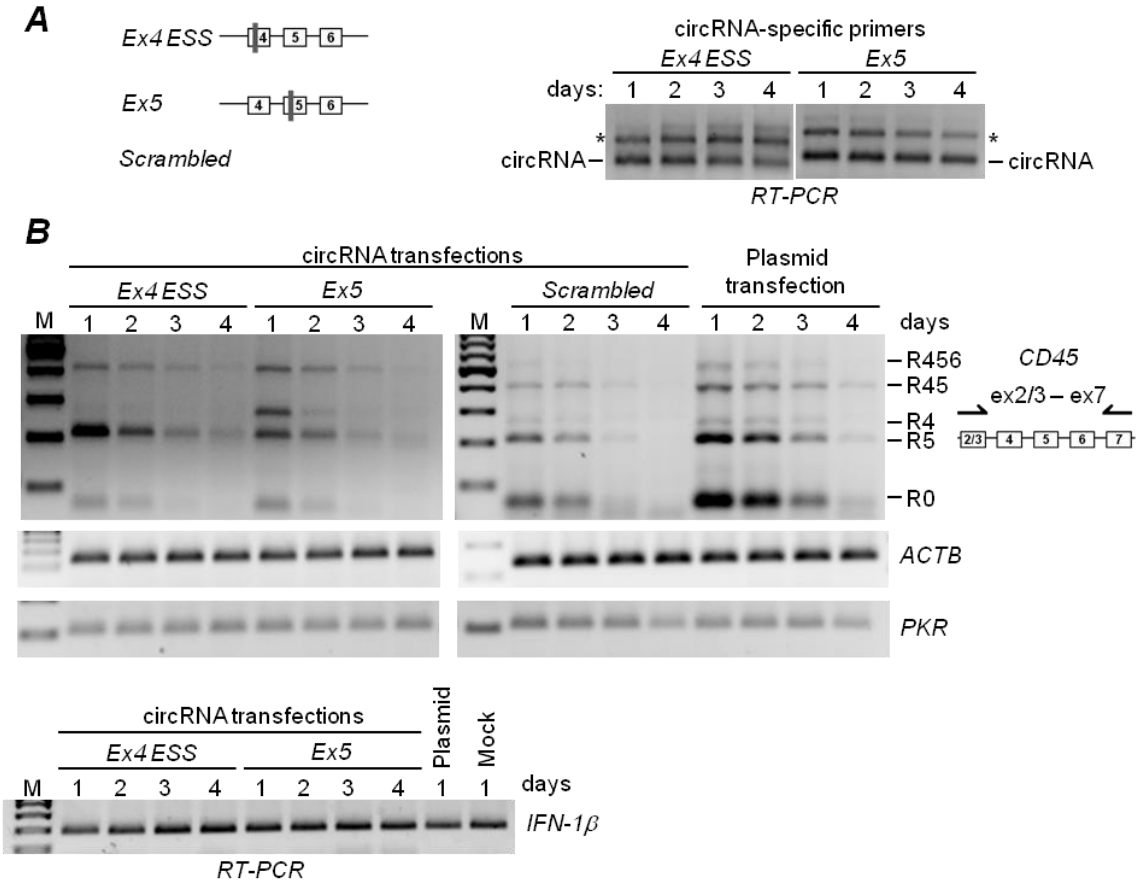

Figure 4.22 Effects of antisense circRNAs on alternative splicing of *CD45* minigene in a time-course experiment.

HeLa cells were co-transfected with *CD45* minigene construct and antisense circRNAs. The *CD45* minigene construct transfection alone, as well as the co-transfection of *Scrambled* circRNA, was used as a control. RNA was isolated one to four days after transfection and used for RT-PCR assays.

(A) CircRNA target sequences and circRNA detection. Left: CircRNA target sequences are schematically marked on the *CD45* minigene. Right: Detection of transfected *Ex4 ESS* and *Ex5* antisense circRNAs by RT-PCR at different time points (one to four days). PCR products derived from the circRNA rolling-circle amplification are marked with asterisks.

(B) Alternative splicing of *CD45* minigene. Total RNA obtained after one to four days post-transfection was used for RT-PCR reactions with the primers spanning constant flanking exons of *CD45* minigene (ex2/3 – ex7). Splice forms R456, R45, R4, R5, and R0 are marked on the right. *ACTB* was used as a loading control. The innate immune response was checked by RT-PCR with the *PKR* and *IFN-β1* primers. *M*, marker (DNA Ladder Mix).

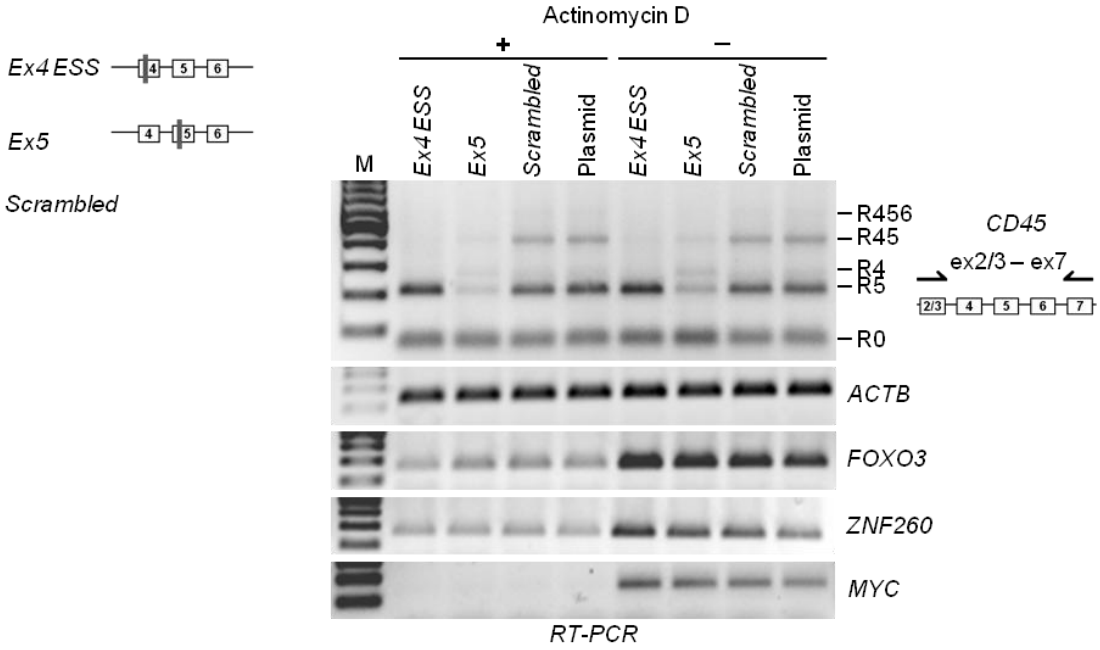

Figure 4.23 Activity of antisense circRNAs under transcription inhibition.
HeLa cells were treated with actinomycin D (+) or left untreated (–). Afterwards, the cells were co-transfected with *CD45* minigene construct and antisense circRNAs, or minigene construct alone. *Scrambled* circRNA was used as a control. After four hours, total RNA was extracted and *CD45* alternative splicing pattern was assayed by RT-PCR. Splice forms R456, R45, R4, R5, and R0 are denoted on the right. Levels of the short-living mRNAs (half-life <1 h: *FOXO3*, *ZNF260*, and *MYC*) were visualized by RT-PCR. *ACTB* served as a loading control. CircRNA target sequences are schematically shown on the left. *M*, marker (DNA Ladder Mix).

4.5.3 Antisense circRNAs reduce mRNA levels of the target gene

The mechanism of antisense circRNA-driven *CD45* splicing modulation might involve splicing, alternative splicing, or splicing-independent mechanism. To find out if the antisense circRNAs act specifically on alternative splicing or if another mechanism is involved, we designed a circRNA antisense to the constant exon 7 (*Ex7* circRNA) of the *CD45* minigene. For a positive control, we used the antisense circRNAs, which effects on alternative splicing of *CD45* minigene were described above. For that, we co-transfected the *CD45* minigene with these circRNAs in HeLa cells and analyzed the alternative splicing patterns of *CD45* (Fig. 4.24A). It appeared that *Ex7* circRNA did not cause any significant change in the alternative splicing of *CD45*. Interestingly, the total expression of *CD45* in Ex7 circRNA-transfected cells was much lower, when compared to *Scrambled* circRNA and transfection of *CD45* construct alone. To probe the effect of antisense circRNAs on the endogenous *CD45* gene, we selected the Burkitt lymphoma B-cell line DG75. DG75 cells lack hnRNP LL but express hnRNP L, which defines *CD45* exon 4 repression resulting in the R56 predominant form (Preussner *et al*., 2012). Consistently, in our study, *CD45* demonstrated a distribution between the R56 and R456 forms, with the major R56 form (Fig. 4.24B). Unexpectedly, no dramatic effect on alternative splicing of *CD45* upon transfection of antisense circRNAs was detected, except for a slight upregulation of the R5 isoform (Fig. 4.24B, “Ex5”).

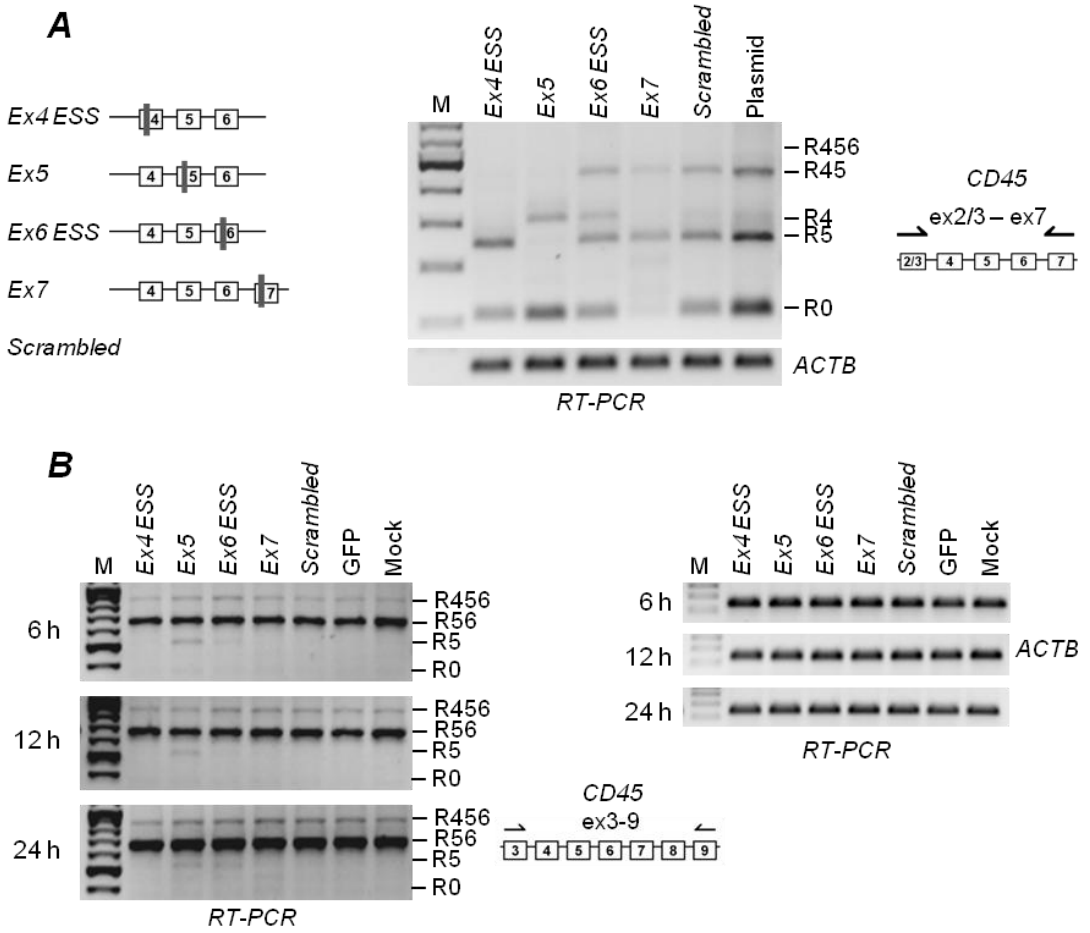

Figure 4.24 Effect of antisense circRNAs: Alternative and constant exons.
HeLa cells ***(A)*** and DG75 cells ***(B)*** were transiently transfected with antisense circRNAs. HeLa cells were co-transfected with the *CD45* minigene, or minigene construct alone ("Plasmid"). *Scrambled* circRNA and GFP plasmid transfections were used as a control. After transfection, aliquots of DG75 cell suspension were taken after indicated time points. HeLa cells were harvested 24 h post-transfection. Total RNA was isolated and *CD45* alternative splicing pattern was assayed by RT-PCR with the primers to flanking constant exons. Splice forms R456, R45, R4, R5, and R0 for HeLa cells and R456, R56, R5, and R0 for DG75 cells are denoted on the right. *ACTB* served as a loading control. CircRNA target sequences are schematically shown on the left. *M*, marker (DNA Ladder Mix).

Since no effect on alternative splicing of endogenous *CD45* was observed, we aimed to investigate if a combination of different circRNAs with proven functionality in HeLa cells, namely, *Ex4 ESS*, *Ex5*, and *Ex6 ESS* circRNAs ("Ex4/5/6"), will affect the alternative splicing pattern of the endogenous *CD45* in DG75 cells. However, no effect on *CD45* alternative splicing was observed (Fig. 4.25A). As we detected the repression of *CD45* minigene expression co-transfected with the Ex7 antisense circRNA in HeLa cells, but did not observe any effects on the endogenous *CD45* in DG75 cells, we decided to assay the absolute levels of the *CD45* transcript by RT-qPCR (Fig. 4.25B). When normalized to scrambled circRNA transfection variant, *Ex4 ESS* and *Ex6 ESS* circRNAs demonstrated down-regulation of the *CD45* expression of to ~70% and 90%, respectively. Additionally in that context, we tried to detect the relative expression of the *CD45* in cells transfected with *Ex7* circRNA (data not shown). However, since a melting curve generated from the qPCR product of this sample

indicated the presence of an additional non-specific qPCR product, which serves as control for quantification, these data could not be quantitated.

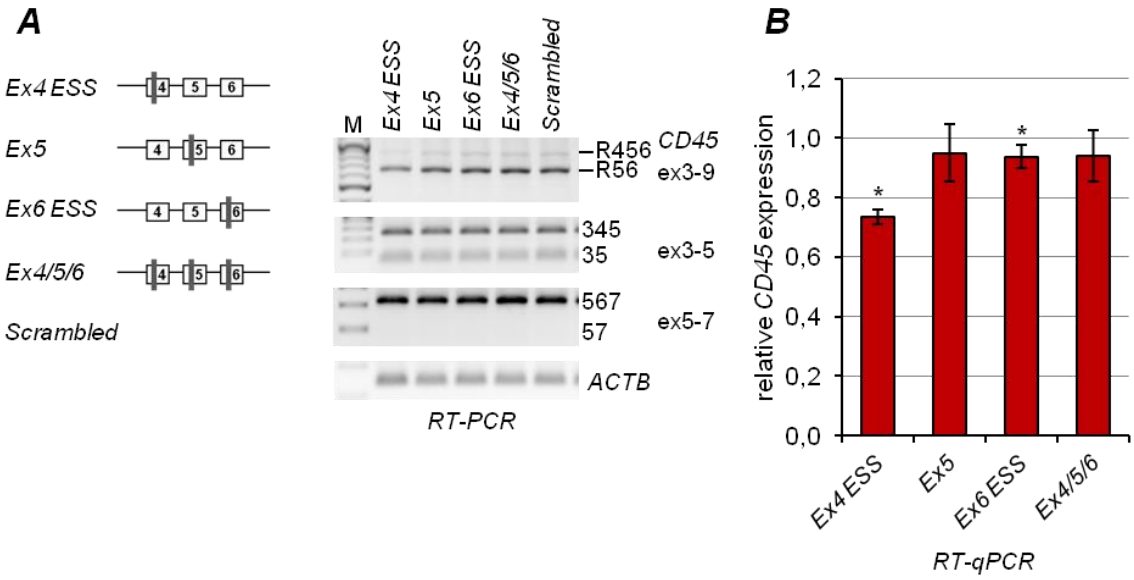

Figure 4.25 Antisense circRNAs act on endogenous *CD45* in the DG75 B-cell line.
Antisense circRNAs *Ex4 ESS*, *Ex5*, *Ex6 ESS*, and in combination *Ex4/5/6* (schematically shown on the left) were transiently transfected in DG75 cells. *Scrambled* circRNA transfection was used as a control. Cells were harvested 24 h after transfection and used for RNA isolation and RT-(q)PCR.
(A) *CD45* alternative splicing pattern in DG75 cells upon transfection of antisense circRNAs. *CD45* alternative splicing was assessed by RT-PCR with the primers spanning constant exons of *CD45* (ex3 – ex9) or flanking individual alternatively spliced exons (ex3 – ex5, ex5 – ex7). Splice forms R456 and R56 are denoted on the right. *ACTB* served as a loading control. *M*, marker (DNA Ladder Mix).
(B) qPCR analysis of total *CD45* expression upon antisense circRNA transfection. To quantify *CD45* expression, primers specific to exon 7 of *CD45* were used. Relative *CD45* expression was normalized to *U6* and *ACTB* RNA. The amount of *CD45* expressed in *Scrambled* circRNA transfection was set as the baseline level to which the transcript levels from the other variants were normalized (data are presented as a fold change). Error bars refer to standard deviations (n = 3, ∗ = $p < 0.05$).

Next, we used the *CD45* minigene to address the effects of a composition of multiple circRNAs on alternative splicing and relative expression of *CD45* in HeLa cells (Fig. 4.26). Thereby, we applied several circRNAs in combination, namely, *Ex4 ESS* and *Ex6 ESS* ("*Ex4/6*"), as well as *Ex4 ESS*, *Ex5*, and *Ex6 ESS* ("*Ex4/5/6*"), and co-transfected those with the *CD45* minigene construct in HeLa cells. These circRNA combinations resulted in averaging of the effects on the alternative splicing (Fig. 4.26A). Specifically, in the *Ex4/6* variant, the R45 form was partially down-regulated, but to a lesser extent than in the *Ex4 ESS* variant alone. In addition, we analyzed total expression of *CD45* upon transfection of antisense circRNAs and detected global downregulation of *CD45* total mRNA levels with all the circRNAs, when compared to scrambled circRNA transfection (Fig. 4.26B). Similar to the effect in DG75 cells, *Ex4 ESS* caused the strongest repression of *CD45* (up to 30% in comparison to *Scrambled* circRNA transfection). As already visually confirmed by RT-PCR, the expression of *CD45* minigene alone without the co-transfection of circRNA proved to be much higher, which possibly reflects differences in transfection efficiency. Namely, the

transfection reagent conveys a better transfection efficiency of the plasmid when plasmid alone is transfected. Overall, we conclude that the antisense circRNAs strongly affect alternative splicing in the case of *CD45* minigene. However, these modulations, at least partially, occur on post-transcriptional level.

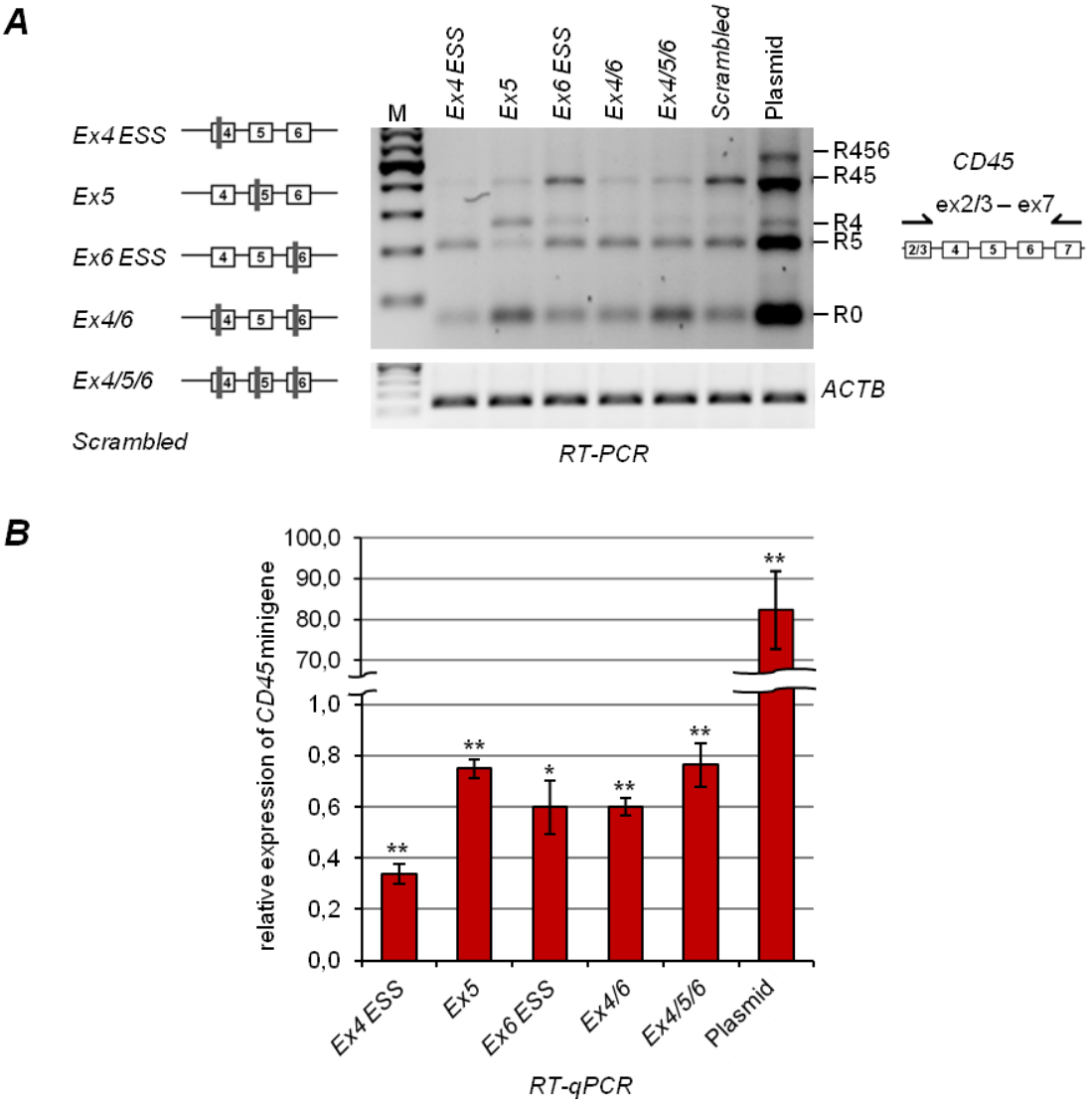

Figure 4.26 Antisense circRNAs modulate alternative splicing of *CD45* minigene and repress its expression in HeLa cells.

Antisense circRNAs *Ex4 ESS*, *Ex5*, *Ex6 ESS*, and their combinations *Ex4/6* and *Ex4/5/6* (schematically shown on the left) were transiently transfected in HeLa cells. *Scrambled* circRNA transfection was used as a control. Cells were harvested 24 h after transfection and used for RNA isolation and RT-(q)PCR.

(A) Detection of *CD45* alternative splicing forms upon transfection of antisense circRNAs. *CD45* alternative splicing was analyzed by RT-PCR with the primers spanning constant exons of *CD45* (ex2/3 – ex7). Splice forms R456, R45, R4, R5, and R0 are noted on the right. *ACTB* served as a loading control. *M*, marker (DNA Ladder Mix).

(B) qPCR analysis of total *CD45* expression upon transfection of antisense circRNA. qPCR reactions were performed with the primers specific to exon 7 of *CD45*. Expression levels were normalized to *U6* and *ACTB* RNA and presented as a fold change relative to *Scrambled* circRNA transfection. Error bars refer to standard deviations (n = 3, ∗ = $p < 0.05$, ∗∗ = $p < 0.01$).

5. Discussion

5.1 Development of optimal vector systems for circRNA production

Upon the discovery of the widespread circRNA formation, many studies focused on the sequence requirements for circRNA biogenesis. It is now known that the process of backsplicing from pre-mRNA is regulated by flanking inverted repeats (Liang & Wilusz, 2014) in combination with protein factors (Conn *et al*., 2015; Rybak-Wolf *et al*., 2015; Aktaş *et al*., 2017). Since circRNAs were reported to exhibit longer half-lifes compared to their linear precursor form (>24 h vs. ~2 h, Liang *et al*., 2017), application of circRNA for RNA and protein expression studies was considered.

Previously, several DNA-based systems for circRNA expression were developed. Some of them are based on endogenous flanking inverted repeats or artificially cloned sequences in a reverse-complementary orientation. Using a minigene construct, which contains sequences derived from the natural *CNTROB* circRNA, Starke *et al*. (2015) could show a up to five-fold enhancement of circularization by cloning the upstream intronic region in a reverse-complementary orientation downstream of the circularized exon. However, transfections of these vectors always resulted in the production of both circRNA and linear precursor, the latter of which could even prevail over circRNA.

In this thesis we could demonstrate, that the extension of flanking complementary regions in the *Plt-circR4* expression vector from 78 bp to 427 bp increased the circularization rate up to 20-fold, simultaneously eliminating the precursor levels (not detectable by RT-PCR, Fig. 4.1B&C). This observation is consistent with the previous data on the minimal required flanking complementary region, where a complementary region of 36 nts with seven mismatches was found as sufficient for minigene-driven *ZKSCAN1* circularization; at the same time, the extension of the complementary region improved circularization (Liang & Wilusz, 2014). However, it had previously been shown that circularization does not absolutely require extended flanking sequences (Starke *et al*., 2015). This might be sequence-specific, different in case of each particular circRNA, and depend on tissue- and cell-specific protein factors that influence splicing decisions.

As an alternative to pre-mRNA-based expression systems, tRNA intron circularization was applied first in a pre-tRNA backbone circRNA expression system (Lu *et al*., 2015), and then in a circRNA expression cassette flanked by ribozymes (Litke & Jaffrey, 2019). Circularization based on the intronic tRNA is associated with high levels of stable co-expressed tRNA and multiple precursors (as shown by Northern blot, Fig. 4.2C). The use of Twister ribozymes offers the advantage of high catalytic rates; these ribozymes produce 5′ hydroxyl and 2′-,3′-cyclic phosphate ends, similar to tRNA-processing enzymes (Roth *et al*., 2014). In the so-called Tornado circRNA expression system, ribozyme-driven autocatalytic cleavage up- and downstream of the circularizing sequence generates RNA ends, which are

recognized and ligated by the endogenous tRNA ligase RtcB. The limiting step of the reaction appears to be endonucleolytic cleavage (Litke & Jaffrey, 2019). Therefore, the intermediate product of the reaction is not accumulating, resulting in fast processing of the precursor into the circRNA, with the circRNA as the main outcome. Consistently, we observed only a minimal amount of the precursor detected by RT-PCR (Fig. 4.10A–C). Notably, the overall intracellular concentration of the expressed circRNA reached the micromolar range, which corresponds to 10^6 – 10^7 circRNA molecules per cell (Fig. 4.12B).

The ribozyme-based circRNA expression system demonstrated high potential for circRNA *in vitro* preparation (Wesselhoeft *et al*., 2018). This permuted intron-exon system is based on the group I catalytic intron from *Anabaena* pre-tRNA and was originally introduced as a backbone for protein expression. This so-called PIE system requires a laborious RNA preparation workflow, such as *in vitro* transcription, RNA extraction, RNase R treatment, and HPLC-purification (Fig. 4.4, Fig. 4.5). Another disadvantage of the PIE system is the generation of multiple by-products in the circularization reaction (Fig. 4.4), which are then co-transfected in cell culture and might interfere with the effects of functional designer circRNAs (Wesselhoeft *et al*., 2019).

Overall, we conclude that the Tornado system is currently the optimal circRNA expression system described. It allows circRNA expression up to 10^7 copies per cell and, additionally, makes it possible to track the RNA by an incorporated fluorescent Broccoli aptamer sequence. Therefore, these Tornado circRNAs could be visualized in total RNA samples (Fig. 4.10E, Fig. 4.11B), which represents a simpler alternative to Northern blot assay. However, all vectors described above have their limitations. Pol III-driven transcription from the tRNA-based vectors limits the size of the circRNA (~<800 nts; Noto *et al*., 2017) and requires the absence of poly(T) stretches, which act as termination signals of the RNA polymerase III. In contrast, the circRNA expression vectors based on pre-mRNA backsplicing are very limited in terms of amounts of produced circRNA and co-express linear precursor. The decision on a particular circRNA expression vector system depends on many factors, such as the length of the sequence of interest, its composition, and the secondary structure.

5.2 Designer circRNAs acting on hnRNP L modulate alternative splicing networks

As miRNA sponging had been described already for endogenous circRNAs, the idea of molecular sequestration of RNA and RNA-binding proteins by circRNAs emerged. Sequestration establishes conditions similar to RNAi-mediated knockdown of an RNA-binding protein, when the endogenous protein or RNA is limiting and its function diminished. As an example, Jost *et al*. (2018) used artificial circRNAs to sponge endogenous miRNA-122, which is required for the reproduction of the hepatitis C virus, and thereby reducing virus propagation. Here it is worth mentioning, that hnRNP L was also shown to be involved in

hepatitis C translation (Hwang *et al*., 2009). In addition, hnRNP L regulates mRNA stability and transport, but its main function is global modulation of alternative splicing networks (Hung *et al*., 2008). In that study, hnRNP L knockdown in combination with microarray analysis resulted in specific changes of alternative splicing of hnRNP L target genes.

In order to sequester hnRNP L, we designed circRNAs containing sequences with a high affinity to hnRNP L, namely, CA-repeats or SELEX-derived hnRNP L-binding sequence (5′-ATACATGACACACACACGCA-3′; Hui *et al*., 2005). These designer circRNAs were either expressed or directly transfected in HeLa cells, and their effects on hnRNP L and its targets were analyzed. Direct physical association of the designer circRNAs with hnRNP L was confirmed *in vivo* by RNA immunoprecipitation. Tornado circRNA accumulated to levels of up to 10^7 molecules per cell, which clearly is sufficient to quantitatively sponge the endogenous hnRNP L (~10^6 molecules per cell, Schreiner *et al*., in press). Another interesting point is whether hnRNP L is accessible for circRNA binding, since it predominately resides in the nucleus, while circRNAs normally accumulate in the cytoplasm. The expression of designer circRNAs shifted the distribution of hnRNP L between the nucleus and the cytoplasm from ~80/20% to ~50/50% (Fig. 4.17A). As hnRNP L is involved in mRNA export from the nucleus to the cytoplasm (Piñol-Roma, 1997), the observed alteration in its localization most likely led to the shift in the endogenous mRNA nuclear/cytoplasmic distribution, as shown for *GAPDH* mRNA (Fig. 4.17B). Additionally, we imaged Broccoli aptamer as a part of designer circRNA containing a single SELEX-derived binding sequence in fixed cells upon transfection. The previously described cytoplasmic localization for this circRNA expression system (Lu *et al*., 2015) was not observed in this case, as we detected equal nuclear-cytoplasmic distribution of the Broccoli-containing RNA by fluorescence imaging (Fig. 4.2). This circRNA distribution pattern may result from a combination of factors, such as circRNA export itself and the effect of this circRNA on hnRNP L and RNA export.

HnRNP L is known to bind CA-repetitive or CA-rich sequences, which represent the most common simple-sequence repeat in the human genome (Waterston *et al*., 2002). Therefore, hnRNP L regulates the splicing of many eukaryotic genes (Hung *et al*., 2008). Our targets for alternative splicing modulation were obtained from the study on hnRNP L knockdown coupled with microarray analysis (Hung *et al.*, 2008), and RNA-seq obtained after $(CA)_{100}$ circRNA transfection or hnRNP L knockdown (Schreiner *et al*., in press). From the initial list of target genes, we could experimentally validate differences in response to hnRNP L sponging for alternative splicing of 14 genes (Fig. 4.16), where hnRNP L promotes either exon skipping, exon inclusion, intron retention, or suppression of multiple exons. Fig. 5.1 summarizes the mechanism of action and the corresponding effects of the designer CA-rich circRNAs. Consistently, we observed significant changes in alternative splicing of hnRNP L target genes in HeLa cells, which either express Tornado-derived circRNA or were

transfected with ribozyme-produced circRNA. However, we detected several differences between *in vitro*-produced and vector-derived circRNAs. For example, the time course experiment showed strongest effects on alternative splicing 48 h after transfection of Tornado constructs, whose abundance remained constant for at least four days (Fig. 4.15), while for PIE circRNA transfections the effect reached its maximum after 24 h and was reduced 48 h post-transfection (Fig. 4.8A). Consistent with the observation of Tornado-derived designer circRNAs, which are present in highest amounts and show strongest effects on alternative splicing, we conclude that in general, the amounts of the expressed/transfected circRNAs determine the efficiency of alternative splicing modulation.

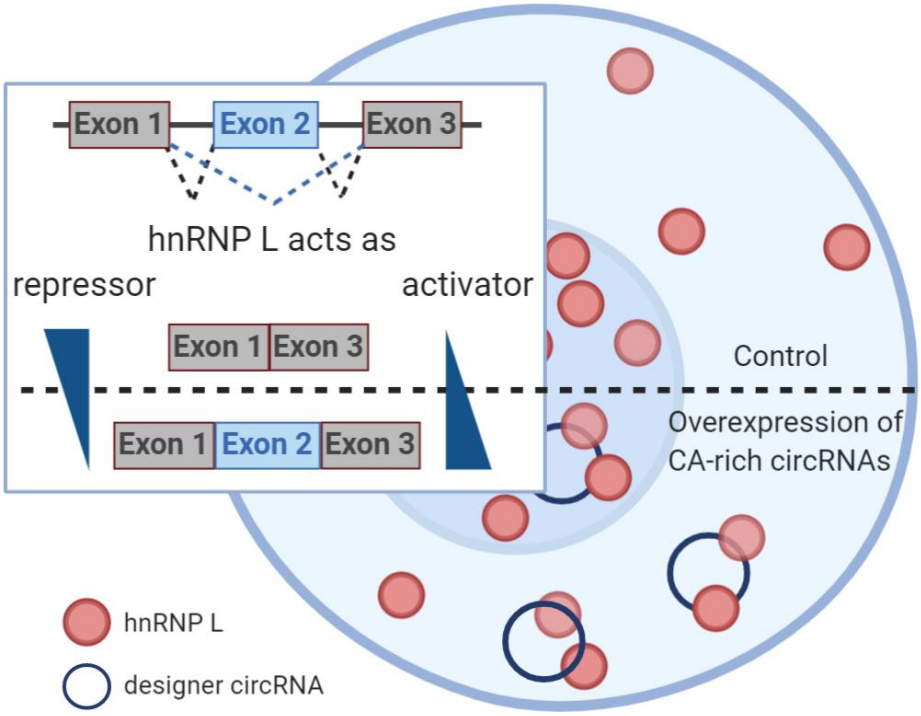

Figure 5.1 Model of action of CA-rich circRNAs with high affinity to hnRNP L.
Upon transfection of designer circRNAs, or their expression from the Tornado construct, accumulation of the circRNA in the cytoplasm shifts the hnRNP L distribution to the cytoplasm, which leads to the depletion of hnRNP L in the nucleus and to corresponding changes in alternative splicing of hnRNP L target genes. Grey boxes designate constant exons, blue boxes – variable exons. The figure was prepared with BioRender tool.

Alternative splicing is deregulated in various pathological conditions, and its targeted restoration has become an important aspect of molecular medicine. Current approaches for targeting alternative splicing are limited to antisense oligonucleotides (ASOs), siRNA-mediated knockdowns, and pharmacological inhibition. However, in clinical applications, these treatments are often accompanied by toxic effects. For example, ASOs and siRNAs are often designed to contain chemical modifications that are intended to overcome endogenous degradation pathways. Therefore, their degradation products are not metabolized efficiently and often accumulate causing various toxic effects. In studies on miRNA sponging, circRNAs were shown to be more efficient than ASOs (Jost *et al*., 2018).

Several ASOs have been successfully implemented or are still undergoing clinical trial process (Quemener *et al*., 2020) and might potentially serve as a basis for circRNA design.
Our proof of principle experiment demonstrated that designer circRNAs with high affinity to hnRNP L cause dramatic effects in hnRNP L distribution and alternative splicing of its target genes. It is worth mentioning, that hnRNP L was determined as a therapeutic target in prostate cancer (Fei *et al*., 2017). Alternative splicing of the the prostate cancer oncogene encoding the androgen receptor was determined to be hnRNP L-dependent, designating hnRNP L as a desease-relevant protein. Application of designer circRNAs can be used for molecular interventions in therapy and applied to other RBPs, since many of them are known to be deregulated in many cancer types, influencing the expression of tumor-suppressors and oncoproteins (reviewed in Pereira *et al*., 2017; Mohibi *et al*., 2019). One example is the RBP Musashi, which is required for propagation of human pancreatic adenocarcinoma and was used as a molecular target to stop tumor penetration (Zearfoss *et al*., 2014). In addition, Fox *et al*. (2016) demonstrated inhibition of Musashi by ASOs, which blocked the growth of primary tumors. Another example is the HuR protein, which was shown to be upregulated in many cancer types. HuR is known to shuttle between the nucleus and cytoplasm and was observed to shift to the cytoplasm in several cancer types (discussed in Mohibi *et al*., 2019).

5.3 Modulation of alternative splicing by antisense circRNA

Alternative splicing is a way to diversify the proteome of the cell. However, aberrations in gene splicing may have serious effects on cell performance. Jung *et al*. (2015) described various splicing aberrations in cancer patients, where single-nucleotide variants caused intron retention and inactivation of tumor suppressor genes. Kahles *et al*. (2018) analyzed splicing alterations in cancer patients and determined thousands of alternative splicing events not detectable in normal samples. Deregulated splicing processes in tumor cells can be a source of tumor neoantigens which are defined as foreign proteins that are absent in normal tissues (Schumacher & Schreiber, 2015). These findings highlight the importance of engineering therapeutic interventions for modulation of alternative splicing. For example, Inoue *et al*. (2019) described the inclusion of a so-called poison exon in *BRD9*, which codes for a component of the chromatin-remodelling complex. This inclusion is driven by a mutated spliceosomal component SF3B1, and eventually leads to a degradation of *BRD9* mRNA, thereby promoting melanomagenesis. Therefore, designer ASOs which correct aberrant *BRD9* splicing and suppress tumor growth were designed and successfully implemented in animal model (Inoue *et al*., 2019).
To investigate the modulation of alternative splicing, we designed antisense circRNAs directed against various regions of the *CD45* pre-mRNA. Their performance was tested in HeLa cells by co-transfections with a *CD45* minigene, where dramatic changes in alternative splicing patterns were observed (Fig. 4.21). HnRNP L and LL are co-expressed in HeLa

cells, which determines R456, R45, R5, and R0 as prevalent forms of alternative splicing of the exons 4, 5, and 6 (Preussner *et al*., 2012). Previous data had demonstrated inhibition of binding of splicing factors to pre-mRNAs and splicing modulation caused by ASOs (Hua *et al*., 2007). To assess antisense circRNA potential for splicing modulation, we targeted ESSs in exons 4 or 6 of *CD45.* These exons are regulated by hnRNP L, as well as in combination with hnRNP LL (exon 4), or by hnRNP LL alone (exon 6). Steric blocking of ESS by antisense sequences potentially blocks the binding sites of RBPs and prevents inclusion of corresponding exons. However, our observations demonstrated the opposite effect: The targeted exons tend to be skipped. In addition, when we targeted exon 5, which is not known to contain regulatory *cis*-elements, we also observed drastic changes in *CD45* alternative splicing. Interestingly, total *CD45* transcript levels were also affected by the antisense circRNAs (Fig. 4.26B). Thus, an mRNA containing a targeted exon may be degraded through the RNAi pathways. The mechanism of this degradation relies on recognition and processing of perfectly complementary dsRNA by Dicer protein; then the complex of bound antisense and target RNA with RNA-induced silencing complex (RISC) promotes mRNA cleavage by AGO2 protein (Hannon, 2002). To the best of our knowledge, circRNAs were not shown to be processed by Dicer. In addition, ASOs acting by steric blocking mechanism can cause aberrant splicing and generation of premature termination codon (PTC)-containing mRNAs, which results in NMD and downregulation of a target mRNA (Ward *et al*., 2014). Recently, the mechanism of the no-go mRNA degradation pathway was deciphered (Navickas *et al*., 2020). In particular, an mRNA containing stacks of stalled ribosomes is cleaved upstream of the stalled sequence and the resulting fragments are further trimmed by exonucleases. Just before, it was demonstrated that this pathway of target mRNA elimination is also activated by the application of ASOs (Liang *et al*., 2019).

In RNA therapy, activation of the cellular immune response is the main dangerous factor which may lead to cytokine storms in patients. Previous studies indicated sensing of exogenous circRNAs by RIG-I, which leads to the development of a typical RIG-I mediated antiviral response (Chen *et al*., 2017). However, other data evidence for non-immunogenic properties of exogenous circRNA without impurities in circRNA preparation (Wesselhoeft et al., 2019). In the context of dsRNA, innate immune response was shown to be activated by dsRNA stretches >33 bp (Husain *et al*., 2012). As our circRNAs were designed to contain 30 or 40 nt antisense sequences, we addressed the mRNA levels of *IFN-1β* and *PKR* (Fig. 4.22B) and detected no upregulation. Therefore, we conclude that, based on these preliminary assays, in the case of *CD45*, the *in vitro*-produced artificial circRNA did not activate the innate immune response.

Next, we approached the effects of the antisense circRNAs targeting the endogenous *CD45* gene in a B-cell line and detected no alterations of alternative splicing (Fig. 4.25A).

Consistently, the effects on the total *CD45* expression were mild and observed only for two antisense circRNAs (Fig. 4.25B). Drawing a comparison with ASOs, we hypothesize that the antisense circRNAs performance may depend on different factors, such as target RNA secondary structure, circRNA sequence specificity, its subcellular localization, stability of both, target and transfected RNA. Lima *et al*. (2014) showed that strong ASO binding correlates with the accessibility of the target mRNA, namely, its secondary structure and association with proteins. In addition, the difference between the effects of the antisense circRNA in HeLa and DG75 cells may rely on different transfection systems. We had switched to electroporation setup for transfections in DG75 cells, which might result in a different intracellular circRNA concentration and preclude the function of these antisense circRNAs.

Taking together our findings on alternative splicing modulation on the *CD45* minigene and endogenous *CD45*, we hypothesize that a complex folding of endogenous *CD45* pre-mRNA may reduce the accessibility of target sites for antisense circRNAs binding, which limits their performance.

5.4 Perspectives

In this thesis, we initially used designer CA-rich circRNAs to sequester the alternative splicing modulator hnRNP L, which resulted in specific alterations of alternative splicing events of hnRNP L target genes. The designer circRNAs were shown to be physically associated with the hnRNP L protein. The observed effects on alternative splicing correlated with the RNAi-mediated hnRNP L downregulation. However, this strategy is limited by the fact that it can only be applied to RBPs with a known and highly specific binding sequence. A promising aspect in this context is that it has already been shown that various members of RBPs are involved in the manifestation of various pathologies (Pereira *et al*., 2017). Therefore, several therapeutic strategies targeting those RBPs are being developed (Mohibi *et al*., 2019). Alternatively, RNA aptamers specific for any protein, including those which are not known to have natural nucleic acid ligands, can be developed and implemented in a similar manner (Bjerregaard et al., 2016). In addition, these SELEX-derived RNA aptamers can be developed and applied for any biomolecule (Ruscito & DeRosa, 2016).

If the upregulation of a particular RBP causes a disease, for example, as previously described for hnRNP L in case of prostate cancer (Fei *et al*., 2017), the protein-sponge strategy seems to be a promising alternative to siRNA-mediated downregulation. In contrast to the latter method, the sponge strategy provides the possibility to regulate the target protein on a broader range, without impairing its complete activity, but rather fulfilling its function at the basal level. Since the function of hnRNP L is essential for cell survival and its total inhibition results in cell death (Gaudreau *et al*., 2016), its partial sponging by circRNAs provides desired hnRNP L sequestration without complete removal.

In parallel, we also applied designer antisense circRNAs directed against *CD45*, an hnRNP L target gene, which exhibits a complex alternative splicing pattern. *CD45* is involved in the modulation of the immune response in T- and B-cells, thereby playing a significant role in infectious- and autoimmune diseases, as well as in tumor progression (reviewed by Rheinländer *et al*., 2018). Here, we could detect significant effects on alternative splicing, although the molecular mechanism behind these changes still remains elusive. However, we hypothesize that the antisense circRNAs act by a similar mechanisms as ASOs, namely splice-switching oligonucleotides (SSOs). Furthermore, antisense circRNAs could be used for modulation of alternative splicing of other genes; however, in case of *CD45*, we demonstrated that splicing of constant exons cannot be affected in this way.

Only 22% of all protein coding genes were estimated to be druggable by two groups of well-established small molecule or antibody-based drugs (Finan *et al*., 2017). RNA can potentially target any types of RNA, including non-coding RNA, which dramatically expands the therapeutic possibilities. In addition, RNA therapy exhibits the great potential in the field of personalized immunotherapy. However, only a limited number of RNA-based drugs have been approved in the last years. Major challenges in RNA therapy are its stability in blood and targeted delivery. In comparison to small molecules, therapeutic RNA has a larger molecular mass and is a highly charged molecule, which impedes its passive delivery through the cell membrane. Moreover, “naked” RNA molecules are highly accessible to degradation and, therefore, possess a short half-life. As double-stranded molecules, siRNAs cannot pass through the cell membrane as easily as single-stranded ASOs; however, they are more effective with fewer molecules.

RNA therapeutics are known to interact with membrane-associated proteins on the cell and can enter the cells by endocytosis. However, only a small amount of RNA molecules are able to escape the endosome and exert their therapeutic effects. The RNA is taken up by endocytosis but remains mainly trapped in endosomal vesicles. This phenomenon is known as non-productive uptake and represents a limiting factor in efficacy of RNA therapy (Crooke *et al.*, 2017). Therefore, new developments to enhance endosomal escape of the therapeutic RNA are needed (Deprey *et al*., 2020).

To improve RNA delivery, polymer- or lipid bilayer-based nanoparticles were successfully implemented (Dahlman *et al*., 2014; Prakash *et al*., 2013; L. Yang *et al*., 2020). Another strategy for RNA delivery is application of specific conjugates, which are designed to bind to cell surface receptors of the target cells (Ämmälä *et al*., 2018). For example, conjugation of *N*-acetylgalactosamine to siRNA and ASO drugs ensures efficient uptake by hepatocytes, as these cells expose large amount of asialoglycoprotein receptor on their cell surface (Nair et al., 2014; Tanowitz et al., 2017). While conjugation of siRNAs with folic acid targets them for internalization in cells expressing the corresponding receptors (Dohmen *et al*., 2012).

However, the efficacy of RNA therapeutics *in vitro* does not always correlate with its *in vivo* efficacy, and up to date the targeted RNA delivery was well-established mainly for liver.

Often, cellular mechanisms against foreign RNA species are activated by RNA therapy, thereby inducing immunogenic response. The strength of this response is dependent on the doses and structure complexity of the therapeutic RNA. Chemical modification of synthetic RNA is one of the sources of immunogenicity (discussed by Bramsen and Kjems, 2012). To extend the half-life of synthetic RNAs and overcome endogenous degradation pathways, chemical modifications of phosphate backbone and ribose are often introduced. Therefore, degradation products of these therapeutic RNAs are not metabolized efficiently and often accumulate causing various toxic effects. Some modifications, such as locked nucleic acids in ASOs were shown to cause hepatic toxicity (Burdick *et al*., 2014).

In spite of recent advances in chemical synthesis of nucleic acid polymers, RNA therapy remains relatively expensive. An alternative to RNA synthesis is a large-scale production of recombinant RNA in bacteria, which has been successfully implemented for production of the therapeutic miRNA against lung cancer (Ho *et al*., 2018).

Lacking extensive modifications, therapeutic circRNA correspond in its safety properties to natural RNAs. Since circRNAs are comparatively stable and do not necessarily require the incorporation of modified nucleotides to extend their half-life time, they offer several advantages for RNA-based therapy; nevertheless, their therapeutic potential is still largely unexplored. The direct delivery of the circRNA-producing vectors is impeded because of their large size. In addition, the efficiency of the circRNA production is often cell-type and tissue-specific. Large-scale production of synthetic circRNAs for therapeutic purposes is still under development. For example, RNA end-modifications for specific targeting, such as *N*-acetylgalactosamine for delivery into hepatocytes, are not possible for circRNA because of its closed configuration. Therefore, exploring the potential of therapeutic circRNA will require further development of specific strategies in the future.

6. References

Ackermann, E. J., Guo, S., Benson, M. D., Booten, S., Freier, S., Hughes, S. G., Kim, T. W., Jesse Kwoh, T., Matson, J., Norris, D., Yu, R., Watt, A., & Monia, B. P. (2016). Suppressing transthyretin production in mice, monkeys and humans using 2nd-Generation antisense oligonucleotides. *Amyloid*, *23*(3), 148–157.

Aktaş, T., Ilik, I. A., Maticzka, D., Bhardwaj, V., Pessoa Rodrigues, C., Mittler, G., Manke, T., Backofen, R., & Akhtar, A. (2017). DHX9 suppresses RNA processing defects originating from the Alu invasion of the human genome. *Nature*, *544*(7648), 115–119.

Alhasan, A. A., Izuogu, O. G., Al-Balool, H. H., Steyn, J. S., Evans, A., Colzani, M., Ghevaert, C., Mountford, J. C., Marenah, L., Elliott, D. J., Santibanez-Koref, M., & Jackson, M. S. (2016). Circular RNA enrichment in platelets is a signature of transcriptome degradation. *Blood*, *127*(9), e1–e11.

Alló, M., Buggiano, V., Fededa, J. P., Petrillo, E., Schor, I., De La Mata, M., Agirre, E., Plass, M., Eyras, E., Elela, S. A., Klinck, R., Chabot, B., & Kornblihtt, A. R. (2009). Control of alternative splicing through siRNA-mediated transcriptional gene silencing. *Nature Structural and Molecular Biology*, *16*(7), 717–724.

Ämmälä, C., Drury, W. J., Knerr, L., Ahlstedt, I., Stillemark-Billton, P., Wennberg-Huldt, C., Andersson, E. M., Valeur, E., Jansson-Löfmark, R., Janzén, D., Sundström, L., Meuller, J., Claesson, J., Andersson, P., Johansson, C., Lee, R. G., Prakash, T. P., Seth, P. P., Monia, B. P., & Andersson, S. (2018). Targeted delivery of antisense oligonucleotides to pancreatic β-cells. *Science Advances*, *4*(10).

Ashwal-Fluss, R., Meyer, M., Pamudurti, N. R., Ivanov, A., Bartok, O., Hanan, M., Evantal, N., Memczak, S., Rajewsky, N., & Kadener, S. (2014). CircRNA biogenesis competes with pre-mRNA splicing. *Molecular Cell*, *56*(1), 55–66.

Aung-Htut, M. T., Comerford, I., Johnsen, R., Foyle, K., Fletcher, S., & Wilton, S. D. (2019). Reduction of integrin alpha 4 activity through splice modulating antisense oligonucleotides. *Scientific Reports*, *9*(1), 1–12.

Barrett, S. P., & Salzman, J. (2016). Circular RNAs: Analysis, expression and potential functions. *Development (Cambridge)*, *143*(11), 1838–1847.

Berget, S. M., Moore, C., & Sharp, P. A. (1977). Spliced segments at the 5’ terminus of adenovirus 2 late mRNA. *Proceedings of the National Academy of Sciences of the United States of America*, *74*(8), 3171–3175.

Birkeland, M. L., Johnson, P., Trowbridge, I. S., & Pure, E. (1989). Changes in CD45 isoform expression accompany antigen-induced murine T-cell activation. *Proceedings of the National Academy of Sciences of the United States of America*, *86*(17), 6734–6738.

Bjerregaard, N., Andreasen, P. A., & Dupont, D. M. (2016). Expected and unexpected features of protein-binding RNA aptamers. *Wiley Interdisciplinary Reviews: RNA*, *7*(6), 744–757.

Bonen, L., & Vogel, J. (2001). The ins and outs of group II introns. *Trends in Genetics : TIG*, *17*(6), 322–331.

Bramsen, J. B., & Kjems, J. (2012). Development of therapeutic-grade small interfering RNAs by chemical engineering. *Frontiers in Genetics, 3*(154).

Breuer, J., & Rossbach, O. (2020). Production and purification of artificial circular RNA sponges for application in molecular biology and medicine. *Methods and Protocols*, *3*(2), 42.

Burdick, A. D., Sciabola, S., Mantena, S. R., Hollingshead, B. D., Stanton, R., Warneke, J. A., Zeng, M., Martsen, E., Medvedev, A., Makarov, S. S., Reed, L. A., Davis, J. W., & Whiteley, L. O. (2014). Sequence motifs associated with hepatotoxicity of locked nucleic acid - modified antisense oligonucleotides. *Nucleic Acids Research*, *42*(8), 4882–4891.

Capel, B., Swain, A., Nicolis, S., Hacker, A., Walter, M., Koopman, P., Goodfellow, P., & Lovell-Badge, R. (1993). Circular transcripts of the testis-determining gene Sry in adult mouse testis. *Cell*, *73*(5), 1019–1030.

Cartegni, L., Hastings, M. L., Calarco, J. A., De Stanchina, E., & Krainer, A. R. (2006). Determinants of exon 7 splicing in the spinal muscular atrophy genes, SMN1 and SMN2. *American Journal of Human Genetics*, *78*(1), 63–77.

Cech, T. R. (1990). Self-splicing of group I introns. *Annual Review of Biochemistry*, *59*(1), 543–568.

Chan, P. P., & Lowe, T. M. (2019). tRNAscan-SE: Searching for tRNA genes in genomic sequences. *Methods in Molecular Biology,* 1962, 1–14.

Chan, S. P., Kao, D. I., Tsai, W. Y., & Cheng, S. C. (2003). The Prp19p-associated complex in spliceosome activation. *Science*, *302*(5643), 279–282.

Chang, X., Li, B., & Rao, A. (2015). RNA-binding protein hnRNPLL regulates mRNA splicing and stability during B-cell to plasma-cell differentiation. *Proceedings of the National Academy of Sciences of the United States of America*, *112*(15), E1888–E1897.

Chen, Y. G., Kim, M. V., Chen, X., Batista, P. J., Aoyama, S., Wilusz, J. E., Iwasaki, A., & Chang, H. Y. (2017). Sensing self and foreign circular RNAs by intron identity. *Molecular Cell*, *67*(2), 228–238.e5.

Chow, L., Gelinas, R., Broker, T., & Roberts, R. (1977). An amazing sequence arrangement at the 5′ ends of adenovirus 2 messenger RNA. *Cell. 12*(1),1–8.

Clement, J. Q., Qian, L., Kaplinsky, N., & Wilkinson, M. F. (1999). The stability and fate of a spliced intron from vertebrate cells. *RNA*, *5*(2), 206–220.

Cocquerelle, C., Mascrez, B., Hétuin, D., & Bailleul, B. (1993). Mis-splicing yields circular RNA molecules. *The FASEB Journal*, *7*(1), 155–160.

Conn, S. J., Pillman, K. A., Toubia, J., Conn, V. M., Salmanidis, M., Phillips, C. A., Roslan, S., Schreiber, A. W., Gregory, P. A., & Goodall, G. J. (2015). The RNA binding protein quaking regulates formation of circRNAs. *Cell*, *160*(6), 1125–1134.

Cordin, O., Hahn, D., & Beggs, J. D. (2012). Structure, function and regulation of spliceosomal RNA helicases. *Current Opinion in Cell Biology 24*(3), 431–438.

Coughlin, S., Noviski, M., Mueller, J. L., Chuwonpad, A., Raschke, W. C., Weiss, A., & Zikherman, J. (2015). An extracatalytic function of CD45 in B cells is mediated by CD22. *Proceedings of the National Academy of Sciences of the United States of America*, *112*(47), E6515–E6524.

Crooke, S. T., Wang, S., Vickers, T. A., Shen, W., & Liang, X. H. (2017). Cellular uptake and trafficking of antisense oligonucleotides. *Nature Biotechnology*, *35*(3), 230–237.

Dahlman, J. E., Barnes, C., Khan, O. F., Thiriot, A., Jhunjunwala, S., Shaw, T. E., Xing, Y., Sager, H. B., Sahay, G., Speciner, L., Bader, A., Bogorad, R. L., Yin, H., Racie, T., Dong, Y., Jiang, S., Seedorf, D., Dave, A., Singh Sandhu, K., … Anderson, D. G. (2014). *In vivo* endothelial siRNA delivery using polymeric nanoparticles with low molecular weight. *Nature Nanotechnology*, *9*(8), 648–655.

Denis, M. M., Tolley, N. D., Bunting, M., Schwertz, H., Jiang, H., Lindemann, S., Yost, C. C., Rubner, F. J., Albertine, K. H., Swoboda, K. J., Fratto, C. M., Tolley, E., Kraiss, L. W., McIntyre, T. M., Zimmerman, G. A., & Weyrich, A. S. (2005). Escaping the nuclear confines: Signal-dependent pre-mRNA splicing in anucleate platelets. *Cell*, *122*(3), 379–391.

Deprey, K., Batistatou, N., & Kritzer, J. A. (2020). A critical analysis of methods used to investigate the cellular uptake and subcellular localization of RNA therapeutics. *Nucleic acids research, 48*(14), 7623–7639.

Dohmen, C., Fröhlich, T., Lächelt, U., Röhl, I., Vornlocher, H. P., Hadwiger, P., & Wagner, E. (2012). Defined folate-PEG-siRNA conjugates for receptor-specific gene silencing. *Molecular Therapy - Nucleic Acids*, *1*(1), e7.

Dowdy, S. F. (2017). Overcoming cellular barriers for RNA therapeutics. *Nature Biotechnology*, *35*(3), 222–229.

Dubin, R. A., Kazmi, M. A., & Ostrer, H. (1995). Inverted repeats are necessary for circularization of the mouse testis Sry transcript. *Gene*, *167*(1–2), 245–248.

Errichelli, L., Dini Modigliani, S., Laneve, P., Colantoni, A., Legnini, I., Capauto, D., Rosa, A., De Santis, R., Scarfò, R., Peruzzi, G., Lu, L., Caffarelli, E., Shneider, N. A., Morlando, M., & Bozzoni, I. (2017). FUS affects circular RNA expression in murine embryonic stem cell-derived motor neurons. *Nature Communications*, *8,* 14741.

Fei, T., Chen, Y., Xiao, T., Li, W., Cato, L., Zhang, P., Cotter, M. B., Bowden, M., Lis, R. T., Zhao, S. G., Wu, Q., Feng, F. Y., Loda, M., He, H. H., Liu, X. S., & Brown, M. (2017). Genome-wide CRISPR screen identifies HNRNPL as a prostate cancer dependency regulating RNA splicing. *Proceedings of the National Academy of Sciences of the United States of America*, *114*(26), E5207–E5215.

Fica, S. M., & Nagai, K. (2017). Cryo-electron microscopy snapshots of the spliceosome: Structural insights into a dynamic ribonucleoprotein machine. *Nature Structural and Molecular Biology, 24*(10), 791–799.

Fica, S. M., Tuttle, N., Novak, T., Li, N. S., Lu, J., Koodathingal, P., Dai, Q., Staley, J. P., & Piccirilli, J. A. (2013). RNA catalyses nuclear pre-mRNA splicing. *Nature*, *503*(7475), 229–234.

Filonov, G. S., & Jaffrey, S. R. (2016). RNA Imaging with dimeric Broccoli in live bacterial and mammalian cells. *Current Protocols in Chemical Biology*, *8*(1), 1–28.

Filonov, G. S., Kam, C. W., Song, W., & Jaffrey, S. R. (2015). In-gel imaging of RNA processing using broccoli reveals optimal aptamer expression strategies. *Chemistry and Biology*, *22*(5), 649–660.

Filonov, G. S., Moon, J. D., Svensen, N., & Jaffrey, S. R. (2014). Broccoli: Rapid selection of an RNA mimic of green fluorescent protein by fluorescence-based selection and directed evolution. *Journal of the American Chemical Society*, *136*(46), 16299–16308.

Finan, C., Gaulton, A., Kruger, F. A., Lumbers, R. T., Shah, T., Engmann, J., Galver, L., Kelley, R., Karlsson, A., Santos, R., Overington, J. P., Hingorani, A. D., & Casas, J. P. (2017). The druggable genome and support for target identification and validation in drug development. *Science Translational Medicine*, *9*(383).

Förch, P., & Valcárcel, J. (2003). Splicing regulation in Drosophila sex determination. In *Progress in molecular and subcellular biology*, *31*, 127–151.

Fox, R. G., Lytle, N. K., Jaquish, D. V., Park, F. D., Ito, T., Bajaj, J., Koechlein, C. S., Zimdahl, B., Yano, M., Kopp, J. L., Kritzik, M., Sicklick, J. K., Sander, M., Grandgenett, P. M., Hollingsworth, M. A., Shibata, S., Pizzo, D., Valasek, M. A., Sasik, R., … Reya, T. (2016). Image-based detection and targeting of therapy resistance in pancreatic adenocarcinoma. *Nature*, *534*(7607), 407–411.

Gagnon, K. T., Li, L., Chu, Y., Janowski, B. A., & Corey, D. R. (2014). RNAi factors are present and active in human cell nuclei. *Cell Reports*, *6*(1), 211–221.

Garikipati, V. N. S., Verma, S. K., Cheng, Z., Liang, D., Truongcao, M. M., Cimini, M., Yue, Y., Huang, G., Wang, C., Benedict, C., Tang, Y., Mallaredy, V., Ibetti, J., Grisanti, L., Schumacher, S. M., Gao, E., Rajan, S., Wilusz, J. E., Goukassian, D., … Kishore, R. (2019). Circular RNA CircFndc3b modulates cardiac repair after myocardial infarction via FUS/VEGF-A axis. *Nature Communications*, *10*(1), 1–14.

Gaudreau, M. C., Grapton, D., Helness, A., Vadnais, C., Fraszczak, J., Shooshtarizadeh, P., Wilhelm, B., Robert, F., Heyd, F., & Möröy, T. (2016). Heterogeneous Nuclear Ribonucleoprotein L is required for the survival and functional integrity of murine hematopoietic stem cells. *Scientific Reports*, *6*.

Good, P. D., Krikos, A. J., Li, S. X. L., Bertrand, E., Lee, N. S., Giver, L., Ellington, A., Zaia, J. A., Rossi, J. J., & Engelke, D. R. (1997). Expression of small, therapeutic RNAs in human cell nuclei. *Gene Therapy*, *4*(1), 45–54.

Grabowski, P. J., Zaug, A. J., & Cech, T. R. (1981). The intervening sequence of the ribosomal RNA precursor is converted to a circular RNA in isolated nuclei of tetrahymena. *Cell*, *23*(2), 467–476.

Graveley, B. R., & Maniatis, T. (1998). Arginine/serine-rich domains of SR proteins can function as activators of pre-mRNA splicing. *Molecular Cell, 1*(5), 765–771.

Hang, J., Wan, R., Yan, C., & Shi, Y. (2015). Structural basis of pre-mRNA splicing. *Science*, *349*(6253), 1191–1198.

Hannon, G. J. (2002). RNA interference. *Nature*, *418*(6894), 244–251.

Hansen, T. B. (2018). Improved circRNA identification by combining prediction algorithms. *Frontiers in Cell and Developmental Biology*, *5*(6), 20.

Hansen, T. B., Jensen, T. I., Clausen, B. H., Bramsen, J. B., Finsen, B., Damgaard, C. K., & Kjems, J. (2013). Natural RNA circles function as efficient microRNA sponges. *Nature*, *495*(7441), 384–388.

Hathcock, K. S., Hirano, H., Murakami, S., & Hodes, R. J. (1992). CD45 expression by B cells. Expression of different CD45 isoforms by subpopulations of activated B cells. *Journal of Immunology*, *149*(7), 2286–2294.

Havens, M. A., & Hastings, N. L. (2016). Splice-switching antisense oligonucleotides as therapeutic drugs. *Nucleic Acids Research*, *44*(14), 6549–6563.

Hermiston, M. L., Xu, Z., & Weiss, A. (2003). CD45: A critical regulator of signaling thresholds in immune cells. *Annual Review of Immunology*, *21*(1), 107–137.

Ho, P. Y., Duan, Z., Batra, N., Jilek, J. L., Tu, M. J., Qiu, J. X., Hu, Z., Wun, T., Lara, P. N., DeVere White, R. W., Chen, H. W., & Yu, A. M. (2018). Bioengineered noncoding RNAs selectively change cellular miRNome profiles for cancer therapy. *Journal of Pharmacology and Experimental Therapeutics*, *365*(3), 494–506.

Holdt, L. M., Stahringer, A., Sass, K., Pichler, G., Kulak, N. A., Wilfert, W., Kohlmaier, A., Herbst, A., Northoff, B. H., Nicolaou, A., Gäbel, G., Beutner, F., Scholz, M., Thiery, J., Musunuru, K., Krohn, K., Mann, M., & Teupser, D. (2016). Circular non-coding RNA *ANRIL* modulates ribosomal RNA maturation and atherosclerosis in humans. *Nature Communications*, *7*(1), 1–14.

House, A. E., & Lynch, K. W. (2006). An exonic splicing silencer represses spliceosome assembly after ATP-dependent exon recognition. *Nature Structural and Molecular Biology*, *13*(10), 937–944.

Hua, Y., Vickers, T. A., Baker, B. F., Bennett, C. F., & Krainer, A. R. (2007). Enhancement of SMN2 exon 7 inclusion by antisense oligonucleotides targeting the exon. *PLoS Biology*, *5*(4), 729–744.

Huang, C., Liang, D., Tatomer, D. C., & Wilusz, J. E. (2018). A length-dependent evolutionarily conserved pathway controls nuclear export of circular RNAs. *Genes & Development*, *32*(9–10), 639–644.

Hui, J., Hung, L.-H., Heiner, M., Schreiner, S., Neumüller, N., Reither, G., Haas, S. A., & Bindereif, A. (2005). Intronic CA-repeat and CA-rich elements: A new class of regulators of mammalian alternative splicing. *The EMBO Journal*, *24*(11), 1988–1998.

Hui, J., Stangl, K., Lane, W. S., & Bindereiff, A. (2003). HnRNP L stimulates splicing of the eNOS gene by binding to variable-length CA repeats. *Nature Structural Biology*, *10*(1), 33–37.

Hung, L.-H., Heiner, M., Hui, J., Schreiner, S., Benes, V., & Bindereif, A. (2008). Diverse roles of hnRNP L in mammalian mRNA processing: A combined microarray and RNAi analysis. *RNA*, *14*(2), 284–296.

Husain, B., Mukerji, I., & Cole, J. L. (2012). Analysis of high-affinity binding of protein kinase R to double-stranded RNA. *Biochemistry*, *51*(44), 8764–8770.

Hwang, B., Lim, J. H., Hahm, B., Jang, S. K., & Lee, S. W. (2009). hnRNP L is required for the translation mediated by HCV IRES. *Biochemical and Biophysical Research Communications*, *378*(3), 584–588.

Inoue, D., Chew, G. L., Liu, B., Michel, B. C., Pangallo, J., D'Avino, A. R., Hitchman, T., North, K., Lee, S. C. W., Bitner, L., Block, A., Moore, A. R., Yoshimi, A., Escobar-Hoyos, L., Cho, H., Penson, A., Lu, S. X., Taylor, J., Chen, Y., … Bradley, R. K. (2019). Spliceosomal disruption of the non-canonical BAF complex in cancer. *Nature*, *574*(7778), 432–436.

Jeck, W. R., & Sharpless, N. E. (2014). Detecting and characterizing circular RNAs. *Nature Biotechnology, 32*(5), 453–461.

Jeck, W. R., Sorrentino, J. A., Wang, K., Slevin, M. K., Burd, C. E., Liu, J., Marzluff, W. F., & Sharpless, N. E. (2013). Circular RNAs are abundant, conserved, and associated with ALU repeats. *RNA*, *19*(2), 141–157.

Jost, I., Shalamova, L. A., Gerresheim, G. K., Niepmann, M., Bindereif, A., & Rossbach, O. (2018). Functional sequestration of microRNA-122 from Hepatitis C Virus by circular RNA sponges. *RNA Biology*, *15*(8), 1032–1039.

Jung, H., Lee, D., Lee, J., Park, D., Jeong Kim, Y., Park, W.-Y., Hong, D., Park, P. J., Lee, E., & Korea, S. (2015). Intron retention is a widespread mechanism of tumor-suppressor inactivation. *Nature Genetics, 47,* 1242–1248.

Kahles, A., Lehmann, K. Van, Toussaint, N. C., Hüser, M., Stark, S. G., Sachsenberg, T., Stegle, O., Kohlbacher, O., Sander, C., Caesar-Johnson, S. J., Demchok, J. A., Felau, I., Kasapi, M., Ferguson, M. L., Hutter, C. M., Sofia, H. J., Tarnuzzer, R., Wang, Z., Yang, L., … Rätsch, G. (2018). Comprehensive Analysis of Alternative Splicing Across Tumors from 8,705 Patients. *Cancer Cell*, *34*(2), 211-224.e6.

Kim, M. S., Pinto, S. M., Getnet, D., Nirujogi, R. S., Manda, S. S., Chaerkady, R., Madugundu, A. K., Kelkar, D. S., Isserlin, R., Jain, S., Thomas, J. K., Muthusamy, B., Leal-Rojas, P., Kumar, P., Sahasrabuddhe, N. A., Balakrishnan, L., Advani, J., George, B., Renuse, S., … Pandey, A. (2014). A draft map of the human proteome. *Nature*, *509*(7502), 575–581.

Kjems, J., & Garrett, R. A. (1988). Novel splicing mechanism for the ribosomal RNA intron in the archaebacterium desulfurococcus mobilis. *Cell*, *54*(5), 693–703.

Kleaveland, B., Shi, C. Y., Stefano, J., & Bartel, D. P. (2018). A Network of Noncoding Regulatory RNAs Acts in the Mammalian Brain. *Cell*, *174*(2), 350-362.e17.

Kos, A., Dijkema, R., Arnberg, A. C., Van Der Meide, P. H., & Schellekens, H. (1986). The hepatitis delta (δ) virus possesses a circular RNA. *Nature*, *323*(6088), 558–560.

Kramer, M. C., Liang, D., Tatomer, D. C., Gold, B., March, Z. M., Cherry, S., & Wilusz, J. E. (2015). Combinatorial control of Drosophila circular RNA expression by intronic repeats, hnRNPs, and SR proteins. *Genes and Development*, *29*(20), 2168–2182.

Lander, E. S., Linton, L. M., Birren, B., Nusbaum, C., Zody, M. C., Baldwin, J., Devon, K., Dewar, K., Doyle, M., Fitzhugh, W., Funke, R., Gage, D., Harris, K., Heaford, A., Howland, J., Kann, L., Lehoczky, J., Levine, R., McEwan, P., … Morgan, M. J. (2001). Initial sequencing and analysis of the human genome. *Nature*, *409*(6822), 860–921.

Legnini, I., Di Timoteo, G., Rossi, F., Morlando, M., Briganti, F., Sthandier, O., Fatica, A., Santini, T., Andronache, A., Wade, M., Laneve, P., Rajewsky, N., & Bozzoni, I. (2017). Circ-ZNF609 is a circular RNA that can be translated and functions in myogenesis. *Molecular Cell*, *66*(1), 22-37.e9.

Li, X. F., & Lytton, J. (1999). A circularized sodium-calcium exchanger exon 2 transcript. *Journal of Biological Chemistry*, *274*(12), 8153–8160.

Li, X., Liu, S., Zhang, L., Issaian, A., Hill, R. C., Espinosa, S., Shi, S., Cui, Y., Kappel, K., Das, R., Hansen, K. C., Zhou, Z. H., & Zhao, R. (2019). A unified mechanism for intron and exon definition and back-splicing. *Nature*, *573*(7774), 375–380.

Liang, D., Tatomer, D. C., Luo, Z., Wu, H., Yang, L., Chen, L. L., Cherry, S., & Wilusz, J. E. (2017). The output of protein-coding genes shifts to circular RNAs when the pre-mRNA processing machinery is limiting. *Molecular Cell*, *68*(5), 940-954.e3.

Liang, D., & Wilusz, J. E. (2014). Short intronic repeat sequences facilitate circular RNA production. *Genes & Development*, *28*(20), 2233–2247.

Liang, X. H., Nichols, J. G., Hsu, C. W., Vickers, T. A., & Crooke, S. T. (2019). MRNA levels can be reduced by antisense oligonucleotides via no-go decay pathway. *Nucleic Acids Research*, *47*(13), 6900–6916.

Lim, K. H., Han, Z., Jeon, H. Y., Kach, J., Jing, E., Weyn-Vanhentenryck, S., Downs, M., Corrionero, A., Oh, R., Scharner, J., Venkatesh, A., Ji, S., Liau, G., Ticho, B., Nash, H., & Aznarez, I. (2020). Antisense oligonucleotide modulation of non-productive alternative splicing upregulates gene expression. *Nature Communications*, *11*(1), 1–13.

Lima, W. F., Vickers, T. A., Nichols, J., Li, C., & Crooke, S. T. (2014). Defining the factors that contribute to on-target specificity of antisense oligonucleotides. *PLoS ONE*, *9*(7), e101752.

Litke, J. L., & Jaffrey, S. R. (2019). Highly efficient expression of circular RNA aptamers in cells using autocatalytic transcripts. *Nature Biotechnology*, *37*(6), 667–675.

Liu, C. X., Li, X., Nan, F., Jiang, S., Gao, X., Guo, S. K., Xue, W., Cui, Y., Dong, K., Ding, H., Qu, B., Zhou, Z., Shen, N., Yang, L., & Chen, L. L. (2019). Structure and degradation of circular RNAs regulate PKR activation in innate Immunity. *Cell*, *177*(4), 865-880.e21.

Lu, Z., Filonov, G. S., Noto, J. J., Schmidt, C. A., Hatkevich, T. L., Wen, Y., Jaffrey, S. R., & Matera, A. G. (2015). Metazoan tRNA introns generate stable circular RNAs *in vivo*. *RNA*, *21*(9), 1554–1565.

Lugowski, A., Nicholson, B., & Rissland, O. S. (2018). Determining mRNA half-lives on a transcriptome-wide scale. *Methods*, *137*, 90–98.

Lynch, K. W., & Weiss, A. (2000). A model system for activation-induced alternative splicing of CD45 pre-mRNA in T cells implicates protein kinase C and Ras. *Molecular and Cellular Biology*, *20*(1), 70–80.

Memczak, S., Jens, M., Elefsinioti, A., Torti, F., Krueger, J., Rybak, A., Maier, L., Mackowiak, S. D., Gregersen, L. H., Munschauer, M., Loewer, A., Ziebold, U., Landthaler, M., Kocks, C., Le Noble, F., & Rajewsky, N. (2013). Circular RNAs are a large class of animal RNAs with regulatory potency. *Nature*, *495*(7441), 333–338.

Memczak, S., Papavasileiou, P., Peters, O., & Rajewsky, N. (2015). Identification and characterization of circular RNAs as a new class of putative biomarkers in human blood. *PLoS ONE*, *10*(10), e0141214.

Mendell, J. R., Goemans, N., Lowes, L. P., Alfano, L. N., Berry, K., Shao, J., Kaye, E. M., & Mercuri, E. (2016). Longitudinal effect of eteplirsen versus historical control on ambulation in Duchenne muscular dystrophy. *Annals of Neurology*, *79*(2), 257–271.

Mendell, J. R., Rodino-Klapac, L. R., Sahenk, Z., Roush, K., Bird, L., Lowes, L. P., Alfano, L., Gomez, A. M., Lewis, S., Kota, J., Malik, V., Shontz, K., Walker, C. M., Flanigan, K. M., Corridore, M., Kean, J. R., Allen, H. D., Shilling, C., Melia, K. R., … Kaye, E. M. (2013). Eteplirsen for the treatment of Duchenne muscular dystrophy. *Annals of Neurology*, *74*(5), 637–647.

Michel, F., & Ferat, J.-L. (1995). Structure and Activities of Group II Introns. *Annual Review of Biochemistry*, *64*(1), 435–461.

Mohibi, S., Chen, X., & Zhang, J. (2019). Cancer the'RBP'eutics–RNA-binding proteins as therapeutic targets for cancer. *Pharmacology and Therapeutics*, *203*, 107390.

Müller-McNicoll, M., Rossbach, O., Hui, J., & Medenbach, J. (2019). Auto-regulatory feedback by RNA-binding proteins. *Journal of Molecular Cell Biology*, *11*(10), 930.

Müller, M., Samel-Pommerencke, A., Legrand, C., Tuorto, F., Lyko, F., & Ehrenhofer-Murray, A. E. (2019). Division of labour: tRNA methylation by the NSun2 tRNA methyltransferases Trm4a and Trm4b in fission yeast. *RNA Biology*, *16*(3), 249–256.

Müller, S., & Appel, B. (2017). *In vitro* circularization of RNA. *RNA Biology*, 14(8), 1018–1027).

Muntoni, F., Torelli, S., & Ferlini, A. (2003). Dystrophin and mutations: One gene, several proteins, multiple phenotypes. *Lancet Neurology 2*(12) 731–740.

Nair, J. K., Willoughby, J. L. S., Chan, A., Charisse, K., Alam, M. R., Wang, Q., Hoekstra, M., Kandasamy, P., Kelin, A. V., Milstein, S., Taneja, N., Oshea, J., Shaikh, S., Zhang, L., Van Der Sluis, R. J., Jung, M. E., Akinc, A., Hutabarat, R., Kuchimanchi, S., … Manoharan, M. (2014). Multivalent N -acetylgalactosamine-conjugated siRNA localizes in hepatocytes and elicits robust RNAi-mediated gene silencing. *Journal of the American Chemical Society*, *136*(49), 16958–16961.

Navickas, A., Chamois, S., Saint-Fort, R., Henri, J., Torchet, C., & Benard, L. (2020). No-Go Decay mRNA cleavage in the ribosome exit tunnel produces 5′-OH ends phosphorylated by Trl1. *Nature Communications*, *11*(1), 1–11.

Nicolet, B. P., Engels, S., Aglialoro, F., van den Akker, E., von Lindern, M., & Wolkers, M. C. (2018). Circular RNA expression in human hematopoietic cells is widespread and cell-type specific. *Nucleic Acids Research*, *46*(16), 8168–8180. https://doi.org/10.1093/nar/gky721

Nigro, J. M., Cho, K. R., Fearon, E. R., Kern, S. E., Ruppert, J. M., Oliner, J. D., Kinzler, K. W., & Vogelstein, B. (1991). Scrambled exons. *Cell*, *64*(3), 607–613.

Noto, J. J., Schmidt, C. A., & Matera, A. G. (2017). Engineering and expressing circular RNAs via tRNA splicing. *RNA Biology*, *14*(8), 978–984.

Oberdoerffer, S., Moita, L. F., Neems, D., Freitas, R. P., Hacohen, N., & Rao, A. (2008). Regulation of CD45 alternative splicing by heterogeneous ribonucleoprotein, hnRNPLL. *Science*, *321*(5889), 686–691.

Ottesen, E. W. (2017). ISS-N1 makes the first FDA-approved drug for spinal muscular atrophy. In *Translational Neuroscience 8*(1), 1–6.

Sharp, P.A. (1991). "Five easy pieces". *Science*, *254*(5032), 663.

Pamudurti, N. R., Bartok, O., Jens, M., Ashwal-Fluss, R., Stottmeister, C., Ruhe, L., Hanan, M., Wyler, E., Perez-Hernandez, D., Ramberger, E., Shenzis, S., Samson, M., Dittmar, G., Landthaler, M., Chekulaeva, M., Rajewsky, N., & Kadener, S. (2017). Translation of circRNAs. *Molecular Cell*, *66*(1), 9-21.e7.

Pan, Q., Shai, O., Lee, L. J., Frey, B. J., & Blencowe, B. J. (2008). Deep surveying of alternative splicing complexity in the human transcriptome by high-throughput sequencing. *Nature Genetics*, *40*(12), 1413–1415.

Park, E., Pan, Z., Zhang, Z., Lin, L., & Xing, Y. (2018). The expanding landscape of alternative splicing variation in human populations. *American Journal of Human Genetics*, *102*(1), 11–26.

Paushkin, S. V., Patel, M., Furia, B. S., Peltz, S. W., & Trotta, C. R. (2004). Identification of a human endonuclease complex reveals a link between tRNA splicing and pre-mRNA 3′ end formation. *Cell*, *117*(3), 311–321.

Pereira, B., Billaud, M., & Almeida, R. (2017). RNA-binding proteins in cancer: Old players and new actors. *Trends in Cancer*, 3(7), 506–528.

Pfafenrot, C., & Preußer, C. (2019). Establishing essential quality criteria for the validation of circular RNAs as biomarkers. *Biomolecular Detection and Quantification*, *17,* 100085.

Piñol-Roma, S. (1997). HnRNP proteins and the nuclear export of mRNA. *Seminars in Cell and Developmental Biology*, *8*(1), 57–63.

Pinol-Roma, S., Swanson, M. S., Gall, J. G., & Dreyfuss, G. (1989). A novel heterogeneous nuclear RNP protein with a unique distribution on nascent transcripts. *Journal of Cell Biology*, *109*(6), 2575–2587.

Piwecka, M., Glažar, P., Hernandez-Miranda, L. R., Memczak, S., Wolf, S. A., Rybak-Wolf, A., Filipchyk, A., Klironomos, F., Jara, C. A. C., Fenske, P., Trimbuch, T., Zywitza, V., Plass, M., Schreyer, L., Ayoub, S., Kocks, C., Kühn, R., Rosenmund, C., Birchmeier, C., & Rajewsky, N. (2017). Loss of a mammalian circular RNA locus causes miRNA deregulation and affects brain function. *Science*, *357*(6357).

Popow, J., Englert, M., Weitzer, S., Schleiffer, A., Mierzwa, B., Mechtler, K., Trowitzsch, S., Will, C. L., Lührmann, R., Söll, D., & Martinez, J. (2011). HSPC117 is the essential subunit of a human tRNA splicing ligase complex. *Science*, *331*(6018), 760–764.

Popow, J., Schleiffer, A., & Martinez, J. (2012). Diversity and roles of (t)RNA ligases. *Cellular and Molecular Life Sciences*, 69(16), 2657–2670.

Prakash, T. P., Lima, W. F., Murray, H. M., Elbashir, S., Cantley, W., Foster, D., Jayaraman, M., Chappell, A. E., Manoharan, M., Swayze, E. E., & Crooke, S. T. (2013). Lipid nanoparticles improve activity of single-stranded siRNA and gapmer antisense oligonucleotides in animals. *ACS Chemical Biology*, *8*(7), 1402–1406.

Preußer, C., Hung, L.-H., Schneider, T., Schreiner, S., Hardt, M., Moebus, A., Santoso, S., & Bindereif, A. (2018). Selective release of circRNAs in platelet-derived extracellular vesicles. *Journal of Extracellular Vesicles*, *7*(1), 1424473.

Preussner, M., Schreiner, S., Hung, L.-H., Porstner, M., Jäck, H.-M., Benes, V., Rätsch, G., & Bindereif, A. (2012). HnRNP L and L-like cooperate in multiple-exon regulation of CD45 alternative splicing. *Nucleic Acids Research*, *40*(12), 5666–5678.

Quemener, A. M., Bachelot, L., Forestier, A., Donnou-Fournet, E., Gilot, D., & Galibert, M. D. (2020). The powerful world of antisense oligonucleotides: From bench to bedside. *Wiley Interdisciplinary Reviews, RNA*, *11*(5), e1594.

Raal, F. J., Santos, R. D., Blom, D. J., Marais, A. D., Charng, M. J., Cromwell, W. C., Lachmann, R. H., Gaudet, D., Tan, J. L., Chasan-Taber, S., Tribble, D. L., Flaim, J. A. D., & Crooke, S. T. (2010). Mipomersen, an apolipoprotein B synthesis inhibitor, for lowering of LDL cholesterol concentrations in patients with homozygous familial hypercholesterolaemia: A randomised, double-blind, placebo-controlled trial. *The Lancet*, *375*(9719), 998–1006.

Raghunathan, P. L., & Guthrie, C. (1998). RNA unwinding in U4/U6 snRNPs requires ATP hydrolysis and the DEIH-box splicing factor Brr2. *Current Biology, 8*(15), 847–855.

Rheinländer, A., Schraven, B., & Bommhardt, U. (2018). CD45 in human physiology and clinical medicine. In *Immunology Letters, 196*, 22–32.

Robb, G. B., Brown, K. M., Khurana, J., & Rana, T. M. (2005). Specific and potent RNAi in the nucleus of human cells. *Nature Structural and Molecular Biology*, *12*(2), 133–137.

Rossbach, O., Hung, L.-H., Schreiner, S., Grishina, I., Heiner, M., Hui, J., & Bindereif, A. (2009). Auto- and cross-regulation of the hnRNP L proteins by alternative splicing. *Molecular and Cellular Biology*, *29*(6), 1442–1451.

Rossbach, Oliver, Hung, L.-H., Khrameeva, E., Schreiner, S., Koñig, J., Curk, T., Zupan, B., Ule, J., Gelfand, M. S., & Bindereif, A. (2014). Crosslinking-immunoprecipitation (iCLIP) analysis reveals global regulatory roles of hnRNP L. *RNA Biology*, *11*(2), 146–155.

Roth, A., Weinberg, Z., Chen, A. G. Y., Kim, P. B., Ames, T. D., & Breaker, R. R. (2014). A widespread self-cleaving ribozyme class is revealed by bioinformatics. *Nature Chemical Biology*, *10*(1), 56–60.

Ruscito, A., & DeRosa, M. C. (2016). Small-molecule binding aptamers: Selection strategies, characterization, and applications. *Frontiers in Chemistry*, *4*(14).

Ruth Zearfoss, N., Deveau, L. M., Clingman, C. C., Schmidt, E., Johnson, E. S., Massi, F., & Ryder, S. P. (2014). A conserved three-nucleotide core motif defines musashi RNA binding specificity. *Journal of Biological Chemistry*, *289*(51), 35530–35541.

Rybak-Wolf, A., Stottmeister, C., Glažar, P., Jens, M., Pino, N., Hanan, M., Behm, M., Bartok, O., Ashwal-Fluss, R., Herzog, M., Schreyer, L., Papavasileiou, P., Ivanov, A., Öhman, M., Refojo, D., Kadener, S., & Rajewsky, N. (2015). Circular RNAs in the mammalian brain are highly abundant, conserved, and dynamically expressed. *Molecular Cell*, *58*(5), 870–885.

Salzman, J., Gawad, C., Wang, P. L., Lacayo, N., & Brown, P. O. (2012). Circular RNAs are the predominant transcript isoform from hundreds of human genes in diverse cell types. *PLoS ONE*, *7*(2).

Sanger, H. L., Klotz, G., Riesner, D., Gross, H. J., & Kleinschmidt, A. K. (1976). Viroids are single stranded covalently closed circular RNA molecules existing as highly base paired rod like structures. *Proceedings of the National Academy of Sciences of the United States of America*, *73*(11), 3852–3856.

Schmidt, C. A., & Matera, A. G. (2020). tRNA introns: Presence, processing, and purpose. *WIREs RNA*, *11*(3).

Schneider, T., & Bindereif, A. (2017). Circular RNAs: Coding or noncoding? *Cell Research*, *27*(6), 724–725.

Schneider, T., Hung, L.-H., Aziz, M., Wilmen, A., Thaum, S., Wagner, J., Janowski, R., Müller, S., Schreiner, S., Friedhoff, P., Hüttelmaier, S., Niessing, D., Sattler, M., Schlundt, A., & Bindereif, A. (2019). Combinatorial recognition of clustered RNA elements by the multidomain RNA-binding protein IMP3. *Nature Communications*, *10*(1), 1–18.

Schneider, T., Schreiner, S., Preußer, C., Bindereif, A., & Rossbach, O. (2018). Northern blot analysis of circular RNAs. *Methods in Molecular Biology, 1724*, 119–133.

Schreiner, S., Didio, A., Hung, L.-H., & Bindereif, A. Design and application of circular RNAs with protein-sponge function. *Nucleic Acids Research*, *in press.*

Schumacher, T. N., & Schreiber, R. D. (2015). Neoantigens in cancer immunotherapy. *Science, 348*(6230), 69–74.

Semlow, D. R., Blanco, M. R., Walter, N. G., & Staley, J. P. (2016). Spliceosomal DEAH-Box ATPases remodel pre-mrna to activate alternative splice sites. *Cell*, *164*(5), 985–998.

Shukla, S., Kavak, E., Gregory, M., Imashimizu, M., Shutinoski, B., Kashlev, M., Oberdoerffer, P., Sandberg, R., & Oberdoerffer, S. (2011). CTCF-promoted RNA polymerase II pausing links DNA methylation to splicing. *Nature*, *479*(7371), 74–79.

Singh, N. K., Singh, N. N., Androphy, E. J., & Singh, R. N. (2006). Splicing of a critical exon of human survival motor neuron is regulated by a unique silencer element located in the last intron. *Molecular and Cellular Biology*, *26*(4), 1333–1346.

Staley, J. P., & Guthrie, C. (1999). An RNA switch at the 5’ splice site requires ATP and the DEAD box protein Prp28p. *Molecular Cell*, *3*(1), 55–64.

Stangl, K., Cascorbi, I., Laule, M., Klein, T., Stangl, V., Rost, S., Wernecke, K. D., Felix, S. B., Bindereif, A., Baumann, G., & Roots, I. (2000). High CA repeat numbers in intron 13 of the endothelial nitric oxide synthase gene and increased risk of coronary artery disease. *Pharmacogenetics*, *10*(2), 133–140.

Starke, S., Jost, I., Rossbach, O., Schneider, T., Schreiner, S., Hung, L.-H., & Bindereif, A. (2015). Exon circularization requires canonical splice signals. *Cell Reports*, *10*(1), 103–111.

Steitz, T. A., & Steitz, J. A. (1993). A general two-metal-ion mechanism for catalytic RNA. *Proceedings of the National Academy of Sciences of the United States of America*, *90*(14), 6498–6502.

Streuli, M., Hall, L. R., Saga, Y., Schlossman, S. F., & Saito, H. (1987). Differential usage of three exons generates at least five different mRNAs encoding human leukocyte common antigens. *Journal of Experimental Medicine*, *166*(5), 1548–1566.

Surono, A., Takeshima, Y., Wibawa, T., Ikezawa, M., Nonaka, I., & Matsuo, M. (1999). Circular dystrophin RNAs consisting of exons that were skipped by alternative splicing. *Human Molecular Genetics*, *8*(3), 493–500.

Tanowitz, M., Hettrick, L., Revenko, A., Kinberger, G. A., Prakash, T. P., & Seth, P. P. (2017). Asialoglycoprotein receptor 1 mediates productive uptake of N-Acetylgalactosamine-conjugated and unconjugated phosphorothioate antisense oligonucleotides into liver hepatocytes. *Nucleic Acids Research*, *45*(21), 12388–12400.

Tatomer, D. C., Liang, D., & Wilusz, J. E. (2017). Inducible expression of eukaryotic circular RNAs from plasmids. *Methods in Molecular Biology*, *1648*, 143–154.

Trotta, C. R., Miao, F., Arn, E. A., Stevens, S. W., Ho, C. K., Rauhut, R., & Abelson, J. N. (1997). The yeast tRNA splicing endonuclease: A tetrameric enzyme with two active site subunits homologous to the archaeal tRNA endonucleases. *Cell*, *89*(6), 849–858.

Turunen, J. J., Niemelä, E. H., Verma, B., & Frilander, M. J. (2013). The significant other: Splicing by the minor spliceosome. *Wiley Interdisciplinary Reviews: RNA, 4*(1), 61–76.

Vo, J. N., Cieslik, M., Zhang, Y., Shukla, S., Xiao, L., Zhang, Y., Wu, Y. M., Dhanasekaran, S. M., Engelke, C. G., Cao, X., Robinson, D. R., Nesvizhskii, A. I., & Chinnaiyan, A. M. (2019). The landscape of circular RNA in cancer. *Cell*, *176*(4), 869-881.e13.

Wang, E. T., Sandberg, R., Luo, S., Khrebtukova, I., Zhang, L., Mayr, C., Kingsmore, S. F., Schroth, G. P., & Burge, C. B. (2008). Alternative isoform regulation in human tissue transcriptomes. *Nature*, *456*(7221), 470–476.

Wang, G. S., & Cooper, T. A. (2007). Splicing in disease: Disruption of the splicing code and the decoding machinery. *Nature Reviews Genetics, 8*(10), 749–761.

Wang, M., Hou, J., Müller-McNicoll, M., Chen, W., & Schuman, E. M. (2019). Long and repeat-rich intronic sequences favor circular RNA formation under conditions of reduced spliceosome activity. *Science*, *20*, 237–247.

Wang, Z., & Burge, C. B. (2008). Splicing regulation: From a parts list of regulatory elements to an integrated splicing code. *RNA*, 14(5), 802–813.

Ward, A. J., Norrbom, M., Chun, S., Bennett, C. F., & Rigo, F. (2014). Nonsense-mediated decay as a terminating mechanism for antisense oligonucleotides. *Nucleic Acids Research*, *42*(9), 5871–5879.

Waterston, R. H., Lindblad-Toh, K., Birney, E., Rogers, J., Abril, J. F., Agarwal, P., Agarwala, R., Ainscough, R., Alexandersson, M., An, P., Antonarakis, S. E., Attwood, J., Baertsch, R., Bailey, J., Barlow, K., Beck, S., Berry, E., Birren, B., Bloom, T., … Lander, E. S. (2002). Initial sequencing and comparative analysis of the mouse genome. *Nature*, *420*(6915), 520–562.

Weiner, A. J., Choo, Q. L., Wang, K. S., Govindarajan, S., Redeker, A. G., Gerin, J. L., & Houghton, M. (1988). A single antigenomic open reading frame of the hepatitis delta virus encodes the epitope(s) of both hepatitis delta antigen polypeptides p24 delta and p27 delta. *Journal of Virology*, *62*(2), 594–599.

Wesselhoeft, R. A., Kowalski, P. S., & Anderson, D. G. (2018). Engineering circular RNA for potent and stable translation in eukaryotic cells. *Nature Communications*, *9*(1), 2629.

Wesselhoeft, R. A., Kowalski, P. S., Parker-Hale, F. C., Huang, Y., Bisaria, N., & Anderson, D. G. (2019). RNA circularization diminishes immunogenicity and can extend translation duration *in vivo*. *Molecular Cell, 74*(3), 508–520.e4.

Wilkinson, M. E., Charenton, C., & Nagai, K. (2020). RNA Splicing by the Spliceosome. *Annual Review of Biochemistry*, *89*(1), 359–388.

Xu, Z., & Weiss, A. (2002). Negative regulation of CD45 by differential homodimerization of the alternatively spliced isoforms. *Nature Immunology*, *3*(8), 764–771.

Yang, L., Ma, F., Liu, F., Chen, J., Zhao, X., & Xu, Q. (2020). Efficient delivery of antisense oligonucleotides using bioreducible lipid nanoparticles *in vitro* and *in vivo*. *Molecular Therapy - Nucleic Acids*, *19*, 1357–1367.

Yang, Y., Fan, X., Mao, M., Song, X., Wu, P., Zhang, Y., Jin, Y., Yang, Y., Chen, L. L., Wang, Y., Wong, C. C. L., Xiao, X., & Wang, Z. (2017). Extensive translation of circular RNAs driven by N 6 -methyladenosine. *Cell Research*, *27*(5), 626–641.

Zaphiropoulos, P. G. (1997). Exon skipping and circular RNA formation in transcripts of the human cytochrome P-450 2C18 gene in epidermis and of the rat androgen binding protein gene in testis. *Molecular and Cellular Biology*, *17*(6), 2985–2993.

Zaphiropoulos, P. G. (1996). Circular RNAs from transcripts of the rat cytochrome P450 2C24 gene: Correlation with exon skipping. *Proceedings of the National Academy of Sciences of the United States of America*, *93*(13), 6536–6541.

Zhang, Y., Xue, W., Li, X., Zhang, J., Chen, S., Zhang, J.-L., Yang, L., & Chen, L.-L. (2016). The biogenesis of nascent circular RNAs. *Cell Reports*, *15*(3), 611–624.

Zhao, Y., Zhou, J., He, L., Li, Y., Yuan, J., Sun, K., Chen, X., Bao, X., Esteban, M. A., Sun, H., & Wang, H. (2019). MyoD induced enhancer RNA interacts with hnRNPL to activate target gene transcription during myogenic differentiation. *Nature Communications*, *10*(1), 5787.

7. Abbreviations

2′-MOE	2′-O-methoxyethyl
2′Ome	2′-O-methyl
A	adenosine
A	ampere
AGO2	argonaute-2 protein
ANRIL	antisense non-coding RNA in the INK4 locus
APOB	apolipoprotein B
ASO	antisense oligonucleotide
AU	absorbance units
BGH	bovine growth hormone
bp	base pair(s)
BP-A	branch point adenosine
BRD9	bromodomain-containing protein 9
BSA	bovine serum albumin
C	cytidine
CD45	cluster of differentiation antigen 45
CDR1as	cerebellar degeneration-related protein 1 antisense
circRNA	circular RNA
CLIP	crosslinking and immune- precipitation
CNTROB	centrobin, centriole duplication and spindle assembly protein
Da	dalton
DFHBI	3,5-difluoro-4-hydroxy-benzylidene imidazolinone
DIG	digoxigenin
DMD	Duchenne muscular dystrophy
DMEM	Dulbecco's modified eagle medium
DMPC	dimethyl pyrocarbonate
DNA	deoxyribonucleic acid
DNase	deoxyribonuclease
DTT	dithiothreitol
E.	*Escherichia*
EDTA	ethylenediamine tetraacetic acid
eNOS	endothelial nitric oxide synthase
ESE	exonic splicing enhancer
ESS	exonic splicing silencer
ESTs	expressed sequence tags
et al.	*et alii*
ex	exon
FDA	Food and Drug Administration
fwd	forward
g	acceleration of gravity
g	gram
G	guanosine
GAPDH	glyceraldehyde-3-phosphate dehydrogenase
GFP	green fluorescence protein
h	hour(s)

hnRNP L	heterogenous nuclear ribonucleoprotein L
hnRNP LL	hnRNP L-like
HPLC	high-performance liquid chromatography
HSC	hematopoietic stem cells
IFN-1β	Interferon type I β
inp	input
intr	intron
ISE	intronic splicing enhancer
ISS	intronic splicing silencer
ITGA4	integrin subunit alpha 4
LDL	low-density lipoprotein
M	marker
m6A	N6-methyladenosine
min	minute
miRNA	microRNA
ml	milliliter
mRNA	messenger RNA
MS	mass spectrometry
MYL6	myosin light polypeptide 6
ng	nanogram
nM	nanomolar
NMD	nonsense-mediated decay
nt	nucleotide(s)
NTC	NineTeen complex
NTR	NTC-related complex
OH	hydroxyl group
PAPOLA	poly(A) polymerase alpha
PARK7	Parkinson disease protein 7
PBS	phosphate buffered saline
PCR	polymerase chain reaction
PIE	permuted intron-exon
PKR	protein kinase R
PMO	phosphorodiamidate morpholino
Pol II/III	RNA polymerase II/III
pre-mRNA	precursor mRNA
pre-tRNA	precursor tRNA
PS	phosphorothioate
PTC	premature termination codon
RBP	RNA-binding protein
rev	reverse
RIP	RNA immunoprecipitation
RISC	RNA-induced silencing complex
Rlg1/Trl1	tRNA ligase
RNA	ribonucleic acid
RNAi	RNA interference
RNase	ribonuclease
RRM	RNA recognition motif

rRNA	ribosomal RNA
RT	reverse transcription
RtcB	RNA 2′,3′-cyclic phosphate and 5′-OH ligase
SDS	sodium dodecyl sulfate
SELEX	systematic evolution of ligands by exponential enrichment
Seq	sequencing
SF3B1	splicing factor 3b subunit 1
siRNA	small interfering RNA
SMA	spinal muscular atrophy
SMN	survival of motor-neuron
snRNA	small nuclear RNA
snRNP	small nuclear ribonucleoprotein
SR	serine-arginine-rich
SRSF1	serine/arginine-rich splicing factor 1
SS	splice site
SSO	splice-switching oligonucleotide
TBS	tris-buffered saline
TJP1	tight junction protein-1
Tornado	twister-optimized RNA for durable overexpression
tricRNA	tRNA intronic circular RNA
Trm4	methyltransferase
tRNA	transfer RNA
TSEN	tRNA splicing endonuclease
U	unit
U	uracil
UV	ultraviolet
U1 – U6	small nuclear RNA U1 – U6
U2AF	U2-auxiliary factor
V	volt
v/v	volume per volume
w/v	weight per volume
ZKSCAN1	zinc finger with KRAB and SCAN domains 1
µg	microgram
µl	microliter

8. Scientific achievements

Publication

Schreiner, S., Didio, A., Hung L.-H., & Bindereif, A. Design and application of circular RNAs with protein-sponge function. *Nucleic Acids Research*, *in press*.

Poster presentations

Annual GGL Conference
September 4th to September 5th 2019, Giessen, Germany
Didio A, Bindereif A. Circular RNA sponges as splicing modulators.

BIMSB Grand Opening Symposium
October 25th to October 27th 2018, Berlin, Germany
Didio A, Bindereif A. The establishment of circRNA expressing vectors.

Annual GGL Conference
September 19th to September 20th 2018, Giessen, Germany
Didio A, Bindereif A. Analysis of factors and sequences determining circular RNA biogenesis.

Oral presentations

First Online GGL Conference
September 29th to September 30th 2020, Giessen, Germany
Didio A, Bindereif A. Designer circular RNAs for protein sponging.

ITN circRTrain Network meeting
February 4th to February 5th 2019, Rome, Italy
Didio A, Bindereif A. The establishment of circRNA expressing vectors.

9. Acknowledgements

In the beginning, I would like to thank my supervisor Prof. Dr. Albrecht Bindereif for guiding me well throughout the research work. I appreciate his contributions of time, ideas, and funding to make my Ph.D. experience well-turned.

I would like to address special thanks to Dr. Christian Preußer, Dr. Tim Schneider, and Dr. Oliver Rossbach for giving the encouragement and sharing insightful suggestions.

I would like to thank Silke Schreiner who supported the methodological part of my work and provided many genetic constructs. I appreciate her contributions of time and ideas to make my work productive.

I am grateful to all my colleagues with whom I have had the pleasure to work, namely Christina Pfafenrot and Marie Mosbach for their help, company, and wonderful sense of humor. I would like to thank Stephen Nuthalapati for bringing greater cultural diversity and encouraging spirit to the workplace. I also wish to thank Corinna Ulshöfer for always being there for me from my very first days in the lab, her instant support and wise advises.

I express my sincere appreciation to my parents who supported me a lot.

This work would not be possible without circRTrain funding from the European Union's Horizon 2020 research and innovation programme under the Marie Sklodowska-Curie grant, which funded the whole project and provided me an opportunity to attend international conferences as well as internal meeting and to present my work there.

I am thankful to International Giessen Graduate Centre for the Life Sciences for providing useful workshops for personal development.

Last but not least, I would like to thank my husband, Philipp Weinhold, who supported me throughout this journey.

10. Eidesstattliche Erklärung

Ich erkläre: Ich habe die vorgelegte Dissertation selbstständig und ohne unerlaubte fremde Hilfe und nur mit den Hilfen angefertigt, die ich in der Dissertation angegeben habe. Alle Textstellen, die wörtlich oder sinngemäß aus veröffentlichten Schriften entnommen sind, und alle Angaben, die auf mündlichen Auskünften beruhen, sind als solche kenntlich gemacht. Ich stimme einer evtl. Überprüfung meiner Dissertation durch eine Antiplagiat-Software zu. Bei den von mir durchgeführten und in der Dissertation erwähnten Untersuchungen habe ich die Grundsätze guter wissenschaftlicher Praxis, wie sie in der „Satzung der Justus-Liebig-Universität Gießen zur Sicherung guter wissenschaftlicher Praxis“ niedergelegt sind, eingehalten.

I declare that I have completed this dissertation single-handedly without the unauthorized help of a second party and only with the assistance acknowledged therein. I have appropriately acknowledged and cited all text passages that are derived verbatim from or are based on the content of published work of others, and all information relating to verbal communications. I consent to the use of an anti-plagiarism software to check my thesis. I have abided by the principles of good scientific conduct laid down in the charter of the Justus Liebig University Giessen „Satzung der Justus-Liebig-Universität Gießen zur Sicherung guter wissenschaftlicher Praxis“ in carrying out the investigations described in the dissertation.

Gießen, den 25. November 2020

Anna Didio